UNIVERSITY OF SOUTHAMPTON

FACULTY OF ENGINEERING, SCIENCE AND MATHEMATICS

OPTOELECTRONICS RESEARCH CENTRE

An Investigation into Using Optical Amplifiers for Enhancing Brillouin based Optical Time Domain Reflectometry

by

Yuh Tat Cho

Thesis submitted for the degree of Doctor of Philosophy

July 2004

UNIVERSITY OF SOUTHAMPTON

ABSTRACT

FACULTY OF ENGINEERING, SCIENCE AND MATHEMATICS
OPTOELECTRONICS RESEARCH CENTRE

Doctor of Philosophy

An Investigation into Using Optical Amplifiers for Enhancing Brillouin based Optical Time Domain Reflectometry

by Yuh Tat Cho

Distributed fibre sensors have been successfully demonstrated and used in various industries for performing continuous measurements of the physical parameters such as temperature and strain. However, the measurement range and the performance of such sensors are limited by the intrinsic attenuation of the signal in the sensing fibre. This thesis investigates using optical amplification within the sensing fibre to enhance the range and the performance of the distributed Brillouin based sensors.

The preliminary investigation involved using a CW Raman pump launched at the front end of the sensing fibre for amplifying both the pulse and backscattered signals. This technique demonstrated the expected Raman gain. However, the enhanced performance of the sensor was limited by the onset of the nonlinear effects. To overcome this problem, a delayed pulse Raman amplification technique was developed. This technique involves amplifying the probe pulse with the pump pulse at some distance along the sensing fibre. A temperature resolution of 1^{o}C at the front end rising to 13^{o}C at 50 km was achieved with this technique.

To extend the range beyond this, remote amplification was also investigated using CW Raman amplification in which a Raman pump is injected at the midpoint of a 100 km sensing fibre and a remotely pumped Erbium doped fibre amplifier is also situated at the midpoint. The performance achieved using each technique was measured and the relative advantages of each configuration were identified and discussed.

Contents

List of Figures

List of Tables

DECLARATION OF AUTHORSHIP

I, *Yuh Tat Cho*,
declare that the thesis entitled
'*An Investigation into Using Optical Amplifiers for Enhancing Brillouin based Optical Time Domain Reflectometry*'
and the work presented in it are my own. I confirm that:

- this work was done wholly or mainly while in candidature for a research degree at this University;
- where any part of this thesis has previously been submitted for a degree or any other qualification at this University or any other institution, this has been clearly stated;
- where I have consulted the published work of others, this is always clearly attributed;
- where I have quoted from the work of others, the source is always given. With the exception of such quotations, this thesis is entirely my own work;
- I have acknowledged all main sources of help;
- where the thesis is based on work done by myself jointly with others, I have made clear exactly what was done by others and what I have contributed myself;
- parts of this work have been published as:
  Refer to Appendix A (List of Publications)

Signed: Yuh Tat Cho
Date: 30/07/04

Acknowledgements

I wish to acknowledge the guidance and support of my supervisor, Dr Trevor Newson. I am indebted to him for giving me this opportunity to work on the project. I would like to thank my colleague, Mohamed, for the fruitful collaboration and for the assistance in the laboratory. I would like to extend my thanks to Dr Gilberto Brambilla and Dr Mark Gunning for providing the fibre Bragg gratings for my work.

I wish to express my gratitude to the following people for their help and also for the stimulating discussions on various subjects (not necessary related to work): Dr Peter Smith, Dr Eleanor Tarbox, Professor James Wilkinson, Dr Jayanta Sahu, Dr Elizabeth Taylor, Dr Angelique Favre, Dr Stuart Russell, Dr Bruce Kapplauf, Kentaro Furusawa, Fabio Ghiringhelli, Costa Corbari, Hock Aun Tan and Jerry Prawiharjo.

I am grateful to all my other friends and colleagues for their support and encouragement: Dr Katia Gallo, Dr Christos Grivas, Dr Jacob Mackenzie, Walter Belardi, Francesca Parmigiani, Paulo Almeida, Denis Guilhot, Patrick Hole, Paul Chambers, Jin Yee Chung, Chong Yew Lee, Jennifer Morley, Janet Mansour, Wendy White, Eveline Smith and Edwin Weatherby.

Finally, I would like to thank my wonderful family for all their support and encouragement over the years.

Definitions

Fictive Temperature	The temperature at which liquid glass turns into solid glass.
Measurement/Sensing Range	The maximum length of the fibre optic cable.
Spatial Resolution	The distance between the 10% and 90% points.
Strain Resolution	Standard deviation of the strain measurement over a certain length of the fibre maintained at a uniform strain. It is measured at one standard deviation value.
Temperature Resolution	Standard deviation of the temperature measurement over a certain length of the fibre maintained at a uniform temperature It is measured at one standard deviation value.

Abbreviations

AOM	Acousto-optic Modulator
ASE	Amplified Spontaneous Emission
BOTDR	Brillouin based Optical Time Domain Reflectometry
BOTDA	Brillouin based Optical Time Domain Analysis
BOCDA	Brillouin based Optical Correlation Domain Analysis
CRN	Coherent Rayleigh Noise
CW	Continuous Wave
DFB	Distributed Feedback
DPMZ	Double Pass Mach-Zehnder
DTS	Distributed Temperature Sensor
EDFA	Erbium Doped Fibre Amplifier
EOM	Electro-optic Modulator
ESA	Excited State Absorption
FBG	Fibre Bragg Grating
FTDFA	Fluoride based Thulium Doped Fibre Amplifier
FSR	Free Spectral Range
FWHM	Full Width Half Maximum
GHz	Gigahertz
InGaAs	Indium Gallium Arsenide
kHz	kilohertz
LPR	Landau Placzek Ratio
MI	Modulation Instability
μm	micrometer
MFD	Mode Field Diameter
MHz	Megahertz
mW	milliwatt
ns	nanoseconds
nm	nanometer
NZDF	Nonzero Dispersion Shifted Fibre

OSA	Optical Spectrum Analyzer
OTDR	Optical Time Domain Reflectometry
ppm	Parts Per Million
RF	Radio Frequency
SMF	Singlemode Fibre
SBS	Stimulated Brillouin Scattering
SRS	Stimulated Raman Scattering
SPM	Self-Phase Modulation
STDEV	Standard Deviation
THz	Terahertz
TDFA	Thulium Doped Fibre Amplifier
YIG	Yttrium Iron Garnet
WDM	Wavelength Division Multiplexer

List of Symbols

A_{eff}	Effective area
α_B	Brillouin scattering coefficient
α_R	Rayleigh scattering coefficient
c	speed of light in vacuum
D	Dispersion parameter
g_B	Brillouin gain coefficient
g_R	Raman gain coefficient
h	Planck's constant
k	Boltzmann's constant
$K_{P,T}$	Temperature coefficient of Brillouin power
$K_{\nu,T}$	Temperature coefficient of Brillouin frequency shift
$K_{P,\varepsilon}$	Strain coefficient of Brillouin power
$K_{\nu,\varepsilon}$	Strain coefficient of Brillouin frequency shift
L_{eff}	Effective length
λ	Wavelength
n	Refractive index
n_2	Nonlinear refractive index
ν_g	Group velocity
W	Pulse width

Chapter 1

Introduction

1.1 Objective and Outline of Thesis

The majority of sensors involve the measurement of some physical, chemical or biological parameters at a discrete position. In applications where the parameter to be measured is spatially varying, large number of sensors maybe required to map the field. As the required number increases, this approach becomes less attractive due to the increased complexity and cost. Distributed fibre optic sensors, which are capable of spatially resolving a measurand in a continuous fashion along the sensing length, provide a useful technique to overcome such problems. An important category of distributed fibre optic sensors are those based on the technique referred to as optical time domain reflectometry (OTDR). The OTDR is based on measuring the Rayleigh backscattered light as a pulse travels along the optical fibre. The time for the pulse to travel through the fibre and the backscattered light to be detected can be converted into distance.

Sensors based on the measurement of the Brillouin scattering using the OTDR technique have been developed, for distributed temperature and strain measurements. However, the measurement range of the OTDR technique is limited by the attenuation of the sensing fibre. This thesis investigates using optical amplifiers to enhance the measurement range of Brillouin based distributed optical fibre sensors.

A description of spontaneous Brillouin scattering and its use for distributed sensing is presented in Chapter 2. The differences between Brillouin, Rayleigh and Raman scattering mechanisms are highlighted in this chapter. The principles of Brillouin based OTDR and its development from conventional OTDR are discussed. In addition, this chapter discusses how the intensity and the frequency shift, of the spontaneous Brillouin light maybe used to measure temperature and strain. Different types of distributed Brillouin based sensors are reviewed and the problems encountered in distributed sensing systems caused by nonlinear effects such as stimulated Raman scattering (SRS), stimulated Brillouin scattering (SBS) and self phase modulation (SPM) are analysed and discussed. The effects of the coherent Rayleigh noise on the accuracy of the measurement is presented.

The characteristics of the different types of optical amplifiers and their applications for improving the performance of the long range Brillouin based OTDR are discussed in chapter 3. The research has focussed on using Raman amplification and so this was modelled to facilitate optimisation of the controllable parameters in the subsequent experiments.

The experimental investigation of the use of Raman amplifications in the single-ended distributed Brillouin sensing system is described in chapter 4. The Raman gain coefficient was measured using the pump probe method and the result was compared with the values obtained from the literature. A single-ended Brillouin based OTDR systems based on the CW Raman amplification was demonstrated using a 1450 nm pump source and a Q-switched fibre laser probe source at 1533 nm. The problems encountered with the technique are discussed and a solution is reported. This involved using a pulsed pump source at 1450 nm and exploiting the dispersion properties of the fibre in order to control the position of Raman gain within the fibre. Other modifications include using a more efficient optical filtering system and using a more stable pulse probe source.

Finally, the use of the remote amplification has been explored for applications which permit access to the sensing fibre. The design and implementation of a number of configurations of the remotely pumped amplifiers are discussed in chapter 5. The relative performance of each configuration is compared based on the temperature resolution capability at the far end of the sensing fibre.

Chapter 6 provides a summary of the key results and conclusions. It also outlines some future directions for continuing the advance of Brillouin based distributed fibre optic sensors.

Chapter 2

Distributed Optical Fibre Sensors

2.1 Introduction

Distributed optical fibre sensors provide an excellent means for performing spatially continuous measurements over a long distance. These sensors are based on monitoring the changes to the properties of the sensing fibre due to perturbation from the external environment. The Rayleigh based optical time domain reflectometry (OTDR) provided an early platform for distributed sensing. This technique was developed by Barnoski and Jensen to evaluate the attenuation profile of an optical fibre [1] and eventually evolved into Raman and Brillouin based distributed fibre sensing. The principle of OTDR is based on measuring the Rayleigh backscattering light from a pulse of light launched into the optical fibre. The time interval for the pulse to travel through the fibre to the detection of backscattered light provides the spatial information. The mechanism behind the Rayleigh scattering is due to the random density variations in the silica structure introduced during fabrication. This results in fluctuations in the refractive index, which causes the scattering of light.

It is an elastic scattering mechanism and hence there is no difference in the frequency or wavelength between the probe and the backscattered light. The light scattered in an optical fibre consists of three components: Rayleigh, Brillouin and Raman. The magnitude of the Rayleigh component is approximately 15 dB and 30 dB larger compared to the Brillouin and Raman components respectively. Each component occurs at a different wavelengths due to the scattering mechanism involved; typically the frequency shift is 13.2 THz for Raman scattering and 11 GHz for Brillouin scattering at 1.5 μm. Brillouin and Raman scattering are sensitive to certain physical parameters: The intensity of the Raman scattered light is a function of temperature and forms the basis of commercially developed distributed temperature sensors (DTS). Whilst the changes in the frequency and intensity of the Brillouin scattered light are functions of both temperature and strain and permit simultaneous measurement of the temperature and strain.

The main applications of distributed sensors include:

1. Downhole temperature monitoring for the oil and gas industry [2, 3]: Downhole monitoring plays a key role in the production of oil and gas in reservoirs. Key parameters such as temperature and pressure provide valuable information on the depletion or extraction rate of fluid in a reservoir. There is a correlation between the temperature distribution of the downhole and the thermal properties of the fluid. It can be used to determine the flow rate of the fluid. Previously, electronic gauges and wirelines have been used to monitor such parameters. However, the reliability of these electronic based devices is greatly reduced in an environment of high temperature and pressure. In particular, the operational temperature for these electronic devices are limited to 130^{o}C [4]. For example, the DTS can be operated beyond the aforementioned temperature, close to 200 ^{o}C with the use of carbon coated optical fibres [4].

The DTS also allows distributed temperature measurement of the reservoir on a real time basis, which will be useful for optimising the oil well production.

2. Temperature profiling of high voltage underground cables [5, 6]: The majority of the energy cables are buried in the ground and usually the cable link is maintained over a duration of 40 years. Over this period, the environment changes and hence the soil characteristics. For example, installation of heating passages in close proximity to the energy cables in urban areas may modify the properties of the soil, which may cause the cable to overheat and may result in its mechanical breakdown. DTS allows real time monitoring of the temperature of the buried cables, and provides important information both to ensure reliability and also to maximise its current carrying capacity.

3. Structural monitoring: Distributed strain sensing has been used for continuous monitoring of the integrity of structures in places such as bridges, tunnels, river embankments, dams and wings of aircraft.

2.2 Brillouin Based OTDR

2.2.1 Spontaneous Brillouin Scattering Mechanism

Spontaneous Brillouin scattering originates from the interactions between the incident probe light and the thermally induced acoustic waves in an optical medium [7]. The travelling acoustic waves modify the refractive index profile. This effect induces a periodic variation in the refractive index and results in scattering of the incident probe light. The acoustic waves are generated by the vibrations of the molecules in the medium and are temperature dependent. The vibrations of molecules which lead to Brillouin scattering are referred to as acoustic phonons and their frequency is approximately 11 GHz at a pump wavelength of 1550 nm. Spontaneous Raman scattering involves the scattering of light induced by the higher frequency oscillations of the molecules. This type of scattering process is much weaker compared to Brillouin scattering and the frequency of oscillations are of the order of THz and are referred to as optical phonons. The scattering process involves an exchange of energy between the phonons and the light, leading to the creation or annihilation of a phonon. When a phonon is created, the energy and the frequency of the light is reduced and it is known as the Stokes signal. When a phonon is annihilated, the energy and the frequency of the light is increased and it is known as the anti-Stokes signal.

The shift in frequency of the Brillouin scattered light relative to the incident light is given by [8]

$$\nu_B = \frac{2\,n\,V_a}{\lambda_p} \sin\left(\frac{\theta}{2}\right) \tag{2.1}$$

where n is the refractive index in the core, V_a is the acoustic velocity, θ is the angle between the Brillouin scattered light and incident light, λ_p is the probe wavelength and ν_B is the Brillouin frequency shift. When $\theta = \pi$, the frequency shift of the Brillouin scattered light is at the maximum in the backward direction. Based on the values of n and V_a quoted in Bansal and Doremus [9], the calculated range of the Brillouin frequency shift is from 10.779 GHz to 11.626 GHz for a temperature range of 25 ^{o}C to 1000 ^{o}C. The occurrence of multiple Brillouin peaks has been reported [10]. They are usually found in fibre with a multi-compositional core structure which, whilst single mode for light propagation, allows a number of longitudinal acoustic modes. Light scattered from such modes leads to the observed multiple Brillouin peaks. For standard single mode fibre, a single Brillouin Stokes and anti-Stokes peaks are observed as in figure 2.1.

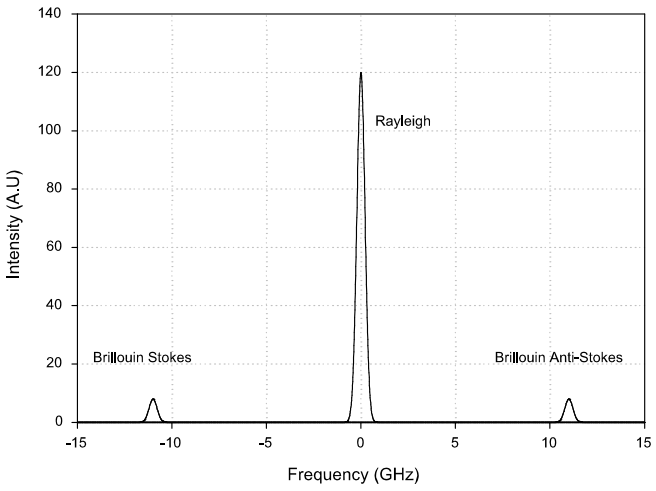

FIGURE 2.1: The spontaneous light scattering consisting of Rayleigh and Brillouin components at 1550 nm.

The acoustic velocity is dependent on Young's modulus and the density of silica. Although the refractive index increases linearly with temperature, it is primarily the change in the Young's modulus with temperature which results in the change in the acoustic velocity [9].

2.2.2 Principle

The principle employed for the distributed spontaneous Brillouin based sensor is similar to that of the conventional Rayleigh based OTDR. The schematic showing the principle of the Brillouin based OTDR is illustrated figure 2.2.

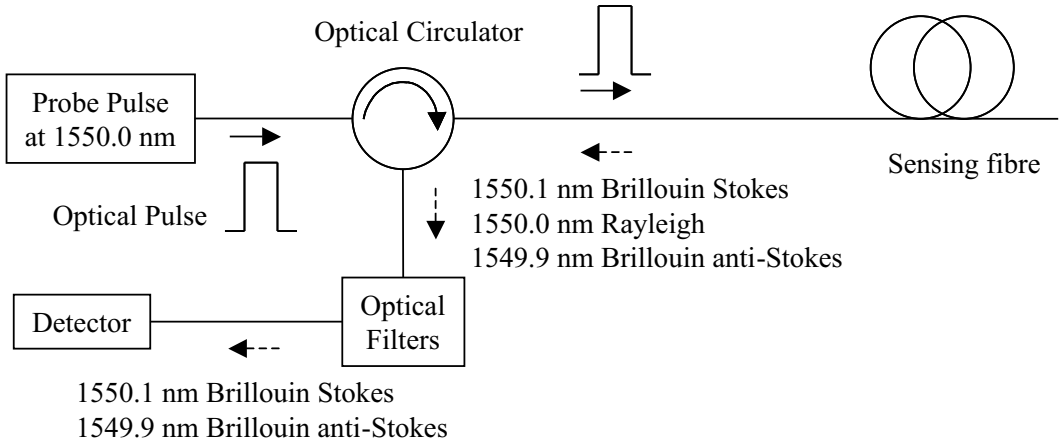

FIGURE 2.2: The schematic of the Brillouin based OTDR. The solid line indicates the path of the optical pulse, while the dashed line denotes the path of the backscattered signals.

Probe pulses at 1550.0 nm was launched into the sensing fibre via an optical circulator. The backscattered signals, which consist of Brillouin Stokes at 1550.1 nm, Rayleigh at 1550.0 nm and Brillouin anti-Stokes at 1549.9 nm, were coupled to the optical filters by an optical circulator. Optical filters were then used to separate both the Brillouin Stokes and anti-Stokes signals from the Rayleigh signal. The Brillouin backscattered signals were transmitted on to a detector and were then processed to produce a plot of the temperature profile as a function of distance.

The spontaneous Brillouin backscattered power as a function of distance can be obtained from the time delay between the launched probe pulse and the arrival of the backscattered signal. The spontaneous Brillouin backscattered power as a function of distance can be expressed in the following form

$$P_B(z) = \frac{1}{2} P_{in} W \alpha_B S v_g \exp(-2\alpha_R z) \tag{2.2}$$

where P_{in} is the launched power of the probe pulse, W is the pulsewidth of the probe, S is the capture fraction which determines the amount of scattered light collected within the numerical aperture of the optical fibre, v_g is the group velocity, α_B and α_R are the Brillouin and Rayleigh scattering coefficients. The exponential term on the right hand side of equation 2.2 accounts for the two way attenuation loss for the forward propagating pulse and the backscattered light. The spatial resolution is the smallest resolvable distance between two scattering positions and it is governed by the width of the probe pulse. The spatial resolution can be expressed in the following form

$$\delta z = \frac{1}{2} \nu_g W \tag{2.3}$$

where δz is the spatial resolution, ν_g is the group velocity in the fibre and W is the width of the probe pulse. The power of the backscattered light is governed by the scattering coefficient and the ratio between α_R and α_B is approximately 15 dB. The intensity of the peaks is determined by the Brillouin scattering coefficient which is given by [11]

$$\alpha_B = \frac{8\pi^3 n^8 p^2 k T}{3\lambda_p^4 \rho V_a^2} \tag{2.4}$$

where p is the photoelastic coefficient, k is the Boltzmann's constant, T is the temperature and ρ is the density of silica. Taking the values of $n = 1.444$, $p = 0.286$, $\rho = 2330\,\mathrm{kg/m^3}$, $k = 1.38\times10^{-23}\,\mathrm{J/K}$, $V_a = 5785\,\mathrm{ms^{-1}}$, $T = 298\,\mathrm{K}$ and $\lambda_p = 1550\,\mathrm{nm}$, resulted in $\alpha_B = 1.17\times10^{-6}\,\mathrm{m^{-1}}$.

To compensate for splice losses and fibre attenuation, the intensity of the Brillouin backscatter is measured and it is normalised using the intensity of the Rayleigh backscattered signal. Since the wavelength separation between the Rayleigh and Brillouin signal is small (0.1 nm), both signals experience similar loss. The ratio between the Brillouin and Rayleigh intensity is given by [11]

$$\frac{I_B}{I_R} = \frac{T}{T_f\,(\rho\,V_a^2\,\beta_T - 1)} \tag{2.5}$$

where I_R is the intensity of the Rayleigh signal, I_B is the intensity of the Brillouin signal, ρ is the density of silica, T_f is the fictive temperature, ie the temperature at which liquid glass turns into solid glass, and β_T is the equilibrium isothermal compressibility of the melt at the fictive temperature.

The coefficients at a wavelength of 1.5 μm were reported to be: $K_{P,T} = 0.30\,\%^oC^{-1}$ [12] and $K_{P,\varepsilon} = -9.03\times10^{-4}\,\%\,(\mu\varepsilon)^{-1}$ [13] are the Brillouin power dependencies on the temperature and strain, while $K_{\nu,T} = 1.1\,\mathrm{MHz}\,^oC^{-1}$ [14, 15] and $K_{\nu,\varepsilon} = 0.048\,\mathrm{MHz}\,(\mu\varepsilon)^{-1}$ [14, 15] are the Brillouin frequency shift dependencies on the temperature and strain. If the percentage intensity change and the Brillouin frequency shift is measured, then the temperature and strain can be calculated.

Table 2.1 summarises the relationship between the Brillouin intensity and frequency shift with temperature and strain.

TABLE 2.1: The variation between the Brillouin intensity and frequency shift with the physical parameters.

Physical Parameter	**Intensity**	**Frequency**
Strain	-9.03×10^{-4} % $(\mu\varepsilon)^{-1}$	0.048 MHz $(\mu\varepsilon)^{-1}$
Temperature	0.30 %^{o}C^{-1}	1.1 MHz ^{o}C^{-1}

The negative coefficient of the strain dependency on the intensity indicated that the intensity is reduced with increased strain. The relationship between the coefficients and the two physical parameters are given as [16]

$$\begin{pmatrix} \Delta P_B \\ \Delta \nu_B \end{pmatrix} = \begin{pmatrix} K_{P,T} & K_{P,\varepsilon} \\ K_{\nu,T} & K_{\nu,\varepsilon} \end{pmatrix} \begin{pmatrix} \Delta T \\ \Delta \varepsilon \end{pmatrix} \tag{2.6}$$

where ΔP_B is the Brillouin power, $\Delta \nu_B$ is the Brillouin frequency shift, $\Delta \varepsilon$ is the applied strain and ΔT is the temperature change. The temperature and strain can be resolved by taking the inverse of the matrix of equation 2.6 provided the determinant of the matrix is nonzero.

2.3 Other Architectures for Distributed Brillouin Sensing

The previous section described BOTDR technique and has the advantage of being single-ended. Alternative schemes based on Brillouin optical time domain analysis (BOTDA) rely on access to both ends of the sensing fibre. Details of these techniques will be presented in the following section.

2.3.1 BOTDA Technique

This technique was developed initially by Horiguchi as an alternative technique offering increased dynamic range to the conventional OTDR, for the loss measurement in the optical fibres [17]. This is achieved by using the stimulated Brillouin interaction between a forward propagating pump and a counter-propagating signal within the fibre. The setup is illustrated in figure 2.3.

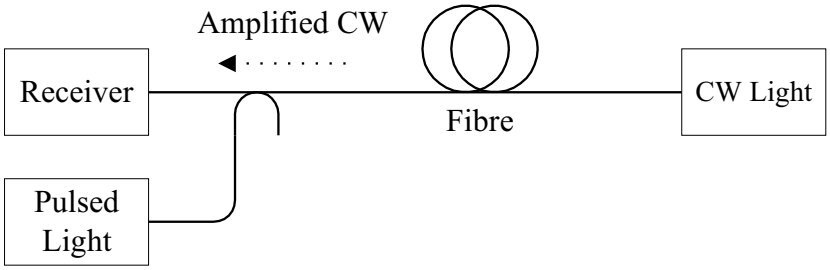

FIGURE 2.3: The experimental setup for the BOTDA technique.

It can be operated in two ways, either in the Brillouin gain or loss method [18]. The Brillouin gain technique is based on the Brillouin amplification of the counter-propagating CW probe light at frequency ν_{cw} using a pulsed pump light at a frequency ν_p where $\nu_p > \nu_{cw}$. The Brillouin gain is at the maximum when the difference between the two frequencies are equivalent to the Brillouin shift, $\nu_B = \nu_p - \nu_{cw}$. The time delay for the pulse to interact with the CW light provides the spatial information. Hence, the amplified CW probe light can be measured as a function of the distance. The sensing length of this technique is limited by the pump pulse due to depletion and attenuation of the pump.

The Brillouin loss technique is based on the amplification of the pulse light at frequency ν_p by the CW light at frequency ν_{cw} where $\nu_p < \nu_{cw}$. The depleted CW light is collected and analysed as a function of time. A longer sensing range has been claimed using the Brillouin loss method as the pulse is amplified and hence it is able to travel further down the sensing fibre, provided that the sensing fibre is at a uniform strain or temperature distribution. In both cases, the Brillouin gain spectrum is obtained by tuning the wavelength of one of the sources over several hundred MHz. The physical parameters such as temperature or strain can be deduced by measuring the changes in the centre frequency of the Brillouin gain spectrum. However, the technique is not capable of distinguishing the two parameters and suffers from requiring access to both ends. The latter problem was partially solved by using reflected light from the far end of the sensing fibre [19].

2.3.2 BOCDA Technique

The Brillouin optical correlation domain analysis technique (BOCDA) was developed to improve the accuracy of the Brillouin frequency shift measurement for applications with very high spatial resolution requirements. The accuracy of the Brillouin frequency shift measurement is degraded when the length of the probe pulse is reduced to less than 10 ns, corresponding to a spatial resolution of 1 m, due to difficulty in determining the centre frequency of the Brillouin spectrum [20]. This is because the measured linewidth of the Brillouin spectrum is the convolution of the pump spectrum and the Brillouin spectrum of a monochromatic source. As the probe pulse gets shorter, its spectrum becomes broader and hence the measured Brillouin linewidth is broadened as well.

Hotate proposed a correlation-based technique to overcome this spatial resolution problem [21]. The SBS interaction between the CW probe and the CW pump along the sensing fibre is obtained by controlling the phase between the two light sources. In this way, the SBS interaction is confined to a certain position within the fibre under test and this position is determined by monitoring the correlation peak.

Distributed measurement is performed by varying the modulation frequency, f_m, of the laser diode. The Brillouin gain is maximised where the pump and probe lights are in phase. Elsewhere the Brillouin gain is significantly reduced. The relationship between the modulation frequency, f_m, and the intervals of the correlation peak, d_m, and the spatial resolution, δ_z, can be expressed as [21]

$$d_m = \frac{v_g}{2\, f_m} \tag{2.7}$$

$$\delta_z = \frac{v_g\, \Delta\nu_B}{2\,\pi\, m\, f_m^2} \qquad f_m < \Delta\nu_B/2 \tag{2.8}$$

where $\Delta\nu_B$ is the width of the Brillouin gain spectrum, ν_g is the speed of the light in the fibre and m is the modulation index.

The experimental setup for the BOCDA technique is illustrated in figure 2.4.

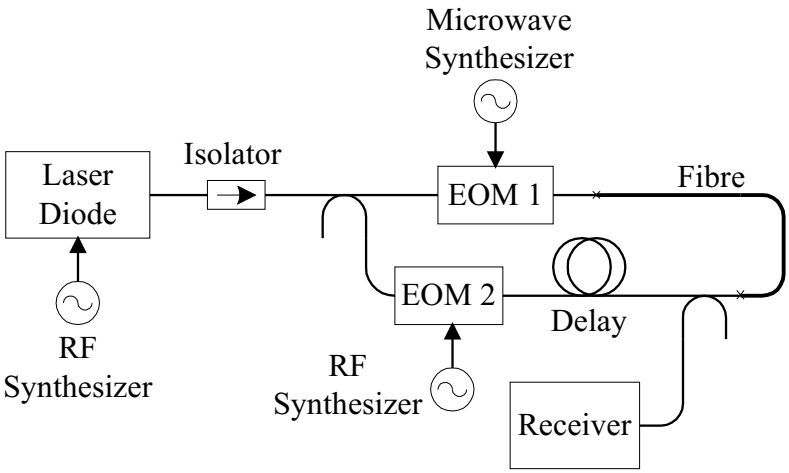

FIGURE 2.4: The setup for the correlation based technique.

The frequency modulated CW light from a laser diode is launched into a coupler. The CW light from the output of the coupler is used as a probe and is modulated at microwave frequency with EOM 1 to generate the lower sideband at frequency $\nu_o - \nu_B$. While, the CW light in the other output of the coupler is used as a pump at frequency ν_o and is modulated at a lower frequency using a RF synthesizer on EOM 2. The electronic signal from the RF synthesizer is used as a reference signal for the lock-in amplifier in order to detect the SBS amplified CW probe. The Brillouin gain spectrum is obtained by tuning the frequency of the probe through the EOM 1. The following section provides an overview of the recent progress achieved using the distributed Brillouin sensors with different measurement techniques.

2.3.3 Recent Progress of Distributed Brillouin Sensors

This section summarises in chronological order the key developments of distributed Brillouin based sensing since 1990. The results are described in this section.

The BOTDA technique is mainly based on the measurement of the frequency shift of the Brillouin gain spectrum as a function of either temperature or strain. In 1990, Kurashima reported a distributed temperature sensor using the BOTDA technique. A temperature measurement of 3 ^{o}C and a spatial resolution of 100 m were achieved for a 1.2 km length of SMF using the Brillouin gain method [22]. In 1993, Bao and colleagues extended the measurement range to 22 km using a similar measurement technique, in which a temperature resolution of 1 ^{o}C and a spatial resolution of 10 m was reported [23]. The measurement range was then increased from 22 km to 32 km in the same year using the Brillouin loss technique, with a temperature resolution of 1 ^{o}C, a spatial resolution of 5 m and signal averaging of 20 times [18]. A further increase in range of 51 km was then reported in 1995 using the same technique [24]. This improved measurement was the result of an increase in the signal averaging to 1024 times. In 1994, Horiguchi reported a sensing range of 11 km with spatial resolution of 1 m with the Brillouin gain technique, however the temperature resolution was degraded to 5 ^{o}C due to spectral broadening of the measured Brillouin spectrum [25]. A single-ended access system was demonstrated in 1996 by Nikles [19], using the reflection from the far end of the sensing fibre. The other modification obtained with this technique involves using a single source to generate the pump and probe. A strain resolution of 5 $\mu\varepsilon$, a spatial resolution of 45 m and a sensing range of 1.4 km was reported.

BOCDA technique was developed for improving the accuracy of the frequency based measurement, discussed in section 2.3.2. This technique is capable of performing submetre spatial resolution measurement as it utilised CW sources for measuring the Brillouin frequency shift. A spatial resolution of 45 cm for a measurement range of 7.8 m was initially reported in 1999 [21]. In 2001, the spatial resolution measurement was improved to 4.0 cm [26]. A strain resolution of 70 $\mu\varepsilon$ was reported for a similar sensing range. The correlation peak interval and the spatial resolution of the measurement are inversely proportional to the modulation frequency of the laser diode. This indicated that a high spatial resolution can be obtained by increasing the modulation frequency, however the peak interval will be simultaneously reduced and hence the measurement range.

The BOTDR technique relied on the measurement of the spontaneous Brillouin backscatter. This technique can be further divided into two other methods, coherent and direct detection. The coherent detection system is focussed on the measurement of the Brillouin frequency shift, while the direct detection is focussed on the intensity measurement. This section summarises the result in a chronological order of the development of the coherent detection system. In 1993, Shimizu reported a BOTDR system with a spatial resolution of 100 m and a sensing range of 10 km [27]. It utilised an AOM loop frequency translator for generating a probe light shifted by an amount almost equal to the Brillouin shift, such that the beat signal could be measured by a 100 MHz detector. In 1996, this configuration was simplified by Izumita using the technique described by Nikles to generate the pump and the frequency shifted probe [28]. They obtained a spatial and a strain resolution of 100 m and 20 $\mu\varepsilon$ respectively for a sensing length of 30 km. In the same year, Kurashima reported a high spatial resolution system for measuring distributed strain [29]. A strain resolution of 100 $\mu\varepsilon$, a spatial resolution of 1.5 m and a measurement range of 10 km was reported.

In the following year, the spatial resolution measurement was reduced to 1 m, however the strain resolution was degraded to 120 $\mu\varepsilon$ [30]. In 1999, a new BOTDR configuration was demonstrated by Maughan. The beat Brillouin signal was measured using a wide bandwidth detector of 20 GHz. The technique overcomes the complexity of the earlier BOTDR setup requiring a frequency translator. In this way, the system was simplified and either the Brillouin or Rayleigh signal could be measured and selected by changing the frequency of a YIG synthesizer. A temperature resolution of 3 ^{o}C and a sensing length of 57 km were reported for this configuration, but the spatial resolution was limited to 20 m due to the specification of the commercial electrical spectrum analyser [31]. A simultaneous measurement of the temperature and strain was demonstrated in 2001 using a similar system [15]. A temperature resolution of 4 ^{o}C, strain resolution of 100 $\mu\varepsilon$ was reported for a measurement range of 30 km. In 2001, Lee proposed a new technique for performing simultaneous measurement of the temperature and strain with the BOTDR method, utilising a non-zero dispersion shifted fibre (NZDF) [32]. The difference in the Brillouin frequency shift coefficients between the two peaks were used to resolve the strain and temperature measurements. A temperature and a strain resolution of 5 ^{o}C and 60 $\mu\varepsilon$, for a sensing length of 3.7 km was reported with this technique. Although this technique demonstrated useful resolution measurements for a short measurement range, there is doubt as to whether this technique would be advantageous for long range measurement since the performance of the Brillouin sensor is also dependent on the accuracy of the intensity measurement [15].

Direct measurement of the intensity of the spontaneous Brillouin backscatter as a function of temperature was first reported in 1996 [12]. A Fabry Perot inteferometer was used to filter the Rayleigh from the Brillouin backscatter, resulting in a temperature resolution of 6.5 ^{o}C for a sensing range and spatial resolution of 13 km and 600 m respectively. The temperature resolution and a spatial resolution was subsequently improved to 1.4 ^{o}C and 130 m in the following year [33]. The improvement is obtained as a result of the reduction in the coherent Rayleigh noise by averaging the narrowband Rayleigh signal over many wavelengths. The performance of the system was limited by the loss in the bulk interferometer $\sim$10 dB. A low loss fibre based Mach-Zehnder interferometer $\sim$3 dB was proposed in 1996 to circumvent this problem [34]. A temperature resolution of 2.9 ^{o}C and spatial resolution of 40 m was reported for a sensing range of 12.9 km. The performance of the system was further optimised in 1998. A temperature resolution of 1.4 ^{o}C, a spatial resolution of 3 m and a sensing range of 16 km was reported [35].

In 1997, a simultaneous measurement of the strain and temperature was reported by Parker [14]. The backscattered Brillouin signal was analysed using a bulk scanning Fabry Perot interferometer with a FSR of 9.7 GHz. A temperature and a strain resolution of 4 ^{o}C and 100 $\mu\varepsilon$ was reported for a spatial resolution of 40 m and sensing length of 1.2 km. In order to measure the Brillouin frequency shift accurately, the bandwidth of the interferometer has to be small $\sim$ 30-40 MHz and this may result in the rejection of some the Brillouin signal, depending on the linewidth of the source. This effect will limit the measurement range of the sensor, in particular for high spatial resolution measurements. A simultaneous measurement of the temperature and strain for a sensing length of 15 km using two cascaded all fibre Mach-Zehnder interferometers were reported in 2000 [36].

The first double pass Mach-Zehnder (DPMZ) with FSR of 22 GHz was used to separate the Brillouin from the Rayleigh backscatter to reduce the effects of CRN, while a second single pass Mach-Zehnder (SPMZ) with FSR of 7 GHz was used to collect a signal dependent on the Brillouin frequency shift. The Brillouin intensity change (independent of the Brillouin frequency shift) was obtained by summing the two Brillouin traces when the Rayleigh frequency signal was first tuned to the minimum and later at the maximum. The Brillouin signal was located either at 80 % or 20 % of the transfer function of the SPMZ for the two tuning conditions respectively. In the presence of strain, the increase in the Brillouin frequency shift would result in the decrease in the intensity of signal for the first condition and vice versa for the second condition. The change in the Brillouin frequency shift can be obtained from the change in the intensity in the earlier measurement. A temperature resolution of 4 ^{o}C and a strain resolution of 290 $\mu\varepsilon$ was reported.

A system for measuring distributed temperature with a spatial resolution of 35 cm and a temperature resolution of 4.3 ^{o}C was reported for a sensing length of 1 km [37]. This measurement was feasible with the use of an EOM to generate a pulsewidth of 3.5 ns. The spatial resolution was reduced to 20 cm in the same year. This result was the obtained with the reduction of the probe pulsewidth. A temperature resolution of 4.4 ^{o}C and a sensing length of 500 m was reported [38]. A measurement range of 23 km with a spatial resolution of 2 m was demonstrated by Souza for the direct detection system [39]. The improvement in the measurement range was obtained with the optical preamplification of the backscattered Brillouin signals using an EDFA.

In the same year, a dual frequency source was proposed by Lecoeuche for a heterodyne detection of the backscattered signal [40]. The dual frequency source consists of a probe pulse laser at Brillouin Stokes frequency and a CW local oscillator. The probe pulse was used to generate the anti-Stokes Brillouin backscattered signals, which was then mixed with the unshifted CW local oscillator to produce a low frequency beat Brillouin signal. Using this technique, a temperature resolution of $6\,^{o}$C and a spatial resolution of 7 m for a sensing range of 20 km was reported. In this configuration, only the intensity of the Brillouin signal is measured and hence it cannot be use for the simultaneous measurement of strain and temperature.

The results described in the earlier section are summarised and tabulated in table 2.2.

TABLE 2.2: The recent progress in different Brillouin based sensing since 1990.

Year	**Freq -uency**	**Inten -sity**	**Range** (km)	**Spatial Resolution** (m)	**Tempe -rature** (^{o}C)	**Strain** ($\mu\varepsilon$)	**Ref**
			BOTDA	**Technique**			
1990	x		1.2	100.0	3.0	-	[22]
1993	x		22.0	10.0	1.0	-	[23]
1993	x		32.0	5.0	1.0	-	[18]
1994	x		11.0	1.0	5.0	-	[24]
1995	x		51.0	5.0	1.0	-	[25]
1996	x		1.4	45.0	-	5.0	[19]
			BOCDA	**Technique**			
1999	x		7.8×10^{-3}	0.45	-	-	[21]
2001	x		8.0×10^{-3}	0.04	-	70.0	[26]
			BOTDR	**Technique**			
1993	x		10.0	100.0	-	-	[27]
1996		x	13.0	600.0	6.5	-	[12]
1996		x	13.0	130.0	1.4	-	[33]
1996	x		30.0	100.0	-	20.0	[28]
1996	x		10.0	1.5	-	100.0	[30]
1997	x	x	1.2	40.0	4.0	100.0	[14]
1997	x		30.0	10.0	-	-	[41]
1997	x		10.0	1.0	-	120.0	[29]
1998		x	16.0	3.0	1.0	-	[35]
1999	x	x	15.0	10.0	4.0	100.0	[36]
1999	x		57.0	20.0	3.0	-	[31]
1999	x	x	30.0	20.0	4.0	100.0	[15]
2000		x	1.0	0.35	4.3	-	[37]
2000		x	0.5	0.2	4.4	-	[38]
2000		x	23.0	2.0	6.0	-	[39]
2000		x	20.0	7.0	6.0	-	[40]
2001	x		3.7	2.0	5.0	60.0	[32]

The factors which may limit the performance of the BOTDR are discussed in the next section.

2.4 Factors Limiting the Performance of BOTDR

The performance of BOTDR measurements is strongly governed by the maximum probe power that can be used. This has to be chosen to avoid non-linear effects. The other important contribution is the coherent Rayleigh scattering (CRN). This section describes the thresholds of the various non-linear processes and the nature of and means to minimise CRN.

2.4.1 Coherent Rayleigh Noise

Coherent Rayleigh noise (CRN) influences the accuracy of the measurements [42]. CRN manifests itself as fluctuations in the Rayleigh backscattered signals and it is due to the interference between the light backscattered at different positions along the fibre. It is observed when a narrow linewidth source is used as a probe. Furthermore, it cannot be reduced by signal averaging. The noise on the Rayleigh signal appears as noise in the measured parameter when the Brillouin signal is normalised using the Rayleigh signal in the direct detection technique. Moreover, the CRN will become even more problematic if there is contamination on the Brillouin signal with Rayleigh signal. This will increase the noise on the Brillouin signal measurement and also in the derived measurement after the normalisation process.

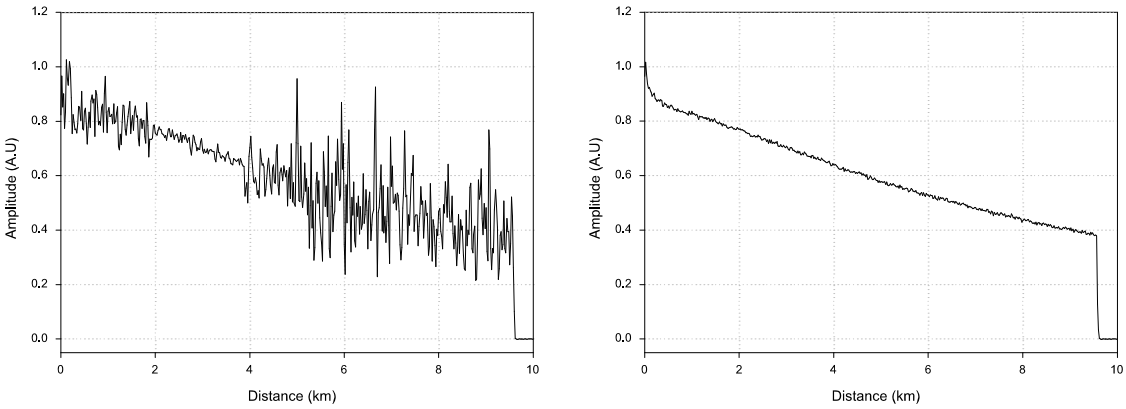

FIGURE 2.5: The effects of coherent Rayleigh noise: (a)The Rayleigh signal generated using a source with linewidth of 2 MHz. (b)The Rayleigh signal generated using a source with linewidth of 255 GHz.

It can be reduced by utilising the frequency shift averaging (FSAV) technique. This technique operates by performing averaging over many different wavelengths. A broadband source can be used for collecting the Rayleigh signal to reduce the effect of the CRN. Figure 2.5 shows the effects of the optical bandwidth of the source on the intensity profile of the Rayleigh backscattered signals. The figure 2.5(a) illustrated the Rayleigh signal, with fluctuations in the intensity, generated using a narrow linewidth source of 2 MHz. It can be seen that the noise on the Rayleigh signal is significantly reduced with the use of a broadband source of 255 GHz, figure 2.5(b).

However, when collecting the Brillouin signal, the linewidth of the source has to be sufficiently narrow, less than $\sim$5 GHz, to avoid overlap of the Rayleigh and Brillouin signal. To minimise the effects of CRN on the Brillouin signal to an acceptable level, the optical filter separating the Brillouin signal from the Rayleigh signal has to provide at least 30 dB rejection of the Rayleigh signal.

2.4.2 Nonlinear Threshold

The permissible launched probe power for the Brillouin based OTDR is governed by the onset of the nonlinear effects. The main influence of the nonlinear effects is to distort the spectral profile of the probe pulse travelling in the optical fibre. Such effects may be useful in applications related to the operation of nonlinear optical devices, but are generally undesirable in the Brillouin based OTDR system. It is vital to quantify the power at which these nonlinear effects occur in the optical fibre, such that these phenomena can be avoided by operating the probe power below the threshold power. Stimulated Raman scattering (SRS), stimulated Brillouin scattering (SBS) and self-phase modulation (SPM) are the three key nonlinear effects that can potentially degrade the performance of the direct detection system.

The SRS and SBS are detrimental as they result in the depletion of the power of the probe pulse. The threshold powers for both cases are defined as the input pump power for which the Stokes power is equivalent to the pump power at the output of the fibre [8]. The critical powers for the SBS and SRS can be expressed as [8]

$$P_{SBS} = \frac{21\ A_{eff}\, K}{L_{eff}\, g_B} \tag{2.9}$$

$$P_{SRS} = \frac{16\ A_{eff}\, K}{L_{eff}\, g_R} \tag{2.10}$$

where g_B is the Brillouin gain coefficient, g_R is the Raman gain coefficient, K is the polarisation factor and A_{eff} is the effective core area. The effective area for the conventional SMF is given by $80\,\mu\text{m}^2$ at 1550 nm [43]. The Brillouin and Raman gain coefficients were reported to be 5×10^{-11} m/W [8] and 3×10^{-14} m/W, at a pump wavelength of 1550 nm[44] respectively. This Brillouin gain coefficient is based on the assumption that the linewidth of the pump is smaller than the Brillouin linewidth.

Its value is affected by the pump linewidth, $\Delta\nu_P$, and consequently the critical power for the SBS may change according to the pump linewidth. The Brillouin gain coefficient as a function of pump linewidth [8], is given by

$$\widetilde{g_B}(\Delta\nu_P) \approx \frac{\Delta\nu_B}{\Delta\nu_B + \Delta\nu_P}\, g_B \quad for \quad \Delta\nu_P > \Delta\nu_B \tag{2.11}$$

where $\widetilde{g_B}(\Delta\nu_P)$ is the new Brillouin gain coefficient, g_B is the Brillouin gain coefficient when the pump linewidth is smaller than the Brillouin linewidth, $\Delta\nu_B$ is the Brillouin linewidth and $\Delta\nu_P$ is the pump linewidth. The main difference in evaluating the critical power for these two nonlinear effects, is the effective length. The effective length of the SBS in the pulse regime is half the pulsewidth, as a result of the counterpropagating nature of the pump and signal. Whereas, the effective length in the pulse regime for the forward SRS is governed by the walk-off length. The effective lengths in the pulse regime for both effects are given by [45, 46]

$$L_{SBS} = \frac{W\, v_g}{2} \tag{2.12}$$

$$L_{SRS} = \frac{W}{D\,\Delta\lambda} \tag{2.13}$$

where D is the dispersion parameter and $\Delta\lambda$ is the difference in wavelength between the pump and signal. Typically, D is 17 ps/nm/km for SMF at 1550 nm [47] and $\Delta\lambda$ is 100 nm. The walk-off length is defined as the interaction length between the probe and pump pulse along the fibre. As a result of dispersion, the two pulses will cease to interact at a certain distance along the fibre. These two nonlinear processes provide an upper limit requirement to the maximum launched pulse power. Moreover further analysis indicates that SPM occurs at a lower power level. The critical powers versus different pulsewidths for the three nonlinear effects are analysed and discussed at the end of this section.

SPM is due to the change in the phase of the pulse resulting from the intensity dependence of the refractive index of the optical fibre. It induces spectral broadening of the pulse and is a function of the effective length and the power. Since the separation between the Rayleigh and Brillouin lines are relatively small ∼11 GHz at 1550 nm, spectral broadening of the pulse exceeding this value is undesirable. The critical power for the SPM can be expressed as [8]

$$P_{SPM} = \frac{\phi_{max}}{\gamma\, L_{eff}} \tag{2.14}$$

where

$$\gamma = \frac{2\,\pi\, n_2}{\lambda\, A_{eff}} \tag{2.15}$$

$$L_{eff} = \frac{1 - exp\,(-\alpha_p\, L)}{\alpha_p} \tag{2.16}$$

where ϕ_{max} is the maximum phase shift, L_{eff} is the effective length, α_p is the Rayleigh scattering coefficient, γ is the nonlinear-index coefficient, A_{eff} is the effective area, n_2 is the nonlinear refractive index and λ is the probe wavelength. Taking the values of $n_2 = 2.2{\times}10^{-20}\,\mathrm{m^2/W}$ [48], $A_{eff} = 80\,\mu\mathrm{m}^2$ at 1550 nm and $\lambda = 1550$ nm, result in $\gamma = 1.1\,\mathrm{W^{-1}km^{-1}}$. The broadening factor of the linewidth is proportional to the maximum phase shift, ϕ_{max}. The relationship between the aforementioned parameters, assuming that the pulse is Fourier transform limited, can be expressed as [8]

$$\delta\nu = \frac{0.86\,\phi_{max}}{W} \tag{2.17}$$

where $\delta\nu$ is the broadening factor and W is the pulsewidth of the source. In order to estimate the threshold power for this effect, we defined it as the power which resulted in the spectrum broadened to 1 GHz. Equation 2.17 is substituted in equation 2.14 and the critical power for SPM, P_{SPM}, is evaluated for different values of pulsewidth, W.

The critical powers for the SBS, SRS and SPM evaluated as a function of pulsewidth in the range of 1 ns to 400 ns are illustrated in figure 2.6.

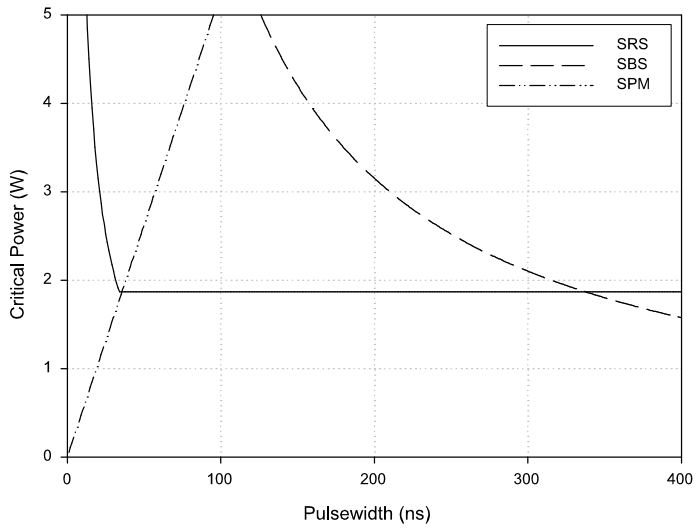

FIGURE 2.6: The plot of the critical power of SBS, SRS and SPM versus pulsewidth for a sensing length of 50 km. The critical power for SBS is indicated by a dashed line, SRS is indicated by a line and SPM is indicated by a dashed double dot line.

For a pulsewidth of less than 35 ns, the nonlinear effects are dominated by SPM as it has a lower threshold compared to SBS and SRS. The threshold power for SPM is calculated to be 50 mW for a pulsewidth of 1 ns and this value increased to 1.9 W at a pulsewidth 35 ns. From a pulsewidth of 35 ns and up to 360 ns, the threshold power is governed by the SRS. The threshold power in this regime is calculated to be 1.9 W. Beyond 360 ns, the threshold power is determined by the SBS effect.

2.5 Summary

This chapter commenced with a description of the process of spontaneous Brillouin scattering. The principle of Brillouin based OTDR and how it can be used for performing distributed measurement of the temperature and strain using conventional SMF was discussed and other sensor architectures utilising Brillouin scattering were reviewed. This included a summary of the recent progress achieved with the different methods and the results obtained with each of the architectures. This chapter concluded with a discussion of the influence of nonlinear effects and coherent Rayleigh noise on the performance of BOTDR.

Bibliography

[1] M.K. Barnoski and S.M. Jensen, "Fiber Waveguides: A Novel Technique for Investigating Attenuation Characteristics," *Applied Optics*, vol. 15, p. 2112, 1976.

[2] A.D. Kersey, "Optical Fiber Sensors for Permanent Downwell Monitoring Applications in the Oil and Gas Industry," *IEICE Transactions Electronics*, vol. E83-C, no. 3, p. 400, March 2000.

[3] M. Al-Asimi, G. Brown and C. Cosad, "Fiber Optic Temperature Monitoring Optimizes Water Injection, Well Production," *WorldOil*, vol. 224, no. 11, p. 39, November 2003.

[4] J. Clowes, J. Edwards, I. Grudinin, E.L.E. Kluth, M.P. Varnham, M.N. Zervas, C.M. Crawley and R.L. Kutlik, "Low Drift Fibre Optic Pressure Sensor for Oil Field Downhole Monitoring," *Electronics Letters*, vol. 35, no. 11, p. 926, 1999.

[5] F.H. Wild and P.Schmetz, "The Applications of Optical Sensors for Temperature, Mechanical Stress and Moisture in Energy Cables in the Netherlands," *14^{th} International Conference on Optical Fiber Sensors Technical Digest (OFS)*, p. 820, 2001.

[6] J.C. Goff and M. Jung, "Thermography of High Voltage Underground Links," *York DTS Seminar*, November 1999.

[7] R.W. Boyd, *Nonlinear Optics*, 2nd ed. Academic Press, 2003.

[8] G.P. Agrawal, *Nonlinear Fiber Optics*, 2nd ed. Academic Press, 1995.

[9] N.P. Bansal and R.H. Doremus, *Handbook of Glass Properties*. Academic Press, 1986.

[10] N. Shibata, Y. Azuma, T. Horiguchi and M. Tateda, "Identification of Longitudinal Acoustic Modes Guided in the Core Region of a Singlemode Optical Fiber by Brillouin Gain Spectra Measurement," *Optics Letters*, vol. 7, no. 13, p. 595, July 1988.

[11] J. Schroeder, R. Mohr, P.B. Macedo and C.J. Montrose, "Rayleigh and Brillouin Scattering in K_2O-SiO_2 Glasses," *Journal of the American Ceramic Society*, vol. 56, no. 10, p. 510, October 1973.

[12] P.C. Wait and T.P. Newson, "Landau Plazcek Ratio Applied to Distributed Fibre Sensing," *Optics Communications*, vol. 122, p. 141, Jun 1996.

[13] K. de Souza, P.C. Wait and T.P. Newson, "Characterisation of Strain Dependence of the Landau-Placzek Ratio for Distributed Sensing," *Electronics Letters*, vol. 33, no. 7, p. 615, 1997.

[14] T.R. Parker, M. Farhadiroushan, V.A. Handerek and A.J. Rogers, "A Fully Distributed Simultaneous Strain and Temperature Sensor Using Spontaneous Brillouin Backscatter," *IEEE Photonics Technology Letters*, vol. 9, no. 7, p. 979, July 1997.

[15] S.M. Maughan, H.H. Kee and T.P. Newson, "Simultaneous Distributed Fibre Temperature and Strain Sensor Using Microwave Coherent Detection of Spontaneous Brillouin Backscatter," *Measurement Science and Technology*, vol. 12, p. 834, February 2001.

[16] J.D.C. Jones, "Review of Fibre Sensor Techniques for Temperature-Strain Discrimination," *12th International Conference on Optical Fiber Sensors Technical Digest (OFS)*, vol. 16, p. 36, 1997.

[17] T. Horiguchi and M. Tateda, "BOTDA Nondestructive Measurement of Singlemode Optical Fiber Attenuation Characteristics using Brillouin Interaction: Theory," *IEEE Journal of Lightwave Technology*, vol. 7, no. 8, p. 1170, August 1989.

[18] X. Bao, D.J. Webb and D.A. Jackson, "32 km Distributed Temperature Sensor Based on Brillouin Loss in an Optical Fiber," *Optics Letters*, vol. 18, no. 18, p. 1561, September 1993.

[19] M. Nikles, L. Thevanez and P.A. Robert, "Simple Distributed Fiber Sensor Based on Brillouin Gain Spectrum Analysis," *Optics Letters*, vol. 21, no. 10, p. 758, May 1996.

[20] A. Fellay, L. Thevenaz, M. Facchini, M. Nikles and P. Robert, "Distributed Sensing Using Stimulated Brillouin Scattering: Towards Ultimate Resolution," *12th International Conference on Optical Fiber Sensors Technical Digest (OFS)*, vol. 16, p. 324, 1997.

[21] K. Hotate and T. Hasegawa, "Measurement of Brillouin Gain Spectrum Distribution Along an Optical Fiber With a High Spatial Resolution Using a Novel Correlation-Based Technique," *13th International Conference on Optical Fiber Sensors Technical Digest (OFS)*, p. 337, 1999.

[22] T. Kurashima, T. Horiguchi and M. Tateda, "Distributed Temperature Sensing Using Stimulated Brillouin Scattering in Optical Silica Fibers," *Optics Letters*, vol. 15, no. 18, p. 1038, September 1990.

[23] X. Bao, D.J. Webb and D.A. Jackson, "22 km Distributed Temperature Sensor Using Brillouin Gain in an Optical Fiber," *Optics Letters*, vol. 18, no. 7, p. 552, April 1993.

[24] X. Bao, J. Dhliwayo, N. Heron, D.J. Webb and D.A. Jackson, "Experimental and Theoretical Studies on a Distributed Temperature Sensor Based on Brillouin Scattering," *IEEE Journal of Lightwave Technology*, vol. 13, no. 7, p. 1340, July 1995.

[25] T. Horiguchi, T. Kurashima and Y. Koyamada, "1 m Spatial Resolution Measurement of Distributed Brillouin Frequency Shift in Single-Mode Fibers," *Proceedings of Optical Fibre Measurement*, p. 73, September 1994.

[26] K. Hotate and M. Tanaka, "Enlargement of Measurement Range of Optical-Fiber Brillouin Distributed Strain Sensor Using Correlation-Based Continuous-Wave Technique," *Conference of Lasers and Electro-Optics Technical Digest (CLEO)*, p. 119, May 2001.

[27] K. Shimizu, T. Horiguchi, Y. Koyamada and T. Kurashima, "Coherent Self-Heterodyne Detection of Spontaneously Brillouin-Scattered Light Waves in a Single-Mode Fiber," *Optics Letters*, vol. 18, no. 3, p. 185, February 1993.

[28] H. Izumita, T. Sato, M. Tateda and Y. Koyamada, "Brillouin OTDR Employing Optical Frequency Shifter Using Side-Band Generation Technique With High-Speed LN Phase Modulator," *IEEE Photonics Technology Letters*, vol. 8, no. 2, p. 1674, December 1996.

[29] T. Kurashima, M. Tateda, K. Shimizu, T. Horiguchi and Y. Koyamada, "A High Performance OTDR for Measuring Distributed Strain and Optical Loss," *European Conference on Optical Communications Technical Digest (ECOC)*, vol. 2, p. 215, 1996.

[30] T. Kurashima, M. Tateda, T. Horiguchi and Y. Koyamada, "Performance Improvement of a Combined OTDR for Distributed Strain and Loss Measurement by Randomizing the Reference Light Polarization State," *IEEE Photonics Technology Letters*, vol. 9, no. 3, p. 360, March 1997.

[31] S.M. Maughan, H.H. Kee and T.P. Newson, "57 km Single-Ended Spontaneous Brillouin-Based Distributed Fiber Temperature Sensor Using Microwave Coherent Detection," *Optics Letters*, vol. 26, no. 6, p. 331, March 2001.

[32] C.C. Lee, P.W. Chiang and S. Chi, "Utilization of a dispersion-shifted fiber for simultaneous measurement of distributed strain and temperature through brillouin frequency shift," *IEEE Photonics Technology Letters*, no. 10, p. 1094, October 2001.

[33] P.C. Wait and T.P. Newson, "Reduction of Coherent Noise in The Landau Placzek Ratio Method For Distributed Fibre Optic Temperature Sensing," *Optics Communications*, vol. 131, p. 285, November 1996.

[34] K.D. Souza, G.P. Lees, P.C. Wait and T.P. Newson, "A Diode-Pumped Landau-Placzek based Distributed Temperature Sensor Utilising an All-Fibre Mach-Zehnder Interferometer," *Electronics Letters*, vol. 32, no. 23, p. 2174, November 1996.

[35] G.P. Lees, P.C. Wait, M.J. Cole and T.P. Newson, "Advances in Optical Fiber Distributed Temperature Sensing Using the Landau-Placzek Ratio," *IEEE Photonics Technology Letters*, vol. 10, no. 1, p. 126, 1998.

[36] H.H. Kee, G.P. Lees and T.P. Newson, "All Fiber System for Simultaneous Interrogation of Distributed Strain and Temperature Sensing by Spontaneous Brillouin Scattering," *Optics Letters*, vol. 25, no. 10, p. 695, May 2000.

[37] H.H. Kee, G.P. Lees and T.P. Newson, "Technique for Measuring Distributed Temperature With 35 cm Spatial Resolution Utilizing the Landau-Placzek Ratio," *IEEE Photonics Technology Letters*, vol. 12, no. 7, p. 873, July 2000.

[38] H.H. Kee and T.P. Newson, "1.5 μm Brillouin-Based Fibre Optical Distributed Temperature Sensor With High Spatial Resolution of 20 cm," *14^{th} International Conference on Optical Fiber Sensors Technical Digest (OFS)*, p. 800, 2000.

[39] K. de Souza and T.P. Newson, "Brillouin-Based Fiber Optic Distributed Temperature Sensor With Optical Preamplification," *Optics Letters*, vol. 25, no. 18, p. 1331, September 2000.

[40] V. Lecoeuche, M.W. Hathaway, D.J. Webb, C.N. Pannell and D.A. Jackson, "20 km Distributed Temperature Sensor Based on Spontaneous Brillouin Scattering," *IEEE Photonics Technology Letters*, vol. 12, no. 10, p. 1367, October 2000.

[41] H. Izumita, T. Horiguchi and T. Kurashima, "Distributed Sensing Techniques Using Brillouin Scattering," *12^{th} International Conference on Optical Fiber Sensors Technical Digest (OFS)*, p. 316, 1997.

[42] K. Shimizu, T. Horiguchi and Y. Koyamada, "Characteristics and Reduction of Coherent Fading Noise in Rayleigh Backscattering Measurement for Optical Fibers and Components," *IEEE Journal of Lightwave Technology*, vol. 10, no. 7, p. 982, July 1992.

[43] Y. Namihira, "Wavelength Dependence of Correction Factor on Effective Area and Mode Field Diameter for Various Singlemode Optical Fibres," *Electronics Letters*, vol. 33, no. 17, p. 1483, August 1997.

[44] D. Mahgerefteh, D.L. Butler, J. Goldhar, B. Rosenberg and G.L. Burge, "Technique for Measurement of the Raman Gain Coefficient in Optical Fibres," *Optics Letters*, vol. 21, no. 24, p. 2026, December 1996.

[45] R.G. Smith, "Optical Power Handling Capacity of Low Loss Optical Fibers as Determined by Stimulated Raman and Brillouin Scattering," *Applied Optics*, vol. 11, no. 11, p. 2489, November 1972.

[46] R.G. Stolen and A.M. Johnson, "The Effect of Pulse Walkoff on Stimulated Raman-Scattering in Fibers," *IEEE Journal of Quantum Electronics*, vol. 22, no. 11, p. 2154, 1986.

[47] L.G. Cohen, W.L. Mammel and S. Lumish, "Dispersion and Bandwidth Spectra in Single-Mode Fibers," *IEEE Journal of Quantum Electronics*, vol. QE-18, no. 1, p. 49, January 1982.

[48] A. Boskovic, S.V. Chernikov, J.R. Taylor, L. Gruner-Nielsen and O.A. Levring, "Direct Continuous-Wave Measurement of n_2 in Various Types of Telecommunication Fiber at 1.55 μm," *Optics Letters*, vol. 21, no. 24, p. 1966, December 1996.

Chapter 3

Optical Amplifiers for Distributed Sensing

3.1 Introduction

The preceding chapter discussed the principles of Brillouin based OTDR and the various factors which can affect the performance of such systems. The transmission range and hence the measurement range of distributed sensors is governed by the loss in the fibre. This effect can be minimised by operating at a low loss wavelength of 1550 nm and by optimising the detection system. Optical amplifiers have been previously used to compensate for transmission losses in long haul optical communication systems and similarly this method can be applied to distributed long range sensors. In this chapter, the different characteristics of various amplifiers and their applications to enhance the performance of distributed sensors are discussed. The optical amplifiers considered are the rare-earth doped amplifiers, such as Erbium doped fibre amplifiers, Brillouin and Raman amplifiers.

3.2 Choice of Optical Amplifiers for Distributed Sensing

3.2.1 Introduction

The characteristics of EDFA, Brillouin and Raman amplifiers and the possible ways that they may be used for improving the performance of the distributed sensors are discussed in this section.

3.2.2 The Erbium Doped Fibre Amplifier

The EDFA provides gain over the wavelength of our interest, ie. 1550 nm, and potentially can provide amplification with low noise. The energy level diagram of the erbium ion in a silica host is illustrated in figure 3.1. The most important transition in the EDFA is the amplifying transition which occurs between the upper level of $^4I_{13/2}$ and the ground state level of $^4I_{15/2}$. The lifetime of the metastable level $^4I_{13/2}$ is 10.8 ms for silica based host material [1]. This relatively long lifetime facilitates achieving the population inversion between the $^4I_{13/2}$ and $^4I_{15/2}$ required for gain. The difference in the energy levels between each excited state levels and the ground state level correspond to the pump wavelengths of 514 nm, 670 nm, 800 nm, 980 nm and 1480 nm. The EDFA is optimally pumped using either 980 nm or 1480 nm as there is little excited state absorption (ESA) at these pump wavelengths [2].

ESA is undesirable as it depletes the population of the metastable level and reduces the efficiency of the pump. The choice between 980 nm or 1480 nm is dependent on the application. For example, in remote pumping applications, the 1480 nm pump wavelength is more appropriate: although it has a lower gain efficiency 6.3 dB/mW [3] compared to 11 dB/mW at 980 nm [4], the propagation loss in SMF is lower for 1480 nm of 0.23 dB/km compared to 1.0 dB/km at 980 nm.

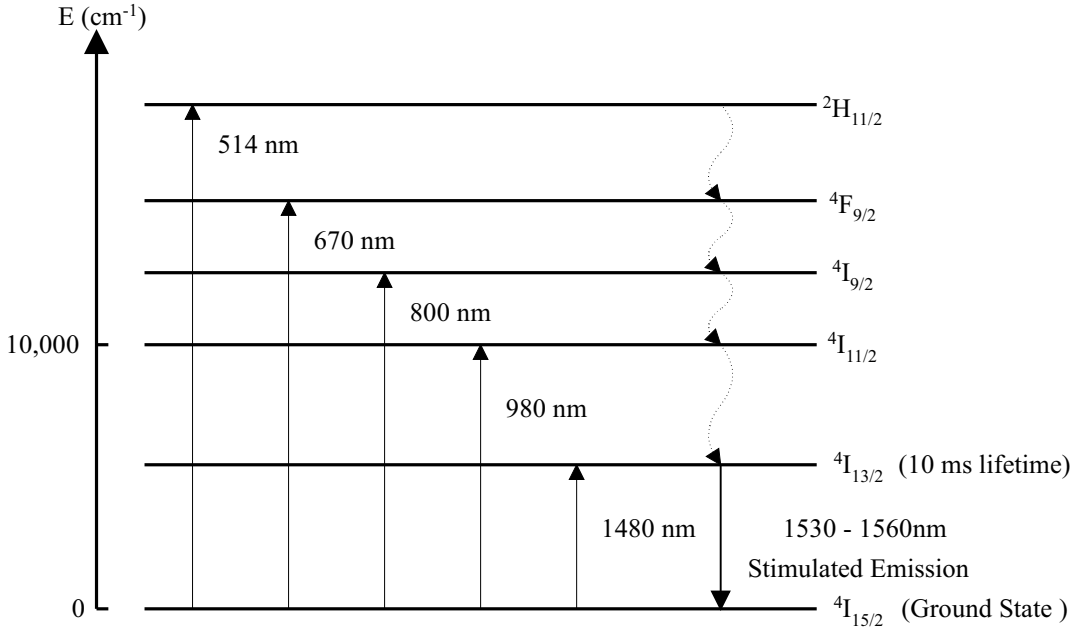

FIGURE 3.1: The energy levels of erbium ions in silica fibres [5]. The dashed line indicates the non-radiative decay.

The EDFA is usually used as a discrete amplifier, ie. the gain occurs over a short length of fibre. Such amplifiers are widely used as inline amplifiers to extend the transmission range of optical communication systems. A transmission length of over 2200 km was demonstrated using 25 EDFA inline amplifiers, located at an interval of 80 km [6]. The EDFA may also be used as a preamplifier to increase the sensitivity of the detector. Such a configuration was used to improve the signal to noise of a Brillouin signal in the Brillouin based OTDR [7].

The EDFA has also been used to amplify both the outgoing pulse and the backscattered signals in an OTDR system [8]; a 10 dB improvement in the OTDR range was reported. The EDFA itself may also be used as a distributed sensing medium by using a long lengths of low doped Erbium fibre with just sufficient gain to achieve transparency ie. the gain equals the fibre loss. Such systems however are likely to be more expensive in comparison to using standard singlemode fibres.

3.2.3 Brillouin Based Optical Amplifiers

In the previous chapter, the spontaneous Brillouin scattering mechanism and how it was used for distributed sensing was described. The Brillouin amplifier, depends on the interactions between the pump, the Stokes wave and the acoustic wave and is described in this section. The interference between the pump and Stokes signal results in the periodic modulation of the refractive index through electrostriction [9]. The pump wave is then scattered to a lower frequency wave at ν_s as a result of the variation in the refractive index and contribute to the growth of the downshifted Stokes wave. A signal counterpropagating with the pump signal and downshifted in frequency by an amount equal to acoustic frequency will experience gain. A diagram indicating the interactions between the three parameters is illustrated in figure 3.2.

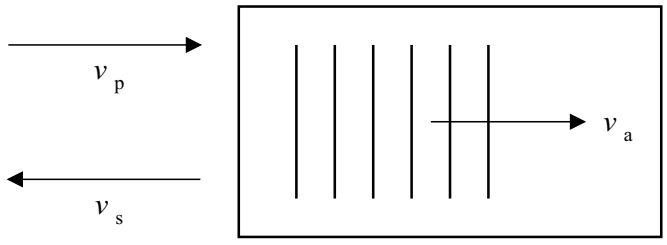

FIGURE 3.2: A diagram indicating the interactions between the pump, Stokes and acoustic wave. Pump frequency is represented by ν_p, Stokes frequency is represented by ν_s and acoustic frequency is represented by ν_a.

SBS exhibits the lowest threshold power compared to the other nonlinear effect such as SRS. This effect is undesirable in optical communication systems as it attenuates the power of the forward propagating pump and provides amplification to the counterpropagating Stokes light. Nevertheless, this effect has been used as a narrowband amplifier to compensate for the propagation loss in the fibre [10]. This is possible as the effective length of this fibre is long and the gain coefficient is relatively high, which allows high gain to be achieved at a relatively low pump power. However, this amplifier may only be used for amplifying signals propagating in the opposite direction to the pump. The expression for the small signal gain at the peak frequency of Brillouin gain is given by [11]

$$G_{SBS} = exp\left(\frac{g_B\, P_{in}\, L_{eff}}{A_{eff}\, K_{SBS}}\right) \tag{3.1}$$

where g_B is the Brillouin gain coefficient, P_{in} is the pump power, K_{SBS} is the polarisation factor and L_{eff} is the effective length. Taking the values of $P_{in} = 1\,\text{mW}$, $g_B = 5{\times}10^{-11}\text{m/W}$ [11], $L_{eff} = 8\,\text{km}$ $A_{eff} = 80\,\mu\text{m}^2$ at 1550 nm [12] and $K_{SBS} = 1.5$ [11] to account the random polarisation, the calculated small signal gain is approximately 14.5 dB.

The Brillouin amplifier has been widely used in double-ended distributed Brillouin based fibre sensors and was reviewed in section 2.3. There is also the possibility that this amplifier may be used to amplify the spontaneous Brillouin backscattered signal and this can be achieved by launching the pump at the front end of the sensing fibre, allowing the system to remain single-ended. The spontaneous noise generated from the pump will affect the performance of the system and generally it is expected that the noise figure for such a Brillouin preamplifier will exceed that of an optimised Erbium-doped fibre amplifier [13].

3.2.4 Raman Based Optical Amplifiers

The Raman amplifier was extensively researched in the 1980s. However, due to the low gain efficiency and high pump power requirements of the Raman amplifier, attention switched to the EDFA. Moreover, as the demand for bandwidth increased and with the recent development of high power lasers, the interest in Raman amplification has been revived.

The operation of the Raman based amplifier is illustrated in figure 3.3. Two photons, representing the pump frequency, ν_p, and downshifted Stokes frequency, ν_s, are incident on a molecule. The pump photon is absorbed and emitted as a downshifted photon following a Stokes transition. This scattered photon adds constructively to the incident photon of frequency ν_s, which is therefore amplified.

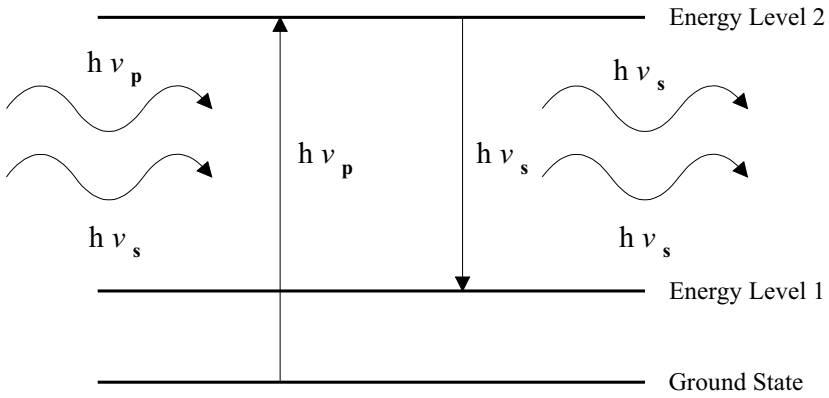

FIGURE 3.3: The energy level diagram of stimulated Raman scattering.

A Raman amplifier may be considered as a distributed amplifier as the gain is distributed over the length of the gain medium. Such distributed gain can be beneficial for distributed sensing systems as it allows the probe signal to be amplified within the sensing fibre and for peak permissible powers to be achieved some distance from the front end of the sensing fibre.

Raman amplification has been used to extend the measurement range in conventional OTDR systems and was first demonstrated by Spirit [14]. An increase in the signal level of 8 dB was obtained in a 100 km dispersion shifted fibre using a combined CW pump power of 160 mW. An alternative method involved using a pulsed Raman pump pulse at 1.53μm to amplify a probe pulse at 1.65μm in a 1.65μm OTDR. A measurement range of up to 100 km in standard singlemode fibre was demonstrated with this technique [15]. Such examples have demonstrated the potential of Raman amplification for extending the range of OTDR measurements. To help to understand its operation a simple model of Raman amplification is described in the next section.

3.2.5 Model for Raman Amplifiers

The intensity profiles of the pump and the Stokes signal are governed by the two coupled equations and can be expressed as [11]

$$\frac{dP_s}{dz} = \frac{g_R}{A_{eff}\,K_{SRS}}\,P_s\,P_p - \alpha_s\,P_s \tag{3.2a}$$

$$\frac{dP_p}{dz} = \frac{-\lambda_s\,g_R}{\lambda_p\,A_{eff}\,K_{SRS}}\,P_s\,P_p - \alpha_p\,P_p \tag{3.2b}$$

where g_R is the Raman gain coefficient, P_s and P_p are the signal and pump power, A_{eff} is the effective area , K_{SRS} is the polarisation factor, α_s and α_p are the scattering coefficients at the signal and pump wavelength to account for the attenuations in the fibre, λ_p and λ_s are the pump and signal wavelength respectively.

The equation 3.2a represents the profile of the signal with distance, the first term on the right hand side indicates the growth of the signal while the second term governs the loss of the signal. The equation 3.2b represents the pump profile with distance, the first term indicates the pump depletion, while the second term describes the pump loss.

These equation may be modified to include multiple pumps and signals interactions and also the evolution of the spontaneous Raman noise [16, 17]. When the pump is significantly bigger than the signal $P_p \gg P_s$ and assuming there is no depletion of pump power, the Raman small signal gain is approximated by the following expression [11]

$$G_{SRS} = exp\left(\frac{g_R\, P_p\, L_{eff}}{A_{eff}\, K_{SRS}}\right) \tag{3.3}$$

or in dBs

$$G_{SRS}(dB) = \frac{4.34\, g_R\, P_p\, L_{eff}}{A_{eff}\, K_{SRS}} \tag{3.4}$$

It can be seen from the equations above that the Raman gain is dependent on several parameters, the launched pump power, polarisation factor, gain coefficient, effective area and length. The gain coefficient is an important parameter as it governs the strength of the coupling between the pump and the signal. The gain coefficient may be obtained by using either direct measurement of the gain in equation 3.3 or from the measurement of the spontaneous Raman cross section. The relationship between the Raman gain coefficient and the scattering cross section is given by [18]

$$g_R(\nu) = \frac{\sigma_0(\nu)\, \lambda^3}{c^2\, h\, n(\nu)^2} \tag{3.5}$$

where λ is the wavelength, h is Planck's constant, c is the speed of light in vacuum, $n(\nu)$ is the refractive index of the glass which is frequency dependent and $\sigma_0(\nu)$ is the Raman cross section at zero Kelvin. The scattering cross section, $\sigma_0(\nu)$, is inversely proportional to λ^4, hence the gain coefficient has an inverse dependence on the pump wavelength [19].

The peak of the gain coefficient was reported to be 1.0×10^{-13} m/W at $1.064\,\mu$m [11] and it may be used to estimate the gain coefficient at other pump wavelengths according to the expression [11]

$$g_R(\lambda_p) = \left(\frac{1.064\,\mu m}{\lambda_p}\right)(1.0 \times 10^{-13}) \tag{3.6}$$

From equation 3.4 and equation 3.6, the Raman gain in dBs is inversely proportional to the pump wavelength. The Raman gain is increased by incorporating dopants such as germanium in the core of a silica fibre, this also reduces the mode field radius and hence the effective area, causing the pump intensity in the core to increase and hence the Raman gain [20]. The addition of germanium increases the Raman gain coefficient, due to its greater scattering efficiency [20]. However, increasing the germanium concentration increases the loss of the fibre and so the length of the fibre has to be optimised. The influence of a number of controllable parameters on the Raman gain is discussed in the next section.

3.2.6 Factors Controlling Raman Gain

The effects of the fibre parameters on the Raman gain are explored in this section. The investigation includes the influence of the pump power, fibre attenuation and the effective area on the Raman gain. The evolution of the pump and signal at different wavelengths is computed.

According to equation 3.4 the Raman gain in dBs is proportional to the pump power and effective length. The effective length equation is given by

$$L_{eff} = \frac{1}{\alpha_p}\left(1 - exp\left(-\alpha_p\, L\right)\right) \tag{3.7}$$

Using the parameters listed in table 3.1, the variation of the Raman gain as a function of distance for increasing pump powers was evaluated and illustrated in figure 3.4.

TABLE 3.1: List of parameters used in the calculation to determine the effect of the pump power on the Raman gain.

Parameters	**Value**
A_{eff}	$75\,\mu\mathrm{m}^2$
g_R	$7.4\times10^{-14}\,\mathrm{m/W}$
α_p	$0.27\,\mathrm{dB/km}$
K_{SRS}	2
L_{fibre}	$200\,\mathrm{km}$
λ_p	$1450\,\mathrm{nm}$

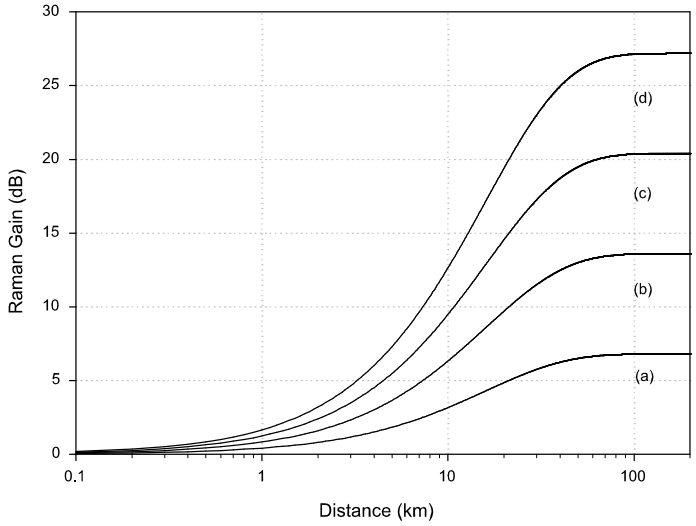

FIGURE 3.4: The Raman gain as a function of distance for different pump powers. The pump power was increased in steps of 200 mW from (a) 200 mW to (d) 800 mW.

The pump power was varied from (a) 200 mW to (d) 800 mW, in steps of 200 mW. It can be seen that the Raman gain increases with increasing pump power. The Raman gain reaches a constant value due to the attenuation of the pump power. The peak Raman gain showed a linear dependence on the pump power ie. 3.4 dB/100 mW.

The gain, G_{SRS} according to equation 3.4, has a linear dependence on the Raman gain coefficient and an inverse dependence on the effective area or the square of the mode field diameter. The effect of reducing the loss coefficient at the pump wavelength increases the effective length and hence will also increase the Raman gain.

Equation 3.2 was used to compute the evolution of the pump and signal powers along the fibre for two different Raman gain coefficients. A loss coefficient of 0.21 dB/km and a launched power of 0.1 W for the probe signal was used for this simulation. Raman gain coefficients of 2×10^{-14} m/W and 8×10^{-14} m/W were chosen to highlight the effect on the evolution of the pump and signal powers along the fibre. The signal and pump profiles with distance for the two gain coefficients are illustrated in figure 3.5(a) and in figure 3.5(b) respectively.

To highlight the effect of pump depletion, the depletion figure in percentage plotted in figure 3.5(b) is normalised with respect to the pump profile obtained due to pump attenuation in the absence of Raman gain. It can be seen that for the signal with the higher gain coefficient, the corresponding signal level at 100 km is approximately 3 dB higher compared to the signal level with a lower gain coefficient. This effect is reflected in the profile of the pump. The pump was depleted by as much as 69 % in the first 10 km for $g_R = 8.0\times10^{-14}$ m/W, in comparison to a value of 16 % for $g_R = 2.0\times10^{-14}$ m/W. This pump depletion effect becomes even more significant as the distance is increased for the trace with a higher gain coefficient value. At 100 km, these values increase to over 99 % and 58% for $g_R = 8.0\times10^{-14}$ m/W and 2.0×10^{-14} m/W respectively.

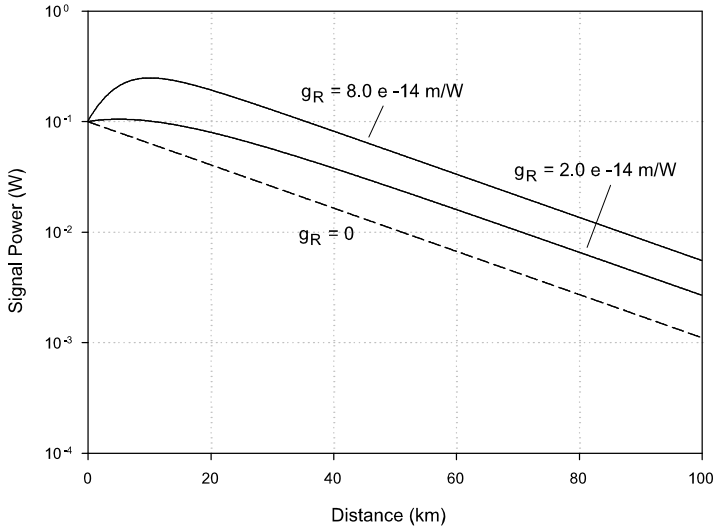

(a)

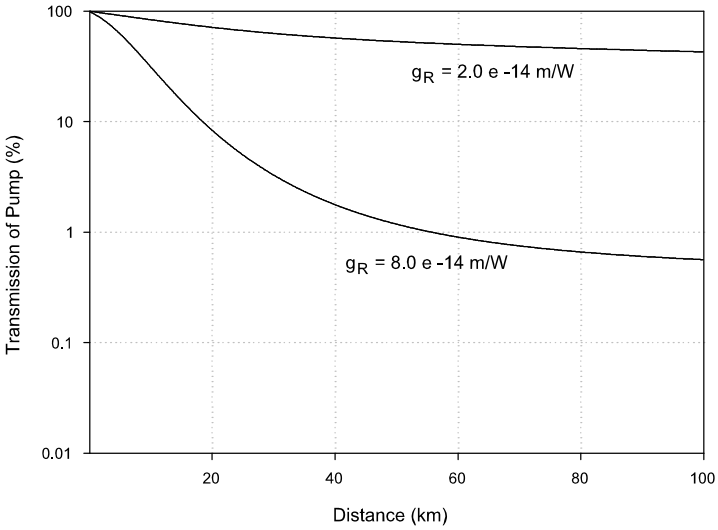

(b)

FIGURE 3.5: The profile of the pump and signal for various Raman gain coefficients: (a)The signal profile as a function of distance for various gain coefficients. (b)The pump profile as a function of distance for various gain coefficients.

3.2.6.1 The Effect of Operating Wavelength

This section describes the effect of the pump and signal wavelength on the Raman gain. The gain coefficient scales inversely with the pump wavelength according to equation 3.6. The relationship between the gain coefficients and the pump wavelengths are shown in table 3.2.

TABLE 3.2: The fibre parameters of conventional SMF for the simulation.

λ_p (μm)	α_p (dB/km)	A_{eff} (μm^2)	g_R ($\times 10^{-14}$ m/W)
1.10	0.82	50.0	9.60
1.30	0.42	65.0	8.20
1.45	0.27	75.0	7.40
1.55	0.21	80.0	6.86

For the other fibre parameters used for the calculation, the values are given in table 3.1. The values of the effective area were obtained from the literature [12] and the gain coefficients were estimated using equation 3.6. The signal wavelength is assumed to be at the peak of the Raman gain curve for each pump wavelength. The traces of Raman gain versus distance for different pump wavelengths are illustrated in figure 3.6. The gain profiles in figure 3.6 corresponded to pump wavelengths of (a) 1.55 μm, (b) 1.45 μm, (c) 1.30 μm and (d) 1.11 μm. Although the gain coefficient at 1.11 μm is higher compared to 1.55 μm, the Raman gain over the full length is higher for the pump at 1.55 μm in comparison to the other wavelengths. This is attributed to the lower fibre attenuation, which results in a longer effective length. For fibre lengths of less than 10 km, a higher Raman gain is obtained for a lower pump wavelength due to the combined effects of the higher gain coefficient and smaller effective area.

This simulation suggest that the best performance is obtained with the pump wavelength at 1.55 μm. However, it is important to appreciate that these gain calculations are ignoring the loss at the signal wavelength. As the signal wavelength is increased to 1.65 μm the loss increases.

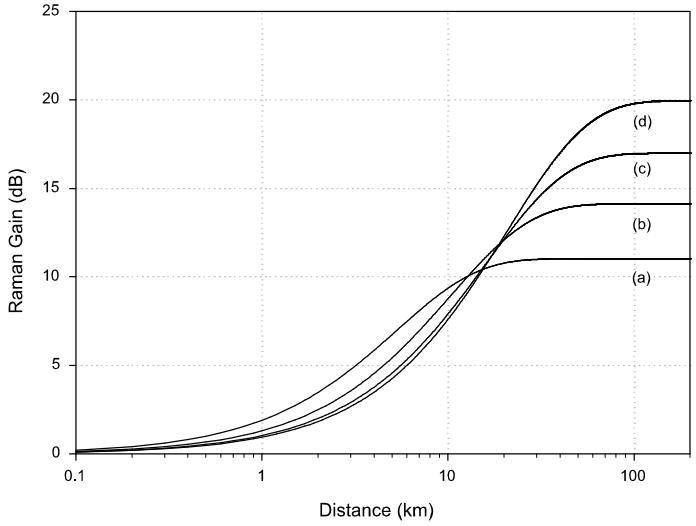

FIGURE 3.6: The Raman gain as a function of distance for four different pump wavelengths. The traces correspond to pump wavelengths of (a) 1.11 μm, (b) 1.30 μm, (c) 1.45 μm and (d) 1.55 μm.

To fully account for this effect, equation 3.2 was used. The loss coefficient for 1.65 μm was assumed to be 0.27 dB/km [21]. The results obtained for the two combinations of pump and signal, at 1.45 μm and 1.55 μm, and, at 1.55 μm and 1.65 μm, respectively are compared and illustrated in figure 3.7, taking into account the signal losses.

The results obtained for the two combinations of pump and signal, at 1.45 μm and 1.55 μm, and, at 1.55 μm and 1.65 μm, respectively are compared and illustrated in figure 3.7, taking into account the signal losses. The pump and signal power at the front end of the fibre for both cases were 0.5 W and 0.1 W respectively. It can be seen that the combination of the pump and signal wavelengths of 1.45 μm and 1.55 μm demonstrated higher gain compared to the other combination. The signal level at 1.55 μm is approximately 18 % higher at 10 km and this value increases to approximately 85% at 50 km, in comparison to the signal level at 1.65 μm. Although the pump at 1.55 μm has a lower fibre loss in comparison to the pump at 1.45 μm, the higher attenuation of the probe signal in conjunction with the smaller gain coefficient obtained at 1.65 μm, resulted in a lower signal level at 100 km compared to 1.55 μm.

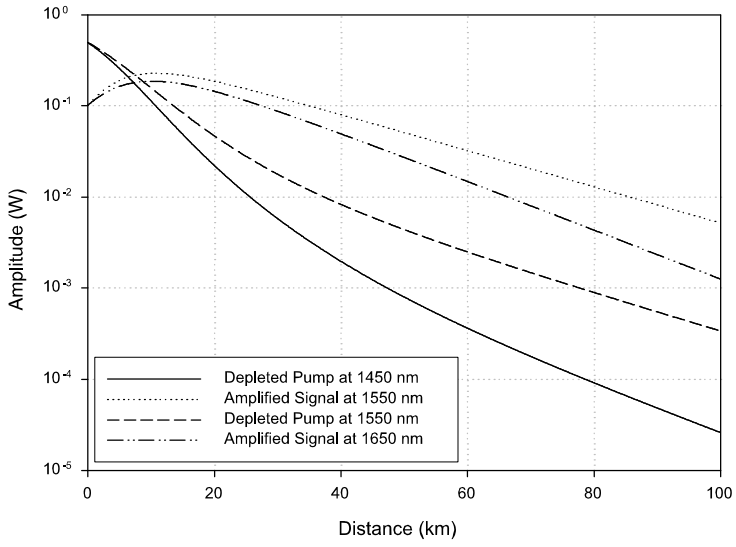

FIGURE 3.7: Raman gain as a function of distance for two different operating pump and signal wavelengths of 1.45/1.55 μm and 1.55/1.65 μm. The profile of the depleted pump at 1.45 μm is represented by a line, the amplified signal at 1.55 μm is represented by a dotted line, the depleted pump at 1.55 μm is represented by a dashed line and the amplified signal at 1.65 μm is represented by a dashed and dotted line.

The signal level profile over a length of 100 km was evaluated using equation 3.6 in order to determine the optimum combinations of pump and signal wavelengths. The parameters varied for this simulation are the attenuation coefficients of the signal and pump wavelengths, gain coefficient and effective area. All the parameters mentioned earlier have dependencies on the operating wavelengths. The values of the attenuation coefficients and effective area at different wavelengths for standard SMF are shown in figure 3.8. These values were estimated from literature [12, 21]. It is important to choose the wavelength of the pump and signal in order to maximise the measurement range of the sensors. Although a pump wavelength at 1.40 μm has a higher gain efficiency compared to 1.45 μm, the higher loss at 1.40 μm corresponding to the tail of the absorption of hydroxyl ions at 1.38 μm for standard SMF, shown in figure 3.8(a), may result in a lower effective length and hence the Raman gain.

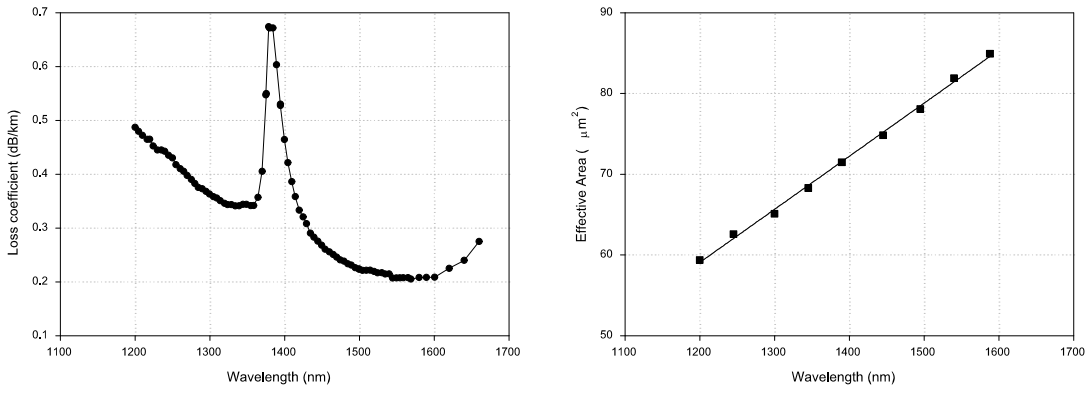

(a) (b)

FIGURE 3.8: The values of the attenuation coefficients and effective area plotted against various wavelengths for standard SMF. (a)The loss coefficients for different wavelength [21]. (b)The effective area for different wavelength [12].

The signal level as a function of distance was evaluated for the wavelengths from 1.50 μm to 1.66 μm at an interval of 10 nm for the cw pump and signal powers of 0.5 W and 0.1 W respectively. The signal wavelength is assumed to be at the peak of the Raman gain curve for each pump and signal wavelength. It can be seen that the amplitude of the signal level at the far end increases as the signal wavelength increases from 1.50 μm up to 1.55 μm. This is primarily due to a higher attenuation of the pump and signal when operated at a lower wavelength, ie. both the pump and signal at 1.41 μm and 1.50 μm have a higher loss compared to 1.45 μm and 1.55 μm. The amplitude of the signal is reduced beyond 1.55 μm as the signal wavelength is increased to 1.66 μm. This is primarily due to an increase in the attenuation of the signal and a small reduction in the gain efficiency and the effective area as the pump wavelength is increased.

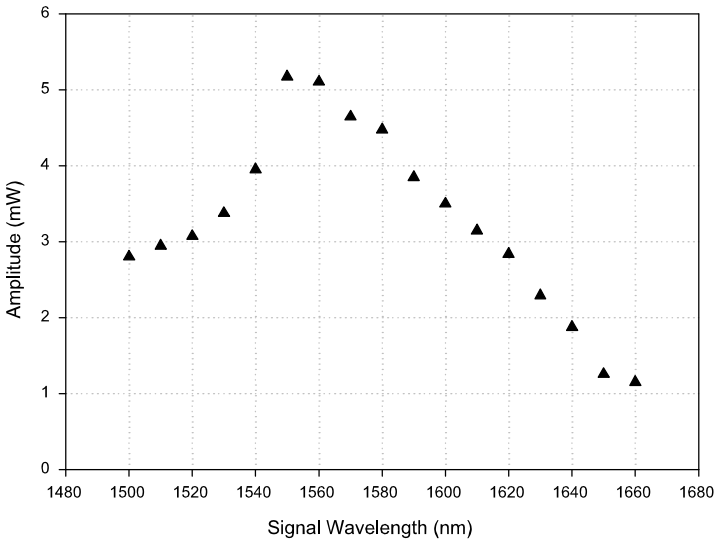

FIGURE 3.9: The amplitude of the signals at 100 km corresponding to different combinations of pump and signal wavelengths.

The simulation suggests that the optimum signal and pump wavelength are located at approximately 1.55 μm and 1.45 μm respectively.

3.3 Summary

The characteristics of the three different optical amplifiers namely the Brillouin, Raman and the EDFA have been reviewed in this section. The influence of the fibre parameters on the Raman gain was simulated and analysed. The choice of the operating pump and signal wavelength is important, as it governs the value of the gain coefficient, effective area, effective fibre length and hence the Raman gain. The other vital variable is the pump power as the Raman gain is primarily governed by this parameter. Although the gain initially increases as the wavelength of operation is increased to around 1.55 μm, this trend is reversed as the signal wavelength approaches 1.65 μm due to increased fibre loss at this wavelength. Further analysis of the different combinations of signal and pump wavelengths obtained in the range of 1.41 μm to 1.66 μm, shows that operating with the Raman pump wavelength of 1.45 μm and signal wavelength of 1.55 μm will achieve near optimal performance.

Bibliography

[1] W.J. Miniscalco, "Erbium-Doped Glasses for Fiber Amplifiers at 1500 nm," *IEEE Journal of Lightwave Technology*, vol. 9, no. 2, p. 234, February 1991.

[2] R.I Laming, S.B. Poole and E.J. Tarbox, "Pump Excited-State Absorption in Erbium-Doped Fibers," *Optics Letters*, vol. 13, no. 12, p. 1084, December 1988.

[3] M. Shimizu, M. Yamada, M. Horiguchi, T. Takeshita and M. Okayasu, "Erbium-Doped Fibre Amplifiers With an Extremely High Gain Coefficient of 11.0 dB/mW," *Electronics Letters*, vol. 26, no. 20, p. 1641, September 1990.

[4] T. Kashiwada, M. Shigematsu, T. Kougo, H. Kanamori and M. Nishimura, "Erbium-Doped Fiber Amplifier Pumped at 1.48 μm with Extremely High Efficiency," *IEEE Photonics Technology Letters*, vol. 3, no. 8, p. 721, August 1991.

[5] E. Desurvire, *Erbium-Doped Fiber Amplifiers: Principles and Applications*. Wiley InterScience, 2002.

[6] S. Saito, T. Imai and T. Ito, "An Over 2200 km Coherent Transmission Experiment at 2.5 GB/s using Erbium-Doped Fiber In-Line Amplifiers," *IEEE Journal of Lightwave Technology*, vol. 9, no. 2, p. 161, February 1991.

[7] K. de Souza and T.P. Newson, "Brillouin-Based Fiber-Optic Distributed Temperature Sensor with Optical Preamplification," *Optics Letters*, vol. 25, no. 18, p. 1331, September 2000.

[8] L.C. Blank and D.M. Spirit, "OTDR Performance Enhancement Through Erbium Fibre Amplification," *Electronics Letters*, vol. 25, no. 25, p. 1693, December 1989.

[9] R.W. Boyd, *Nonlinear Optics*, 2nd ed. Academic Press, 2003.

[10] N.A. Olsson and J.P. Van Der Ziel, "Cancellation of Fiber Loss by Semiconductor Laser Pumped Brillouin Amplification at 1.5 μm," *Applied Physics Letters*, vol. 48, no. 20, p. 1329, May 1986.

[11] G.P. Agrawal, *Nonlinear Fiber Optics*, 2nd ed. Academic Press, 1995.

[12] Y. Namihira, "Wavelength Dependence of Correction Factor on Effective Area and Mode Field Diameter for Various Singlemode Optical Fibres," *Electronics Letters*, vol. 33, no. 17, p. 1483, August 1997.

[13] N.A. Olsson and J.P. Van Der Ziel, "Characteristics of a Semiconductor Laser Pumped Brillouin Amplifier with Electronically Controlled Bandwidth," *IEEE Journal of Lightwave Technology*, vol. LT-5, no. 1, p. 147, January 1987.

[14] D.M. Spirit and L.C. Blank, "Raman Assisted Long Distance Optical Time Domain Reflectometry," *Electronics Letters*, vol. 25, no. 25, p. 1687, December 1989.

[15] H.H. Kee, G.P. Lees and T.P. Newson, "Extended Range Optical Time Domain Reflectometry System at 1.65 μm Based on Delayed Raman Amplification," *Optics Letters*, vol. 23, no. 5, p. 349, March 1998.

[16] Y. Emori and S.Namiki, "Broadband Raman Amplifier for WDM," *IEICE Transactions of Electronics*, vol. E84-C, no. 5, p. 593, May 2001.

[17] H. Kidorf, K. Rottwitt, M. Nissov, M. Ma and E. Rabarijaona, "Pump Interactions in a 100 nm Bandwidth Raman Amplifier," *IEEE Photonics Technology Letters*, vol. 11, no. 5, p. 530, May 1999.

[18] R.H. Stolen and E.P. Ippen, "Raman Gain in Glass Optical Waveguides," *Applied Physics Letters*, vol. 22, no. 6, p. 276, March 1973.

[19] K.J. Cordina, C.R.S. Fludger, "Changes In Raman Gain Coefficient With Pump Wavelength in Modern Transmission Fibres," *Optical Amplifiers and Applications*, pp. OMC3–1, 2002.

[20] F.L. Galeener, J.C. Mikkelsen, Jr., R.H. Geils and W.J. Mosby, "The Relative Raman Cross Sections of Vitreous SiO_2, GeO_2, B_2O_3 and P_2O_5," *Applied Physics Letters*, vol. 32, no. 1, January 1978.

[21] N.R. Haigh and T.C.E. Jones, "The Development of an Optical Fibre Attenuation Standard," *Technical Digest Symposium on Optical Fiber Measurements*, p. 77, 1994.

Chapter 4

Raman Amplification in Single-Ended Distributed Sensors

4.1 Introduction

This chapter investigates the use of Raman amplification for enhancing the signal to noise of spontaneous Brillouin intensity measurements. Raman amplification compensates for the attenuation in the probe pulse in the sensing fibre and hence extends the measurement range. The use of Raman amplification in Rayleigh based OTDR measurement at 1585 nm was initially demonstrated by Spirit [1]. A Raman gain of 8 dB translated to a similar increase in the measurement range using a 100 km dispersion shifted fibre with a Raman pump power of 160 mW operating at 1480 nm. This technique had not previously been applied to Brillouin based OTDR.

4.2 Raman Gain Coefficient

The Raman gain coefficient is an important design parameter of the Raman amplifier. The small signal Raman gain can be measured using a CW pump and a CW counter-propagating probe in the fibre. The counter-propagating configuration minimises the fluctuations in the power levels of the amplified probe arising from the fluctuations in the polarisations of both the pump and probe lights [2]. The Raman gain spectrum can be obtained by tuning the wavelength of the probe and measuring its amplified output using an OSA. The Raman gain coefficient $g_R(\lambda)$ may be expressed as

$$g_R(\lambda) = \frac{0.23\, G(L,\lambda)\, A_{eff}(\lambda)\, K_{SRS}}{P_p\, L_{eff}(\lambda)} \tag{4.1}$$

where $G(L,\lambda)$ is the integrated Raman gain in dBs, $A_{eff}(\lambda)$ is the effective area, K_{SRS} is the polarisation factor, P_p is the input pump power and $L_{eff}(\lambda)$ is the effective length [3]. The expression for $g_R(\lambda)$ is based on the assumption that the probe signal is very much smaller than the pump and that there is no significant pump depletion. The advantage with this measurement technique is that the experimental setup is fairly simple and the Raman ASE noise does not interfere with the gain measurement. This technique requires determination of the fibre attenuation and the effective area. The probe power has to be sufficiently small to avoid depleting the pump power. An alternative technique of measuring the Raman gain is by using the OTDR technique. This method measures the Raman amplified backscattered Rayleigh signal. The ratio between the Raman amplified Rayleigh signal to the unamplified Rayleigh signal provides a measurement of Raman gain. The Raman gain spectrum may be mapped by using a tunable source and a tunable band pass filter to track the Rayleigh backscattered signal at the specified probe wavelength [4]. A band pass filter is used to prevent the Raman ASE from saturating the detector.

To minimise the effects of coherent Rayleigh noise on the Raman gain measurement, the probe signal is either scanned over 10's of GHz or a source with sufficiently broadband is used. The advantage with this technique is that the Raman gain profile may be resolved spatially for long lengths of cascaded fibres with different Raman gain characteristics. However, due to lack of a suitable tunable band pass filter to track the Rayleigh signal, the Raman gain coefficient was measured using the direct measurement of its small signal Raman gain.

4.2.1 Experimental Details

The experimental setup for measuring the small signal Raman gain, is illustrated in figure 4.1. The CW probe consisted of a tunable source which operated over the range of 1480 to 1560 nm. The pump consisted of a Raman fibre laser which had an optical bandwidth of 1.5 nm at 1450 nm. The launched CW pump power at 1450 nm was approximately 400 mW, well below the calculated SBS threshold of 22.2 W for a fibre length of 20 km. A 1450/1550 nm WDM coupler was used for coupling the pump into the test fibre and also for extracting the amplified probe for detection.

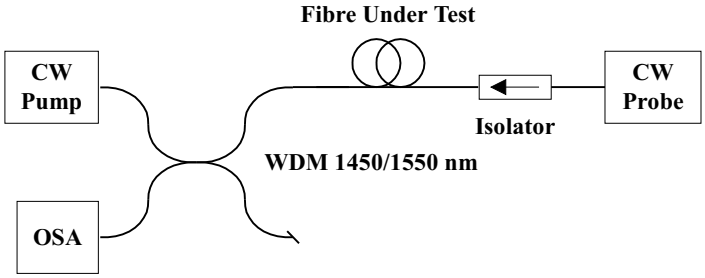

FIGURE 4.1: The experimental setup for measuring the Raman gain.

The procedure for obtaining the Raman gain firstly involves measuring the CW Raman amplified probe signal with the Raman pump and the CW unamplified probe signal without the Raman pump at the far end of the fibre using an OSA. The ratio between the signals obtained under the two different pump conditions provides the Raman gain. The Raman gain from 1480 to 1560 nm was obtained by tuning the probe source. Using the known value of the launched Raman pump power, the effective area and effective length of the fibre, the gain coefficient was evaluated using equation 4.1.

4.2.2 Experimental Results and Discussions

The measurement of the Raman gain coefficients in a standard singlemode fibre, SMF is shown in figure 4.2. It can be seen from figure 4.2 that the peak of the Raman gain coefficient for SMF is located at 1550 nm, for a pump wavelength of 1450 nm. The gain coefficient, g_R, is increased from 2.9×10^{-14} at 1500 nm to 7.0×10^{-14} m/W at 1550 nm corresponding to the peak of the spectrum. The gain coefficient is decreased from 6.9×10^{-14} m/W at 1560 nm to 3.0×10^{-14} at 1570 nm.

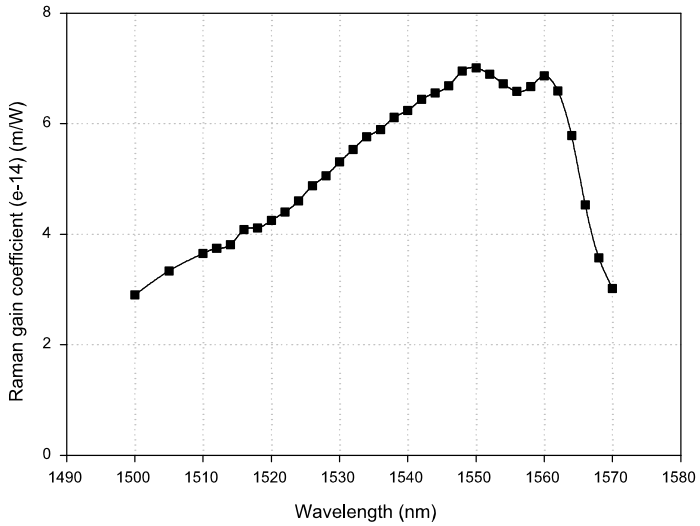

FIGURE 4.2: The plot of Raman gain coefficients for the SMF for pump wavelength of 1450 nm.

Alternatively, the gain coefficient of 7.0×10^{-14} m/W at 1550 nm may be expressed in the form of $0.93\,\mathrm{km^{-1}W^{-1}}$ when normalised by dividing by effective area. This value is in close agreement with the reported value of $1.1\,\mathrm{km^{-1}W^{-1}}$ [5] measured using a similar pump wavelength. This experimental result shows that to obtain the highest Raman gain, the probe wavelength has to be operated close to 1550 nm for the pump at 1450 nm. However, due to the availability of other optical components such as filters and sources at 1533 nm, experiments were conducted at this wavelength.

The errors of the individual parameters for calculating the gain coefficient at 1533 nm are summarised in table 4.1. The estimated gain coefficient at 1533 nm is approximately 5.8×10^{-14} m/W $\pm$ 24 % assuming that the polarisation for the probe and pump light is randomised. For applications in distributed sensors, long lengths of fibres are generally used and the polarisations of the pump and probe lights may be assumed to be scrambled due to random birefringence of the fibre [2].

TABLE 4.1: The estimated errors in the parameters for determining the gain coefficient when K_{SRS}=2 for the pump and signal wavelength of 1450 and 1533 nm respectively.

Parameters	**Value**	**Uncertainty**
Pump Power (mW)	400.0	$\pm$ 8 %
Effective Length (km)	10.8	$\pm$ 5 %
Effective Area (μm^2)	75.0	$\pm$ 8 %
Gain (dB)	7.2	$\pm$ 3 %
Gain Coefficient ($\times 10^{-14}$) (m/W)	5.8	$\pm$ 24 %

4.2.3 Summary

The gain coefficient was deduced based on the Raman gain measurement. This value is used to estimate the Raman gain and the signal to noise improvement in subsequent experiments. The profile of the backscattered signals with CW Raman amplification is calculated in the following section using this measured gain coefficient.

4.3 Simulation of Brillouin based OTDR with CW Raman Amplification

The profile of the Brillouin backscattered signal is evaluated for the condition that the CW Raman pump co-propagates with the probe pulse. The probe pulse is amplified as it co-propagates with the CW Raman pump, resulting in an increase in the backscattered signal. The backscattered signal is then amplified by the counter-propagating CW Raman pump. The intensity profile of the Brillouin backscattered signal as a function of distance with CW Raman amplification can be expressed as

$$P_B(z) = \frac{1}{2} P_{in} W \alpha_B S v_g exp(-2 \alpha_R z) G_r(z) \tag{4.2}$$

where P_{in} is the launched probe power, W is the probe pulsewidth, S is the backscattered factor, α_B and α_R are the Brillouin and Rayleigh scattering coefficients and $G_r(z)$ is the Raman gain. This equation has a similar form to the conventional OTDR equation and an extra term of $G_r(z)$ was included to take into account the Raman gain. The Raman gain experienced by both the probe pulse and its backscattered signal as a function of distance can be represented by

$$G_r(z) = exp\left(\frac{2 g_R P_p L_{eff}}{A_{eff} K_{SRS}}\right) \tag{4.3}$$

where g_R is the Raman gain coefficient, P_p is the CW Raman pump, L_{eff} is the effective length at the Raman pump wavelength, A_{eff} is the effective area and K_{SRS} is the polarisation factor. In equation 4.3, the factor of 2 represents the forward gain of the probe pulse and the backward gain of the backscattered signal. This expression for the Raman gain, $G_r(z)$, is based on the assumption that there is no significant depletion of pump by the signal.

In figure 4.3 the profile of the backscattered signal for a 100 km of standard singlemode fibre is shown, with various pump powers launched from the front end, calculated using equation 4.2. In the forward co-propagating pump configuration, it is anticipated that the maximum Raman gain will be obtained in the first 50 km as the pump power will be highest at the front end of the fibre, and this observation is evident from figure 4.3. It can also be seen that the backscattered signal is increased with a higher launched Raman pump power. With a Raman pump of 100 mW, the increase in signal level at 100 km is approximately 5.3 dB. As the pump power is increased to 500 mW, the calculated increase in the signal level is approximately 27.0 dB.

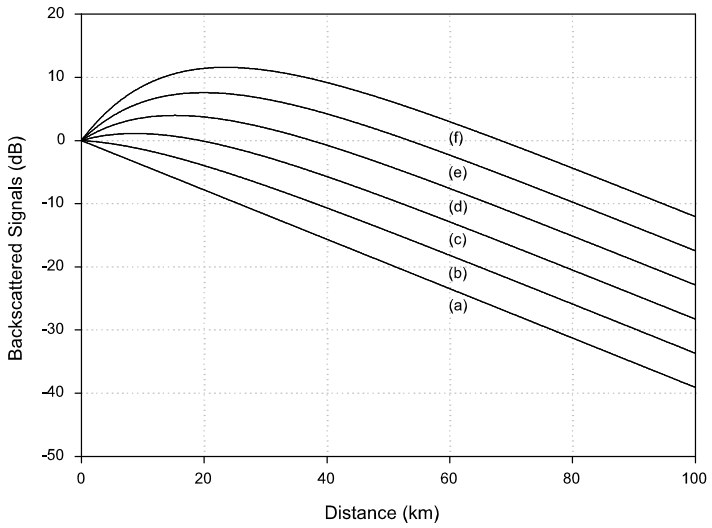

FIGURE 4.3: The profile of backscattered signal for 100 km of standard singlemode fibre with various pump powers launched from the front end. Traces of (a) to (f) indicate launched pump powers of 0 mW to 500 mW, in steps of 100 mW.

4.4 CW Raman Amplification

To investigate a distributed fibre sensor using CW Raman amplification, three key components are required, Raman pump, a narrow linewidth probe pulse laser and an efficient optical filter. A Raman fibre laser at 1450 nm was used as the Raman pump and its operation is described in the next section. A high peak power narrow linewidth probe pulse can be generated using a Q-switched erbium doped fibre laser, in which the operating wavelength and the optical bandwidth of such a fibre laser is primarily governed by the fibre Bragg grating located at the end of the laser cavity. Further details of this laser are described in section 4.4.2. The optical filter used for separating the Brillouin signal from the Rayleigh signal consisted of a low loss double pass Mach-Zehnder interferometer (DPMZ). The operation of the DPMZ is discussed in section 4.4.3.

4.4.1 Raman Fibre Laser at 1450 nm

A Raman fibre laser at 1450 nm was used to provide Raman amplification of signals from 1500 to 1570 nm. This fibre laser was purchased from IPG Photonics. The operation of a CW Raman fibre laser at 1450 nm is now possible with development of the cladding pumped fibre lasers. This method provides an elegant way of converting a high power multimode semiconductor pump light into a single transverse mode output laser source [6]. The cladding pumping technique uses a high power multimode source to pump an optical fibre which consist of a singlemode doped core, surrounded by a lower index of undoped glass forming the inner cladding of the fibre. This layer is then encased with another lower index glass cladding to guide light in the inner cladding. This fibre geometry results in a high acceptance angle and enables the multimode pump light to be coupled more efficiently. The coupled pump light excites the rare earth doped ions in the core as it propagates through the core.

A ytterbium doped fibre laser is generally used as it has an emission band from 1000 to 1200 nm and a high conversion efficiency of 80 %. Such a CW fibre laser is used to pump the cascaded Raman resonators for CW output at 1450 nm [7]. The schematic showing the principle of the Raman fibre laser is illustrated in figure 4.4.

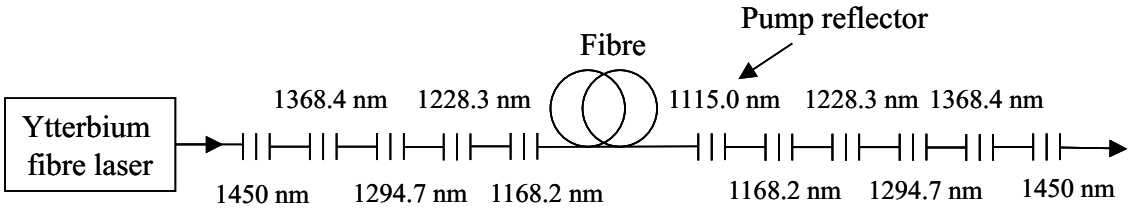

FIGURE 4.4: The schematic of the Raman fibre laser.

The cascaded Raman resonators consist of several hundred metres of fibre in between nested pairs of highly reflective fibre Bragg gratings (FBGs). The identical pairs of FBGs with a reflectivity in excess of 99 % are used to provide feedback for the Stokes light into the cavity. This configuration is essential in order to reduce the threshold for each Raman Stokes transition and to pump the next Raman Stokes light. The frequency shift in the Raman Stokes light is dependent on the dopants used in the core of the silica fibres, ie. for germanium oxide the shift is 13.2 THz. The number of FBGs used is dependent on the desired output wavelength, eg. 5 pairs of FBGs corresponding to 5 Raman Stokes transitions and a single FBG at the pump wavelength of the ytterbium fibre laser to produce an ouput at 1450 nm.

The spectrum of the Stokes lines is illustrated in figure 4.5.

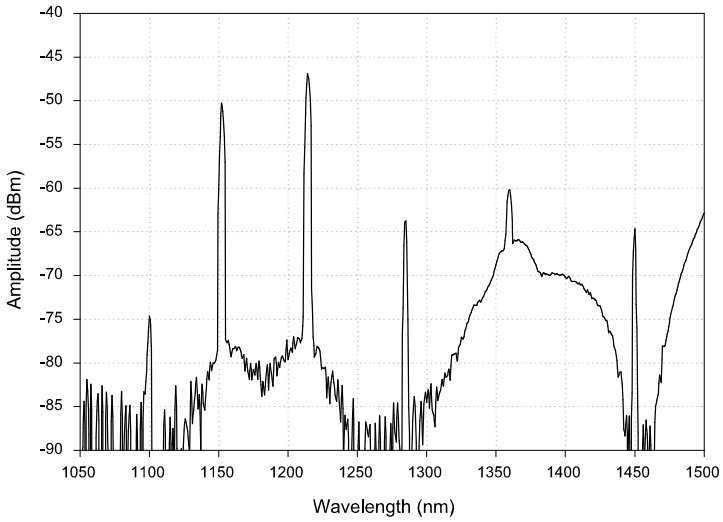

FIGURE 4.5: Spectrum of the Raman fibre laser measured using an OSA.

A CW output power in excess of 1 W has been generated with such a technique.

4.4.2 Q-Switched Erbium Doped Fibre Laser

Q-switched Erbium doped fibre lasers have been used as pulsed sources for Brillouin based OTDR as high peak powers and high repetition rates operating in the range of 1500 to 1560 nm combined with narrow linewidth operation can be obtained using very few optical components. Peak pulse powers of the order of several hundreds of Watts with a pulsewidth of 10 to 20 ns and a repetition rate in excess of 1 kHz have been demonstrated [8, 9, 10]. Such a fibre laser was successfully used as a pulsed source for a 130 km range OTDR system with a spatial resolution of 100 m in 1984 [11] and also in a 16 km range distributed temperature sensor with a spatial resolution of 3 m [12].

The Q-switched fibre laser used in these experiments consists of a pair of mirrors ie. a fibre Bragg grating at one end and a broadband bulk mirror connected at the other end of the cavity, a gain medium, ie. erbium doped fibre and a modulator, ie. an acousto-optic modulator (AOM), within the cavity, see figure 4.6. A fibre based reflector is used since it can be spliced to an erbium doped fibre with relatively low loss. A high loss is induced in the cavity when the AOM is in a low transmission state. The high loss prevents lasing and the gain in the EDFA increases due to optical pumping from a 980 nm laser diode. When the loss in the cavity is reduced by switching the AOM to a high transmission state, the spontaneous emission oscillates in the cavity and is rapidly amplified. A train of pulses can be obtained by periodic modulation of the loss in the cavity.

The experimental arrangement is shown in figure 4.6. The EDFA with an erbium concentration of 900 ppm in the core was pumped by a 980 nm laser diode with an output power of 100 mW. The wavelength of the fibre laser was operated at 1533 nm close to the peak of the EDFA and the centre wavelength of the FBG was centred at a similar wavelength. The optical bandwidth of the FBG was 16 pm (2 GHz) and it governs the linewidth of the fibre laser. This value was chosen such that the Rayleigh and Brillouin signal may be separated optically.

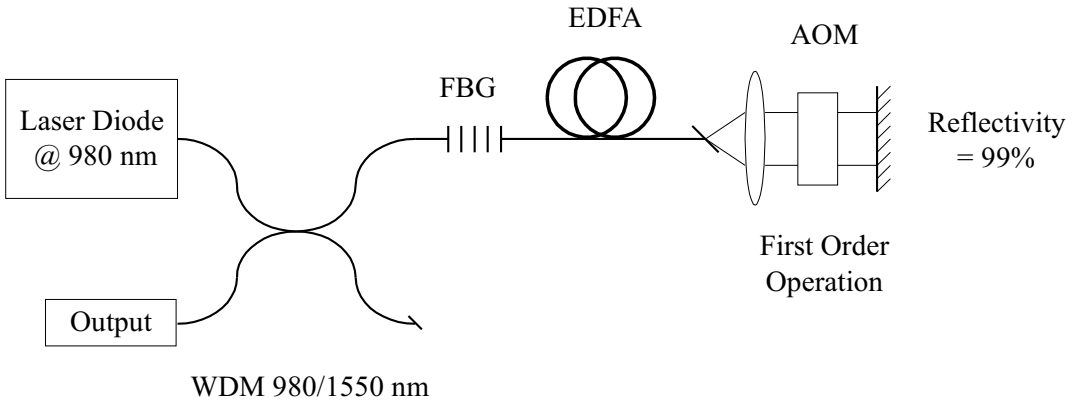

FIGURE 4.6: The schematic for a Q-switched fibre laser.

A peak pulse power of 10.0 W and a pulsewidth of 60 ns could be generated using this configuration. The pulse profile in the time domain was monitored using a fast InGaAs photodiode, with an electrical bandwidth of 400 MHz, connected to an oscilloscope, with an electrical bandwidth 200 MHz, figure 4.7.

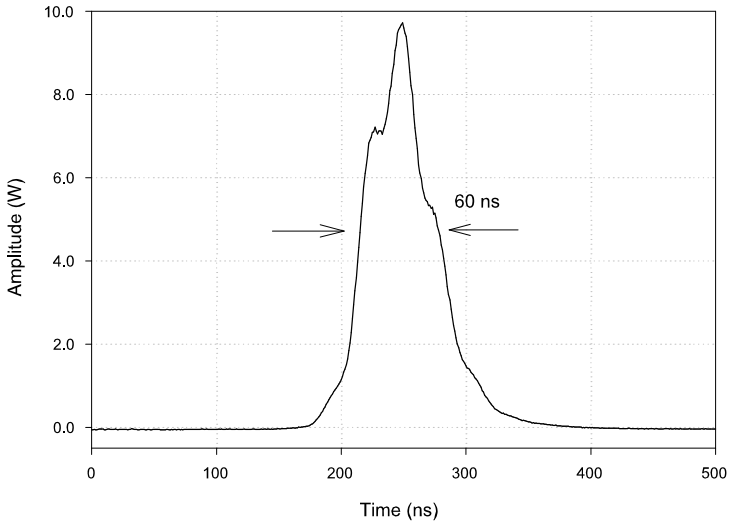

FIGURE 4.7: The temporal and spectral characteristics of the Q-switched fibre laser.

The pulse peak power and the pulsewidth of the Q-switched fibre laser as a function of repetition rate is illustrated in figure 4.8.

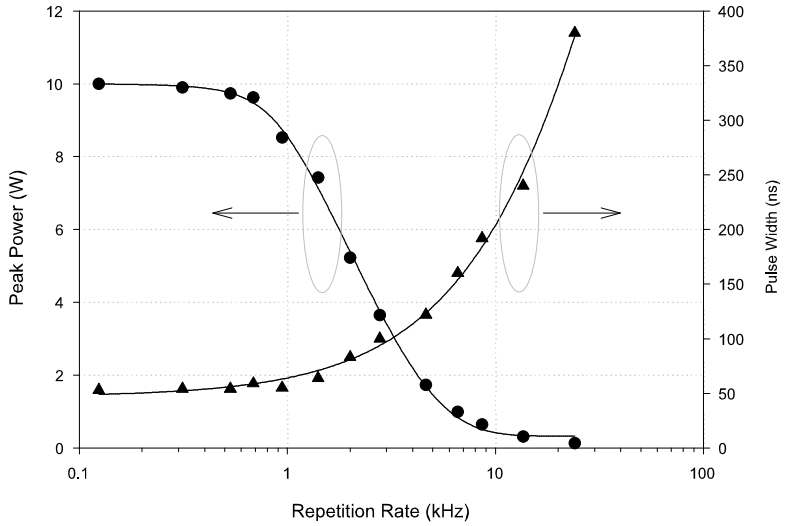

FIGURE 4.8: The pulse peak power (indicated by circles) and pulsewidth (indicated by triangles) of the Q-switched fibre laser with various repetition rate.

At low repetition rate of 0.1 kHz, the pulse peak power and the pulsewidth were measured to be 10.0 W and 50 ns respectively.

When the repetition rate was increased to 1.0 kHz, the pulse peak power was reduced to 8.5 W and the pulsewidth was increased to 55 ns. When the repetition rates was increased beyond 1.0 kHz, the peak power was reduced while the pulsewidth was increased rapidly. This was because at higher repetition rate, the pump did not have sufficient time to replenish the EDFA gain, leading to a reduced pulse peak power. The reduced EDFA gain also caused the ASE light to make more passes through it, leading to an increased in the width of the probe pulse.

The optical bandwidth of the narrowband pulsed fibre laser was measured to be 2.2 GHz using a scanning Fabry Perot. The Fabry Perot interferometer was set to a free spectral range of 11 GHz and had a minimum resolvable bandwidth of 0.5 GHz.

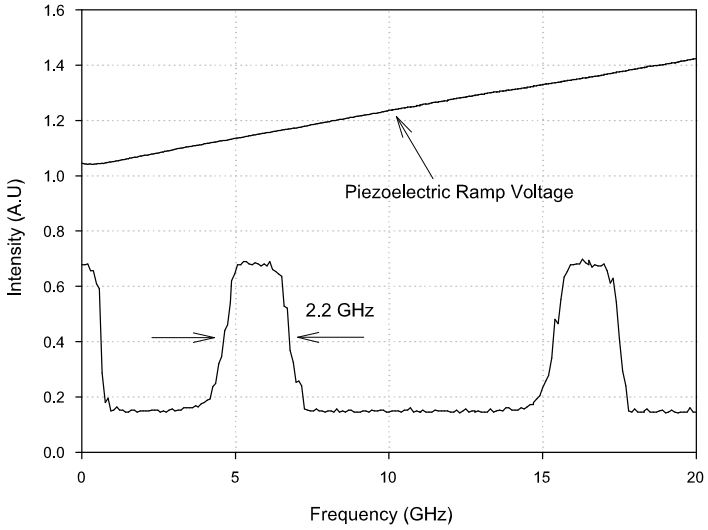

FIGURE 4.9: The spectrum of the Q-switched fibre laser.

4.4.3 Double Pass Mach-Zehnder Interferometer

A bulk Fabry Perot interferometer was used by Wait et al. to optically filter the Brillouin from the Rayleigh signal [13]. However, the loss of such an interferometer of 10 dB limited the measurement range of the sensor. An all fibre Mach-Zehnder interferometer with an insertion loss of 3 dB was developed to overcome this problem [14]. A single pass Mach Zehnder interferometer can be constructed using two 3 dB optical fibre couplers. A path imbalance of 9.1 mm is introduced in one of the arms of the couplers, resulting in a free spectral range (FSR) of 21.9 GHz at 1533 nm. This value matches the separation between the Brillouin Stokes and anti-Stokes light. A double pass Mach-Zehnder (DPMZ) is realised by the addition of an optical isolator and was measured to increase the rejection of the Rayleigh signal and is illustrated in figure 4.10. The transfer function of the DPMZ interferometer can be expressed as [14]

$$M(\nu) = \left[\frac{1}{2}\left[1+\cos\left(\frac{2\,\pi\,\nu}{FSR}\right)\right]\right]^2 \tag{4.4}$$

where

$$FSR = \frac{v}{\Delta\, L} \tag{4.5}$$

where ν is the frequency, v is the speed of light in the fibre and $\Delta\, L$ is the path difference between the two arms. The DPMZ is tuned by heating one of its arms. To separate the Brillouin from the Rayleigh signals, DPMZ is tuned such that the Brillouin signal is coupled into the input port of the optical isolator, resulting in the Brillouin signal being transmitted, whilst the Rayleigh signal is coupled into the output of the optical isolator and is therefore attenuated.

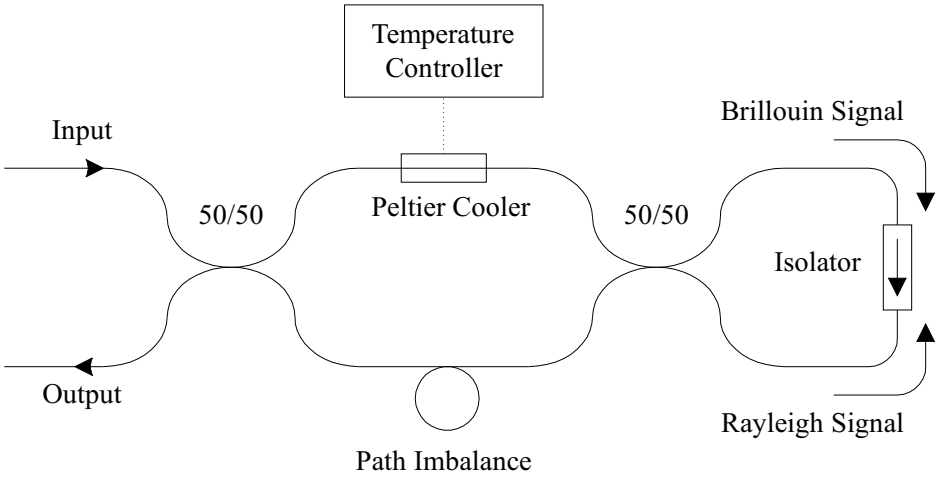

FIGURE 4.10: A diagram of the all fibre double pass Mach-Zehnder interferometer.

Figure 4.11 shows the transfer function of the DPMZ, measured using a tunable laser source with a linewidth of 2 MHz. The measured FSR is 0.17 nm corresponding to 21.7 GHz at 1533 nm, while the optical bandwidth (FWHM) was measured to be approximately 68 pm.

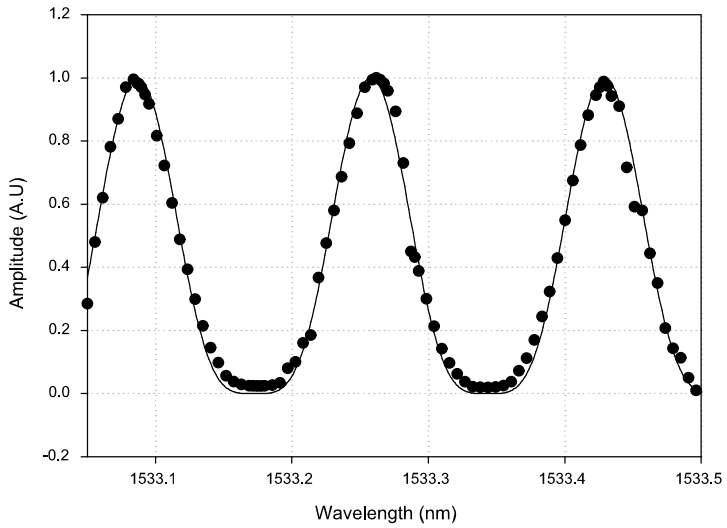

FIGURE 4.11: The spectrum of the double pass Mach-Zehnder optical filter.

The suppression of Rayleigh signal using a DPMZ was measured to be 20 dB for a source with a linewidth of 2 GHz. To achieve greater suppression, a FBG was used in conjunction with the DPMZ and yielded attenuation in excess of 30 dB of the Rayleigh signal.

4.5 Distributed Sensors with CW Raman Amplification

The initial experimental investigation of using CW Raman amplification to enhance the measurement range of a single-ended distributed Brillouin based temperature sensor is described in this section.

4.5.1 Experimental Details

The experimental configuration is illustrated in figure 4.12. A narrowband Q-switched laser was used to generate the Brillouin backscattered signal. Pulses with a power of approximately 200 mW and pulsewidth of 60 ns were launched into the sensing fibre. The CW Raman pump at 1450 nm, with a linewidth of 1.5 nm, was passed through a 1450/1550 nm WDM coupler together with the signal pulse at 1533 nm. The output power of the pump was varied from 0 to 200 mW.

The sensing fibre consisted of six spools of fibres and of lengths of 19 km, 5 km, 2.8 km, 4 km, 0.2 km and 3.8 km respectively. The third and fifth spools of fibres were placed in the oven and heated to approximately 80 ^{o}C. The other spools of fibres were kept at a room temperature of 22 ^{o}C.

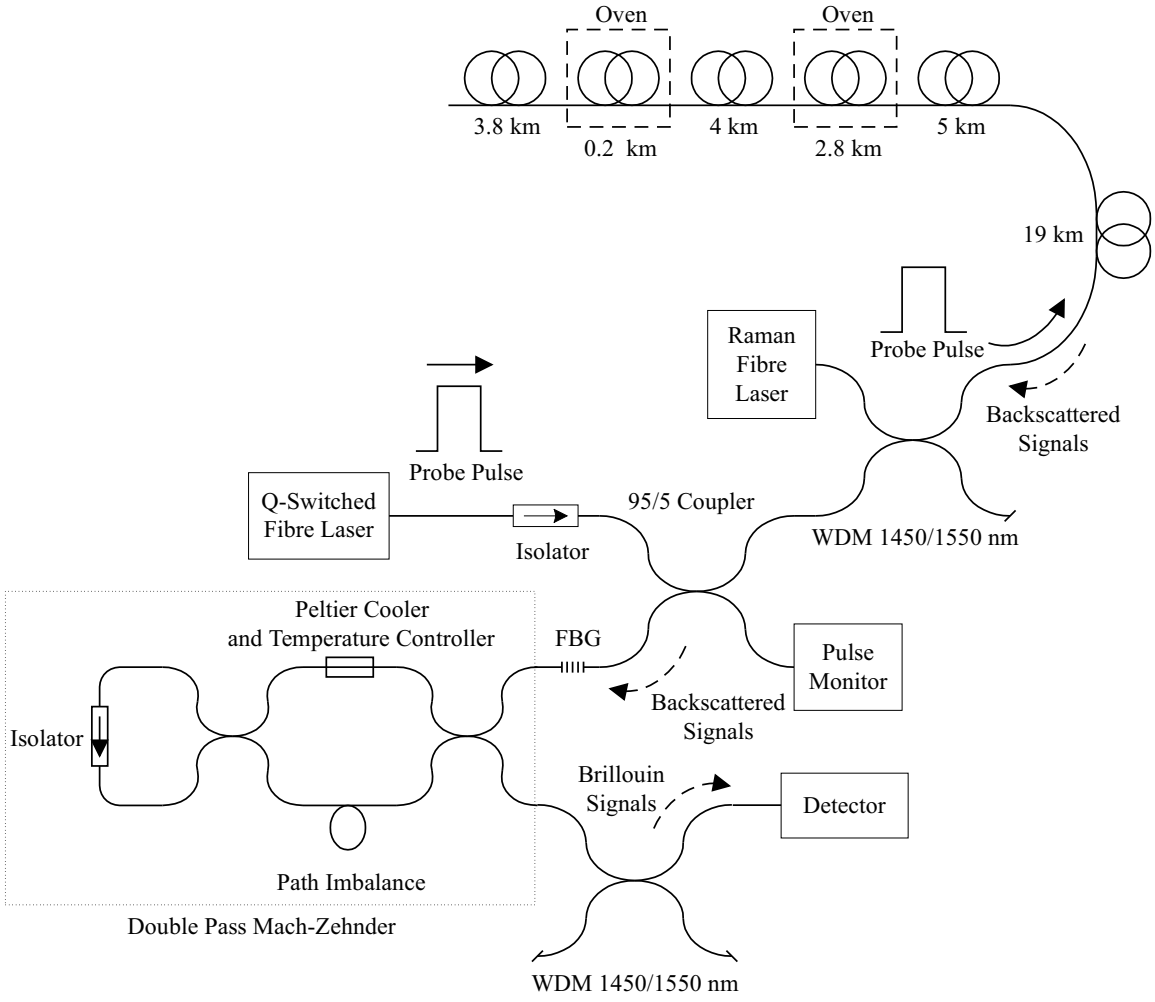

FIGURE 4.12: The experimental setup of the distributed temperature sensors employing CW Raman amplification. The solid line indicates the path of the optical probe pulse, while the dashed line denotes the path of the backscattered signals.

A FBG with a reflectivity of 99.4 %, an optical bandwidth of 0.1 nm and a centre wavelength of 1532.9 nm at 22 ^{o}C was used in conjunction with a DPMZ to attenuate the Rayleigh signal from the probe pulse. Both the FBG and DPMZ were thermally tuned and controlled using two separate Peltier coolers and temperature controllers.

The Rayleigh scattering from the pump at 1450 nm was attenuated using a second 1450/1550 nm WDM coupler. A bulk optical filter shown in figure 4.13 centred at 1520 nm with an optical bandwidth of (FWHM) 23 nm was used to suppress the CW Stokes backscattered noise from 1500 nm to 1570 nm. The spectral profile of the bulk optical filter is illustrated in figure 4.13. For the Rayleigh signal measurement, an additional 11 dB broadband attenuator was required.

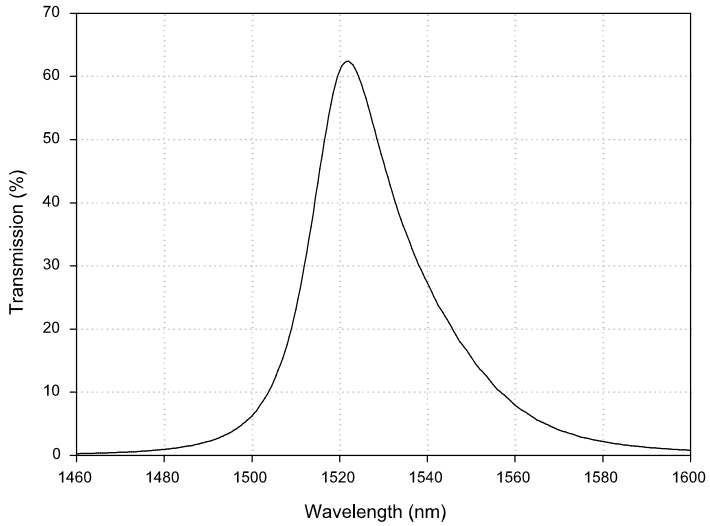

FIGURE 4.13: The profile of the bulk optical filter.

The results obtained from the experiment are discussed in the next section.

4.5.2 Experimental Results and Discussions

Figure 4.14 shows the detailed narrowband Rayleigh backscattered signal for various launched Raman pump powers. The curves of (a) to (f) corresponded to pump power from 0 to 500 mW, increased in steps of 100 mW. For a launched Raman pump power of 500 mW, the intensity of the Rayleigh signal at 12.8 km was approximately 8.6 dB higher compared to the Rayleigh signal without Raman amplification. At 35 km the signal level was increased by 12.9 dB for a pump power of 500 mW.

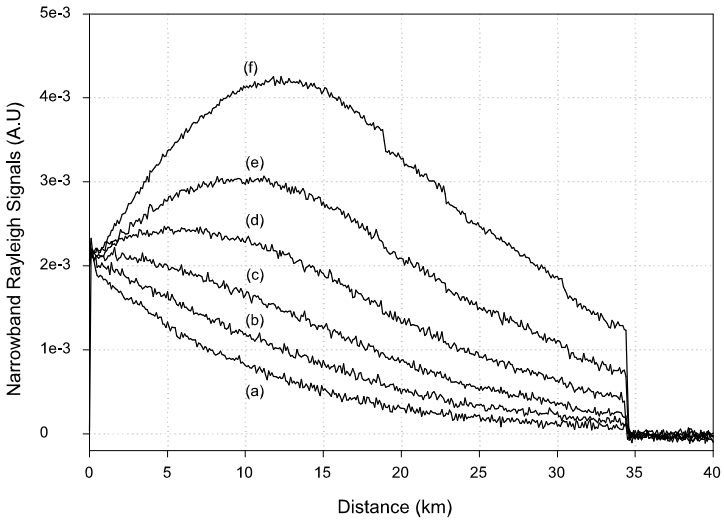

FIGURE 4.14: The amplified narrowband Rayleigh signals with various launched Raman pump power. Traces (a) to (f) corresponded to pump powers of 0 mW to 500 mW, in steps of 100 mW.

The integrated Raman gain over the length of the sensing fibre as the pump powers are increased are illustrated in figure 4.15. The Raman gain profile as a function of fibre length was obtained by taking the ratio of a trace with Raman gain to a trace without Raman gain. It can be seen that the Raman gain is increased when both the pump power and the fibre length are increased. As the fibre length is increased beyond 25 km, the Raman gain saturates due to attenuation of the pump.

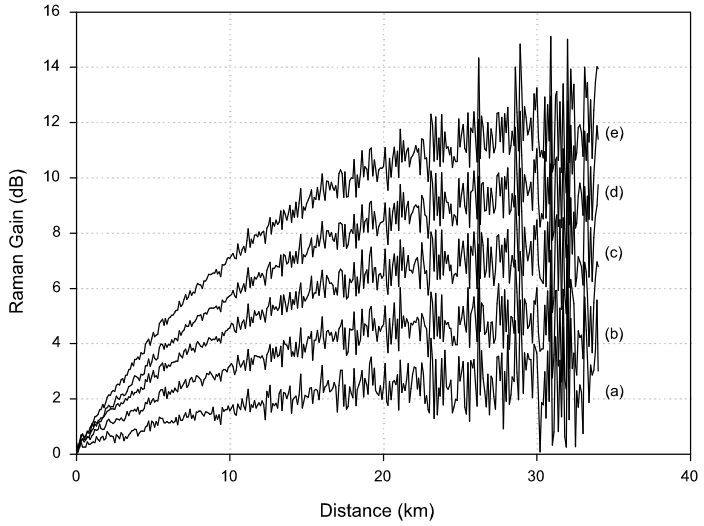

FIGURE 4.15: Raman gain profile over a sensing length of 35 km. Traces (a) to (e) corresponded to pump powers of 100 mW to 500 mW, in steps of 100 mW.

The estimated average gain dependence on the pump power is approximately 2.5 dB/100 mW over a length of 35 km.

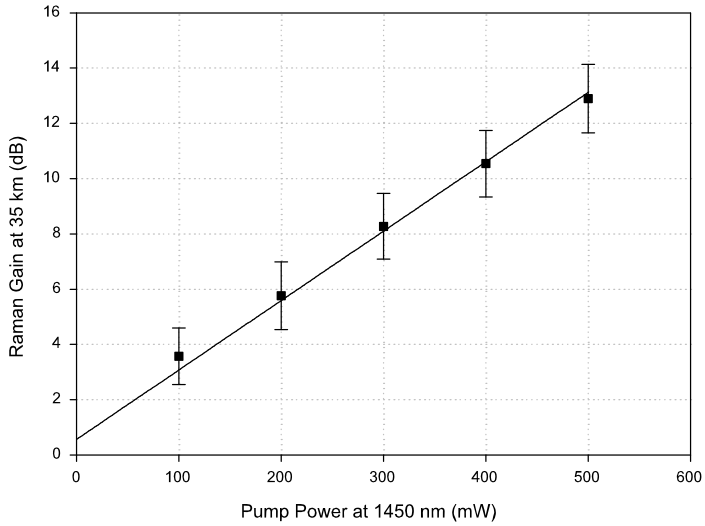

FIGURE 4.16: Raman gain measured at 35 km as a function of pump power.

The amplified Brillouin backscattered signals with different pump powers are shown in figure 4.17. The Brillouin signal level at the far end of the sensing fibre is increased with a higher pump power. However, two peaks located at 3 and 16 km were observed when the launched pump power was increased to 200 mW, but were not observed in the Raman amplified narrowband Rayleigh signals. This observation is attributed to contamination of the Brillouin signal by the Rayleigh signal from the probe pulse as a result of spectral broadening of the probe pulse arising from SPM. This leads to the broadened Rayleigh signal leaking into the transmission band of the DPMZ.

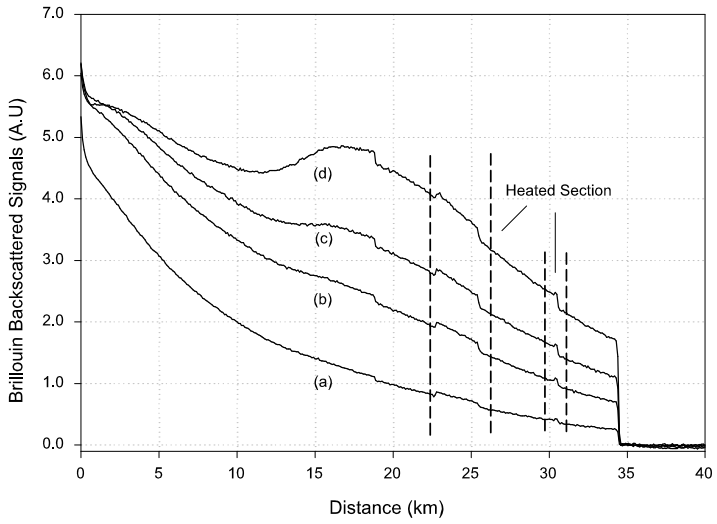

FIGURE 4.17: The amplified Brillouin signals with different pump power. The curves of (a), (b), (c) and (d) corresponded to pump powers of 0, 100, 150 and 200 mW respectively.

This conclusion is supported by the measurement of the temperature coefficients of the 'Brillouin' backscattered power at 25 km for various launched pump powers, figure 4.18. It can be seen that the observed temperature coefficient of the Brillouin power is reduced when the Raman pump is increased. The measured temperature coefficient was reduced from $0.30\,\%^{o}\mathrm{C}^{-1}$ for the condition without pump to $0.13\,\%^{o}\mathrm{C}^{-1}$ when the pump is increased to 200 mW.

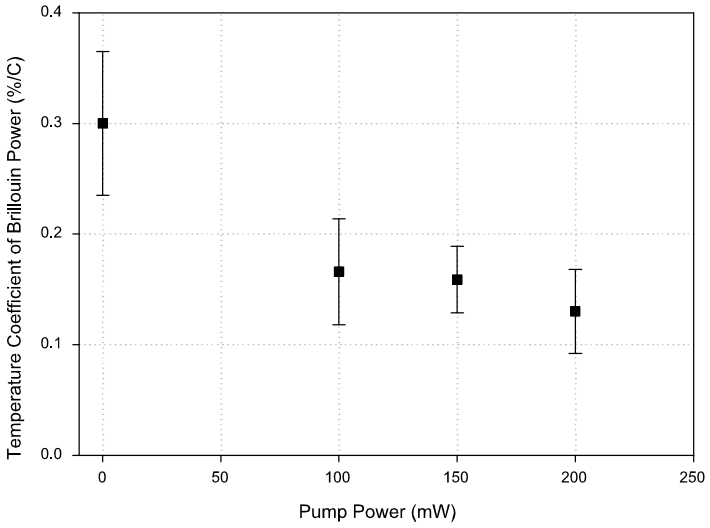

FIGURE 4.18: The temperature coefficients of the Brillouin backscattered power with different launched pump powers measured at 25 km.

The other problem encountered with this experimental setup was the saturation of the detector as a result of CW Raman ASE Stokes noise generated from the pump at 1450 nm. This effect was manifested as an increase in the DC offset in the detector when the pump power is increased. The detector was observed to reach a saturation level when the pump power is increased to 250 mW. This problem may be solved by using an optical filter with a smaller optical bandwidth such as FBG to reduce the Raman ASE noise. The issue related to the optical filtering is discussed in section 4.6.

4.5.3 Summary

The use of CW Raman amplification for enhancing the performance of the Brillouin based OTDR has been demonstrated. This technique demonstrated the expected improvement for the Rayleigh based OTDR. However, the performance of a 35 km Brillouin based OTDR was compromised with a higher launched pump power due to nonlinear effects. The nonlinear effects result in the contamination of the Brillouin signal and this observation was confirmed by the measurement of its temperature coefficient. The improvements using this technique can be achieved by increasing the pump and probe powers close to the onset of nonlinear effects. To enable a much longer measurement range, the Raman gain should be delayed to further down the sensing fibre using a pulsed Raman pump.

4.6 Pulsed Raman Amplification Technique

To investigate the use of pulsed Raman amplification in distributed temperature sensors, several changes to the optical setup were required. An AOM was used in conjunction with a CW Raman pump laser to generate a pulsed pump. This pulsed pump was used to allow amplification of the probe pulse some distance down the sensing fibre to both reduce the Raman ASE noise generated from the pump and the onset of nonlinear effects.

In the preceding section, a Q-switched fibre laser was used to generate the Brillouin signal. However, the narrowband Q-switched fibre laser was not very stable, as the pulse peak power tends to drift over time. Such fluctuations in the peak power level prevents accurate control of the launched power of the probe pulse. This drift is due to thermally induced misalignment of fibre in the free space cavity of the fibre laser. The drift in the probe power was manifested by a 24.1 % variation in the profile of backscattered signals for each successive traces. To overcome this problem, an EDFA amplified DFB pulsed source was used in place of the Q-switched fibre laser source. Using such a fibre laser, the variations in the backscattered signal can be reduced to less than 3.0 %.

The DFB laser was connected to an optical isolator. The CW light from the DFB laser was coupled into EDFA 1, with a length of 6 m and erbium concentration of 100 ppm, by a 980/1550 nm WDM coupler. The amplified CW light was externally modulated using an AOM. The probe pulse light was further amplified by EDFA 2, which had a similar length and erbium concentration as EDFA 1.

The ASE light generated from the EDFA 2 was filtered from the probe pulse light using a second AOM before it was launched into the sensing fibre. This was done to prevent the ASE light of the EDFA 2 from interacting with the probe light in the sensing fibre. Both the AOMs had an extinction ratio in excess of 30 dB.

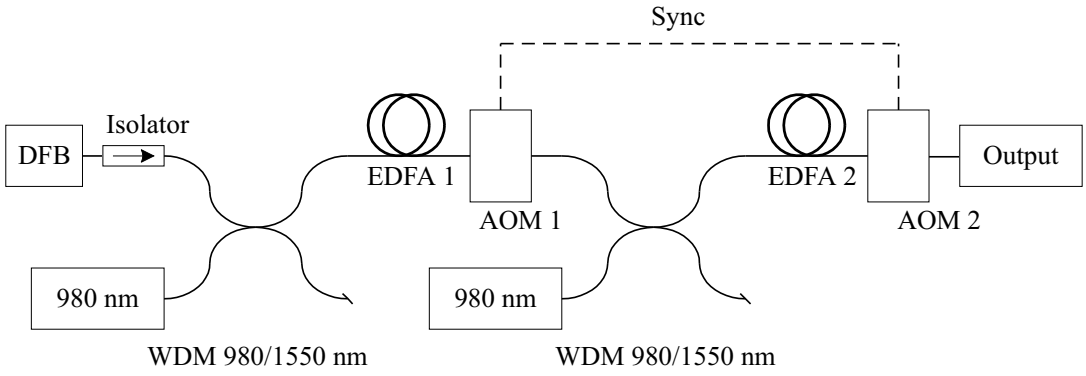

FIGURE 4.19: The setup for the probe source.

Figure 4.20 illustrates the peak probe pulse power. The maximum available output peak power was approximately 400 mW. The intensity profile observed for the probe pulse is due to gain saturation of the EDFA leading to a higher peak power at the leading edge of the pulse.

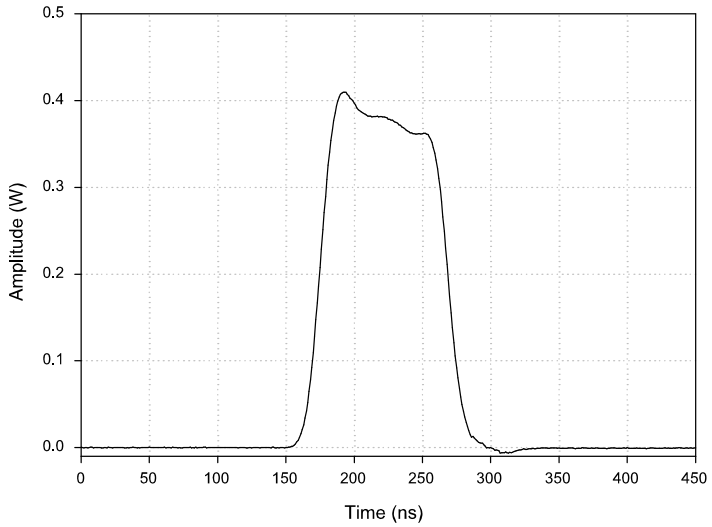

FIGURE 4.20: The peak probe pulse power.

The changes to the optical filtering system are now discussed.

The other modification performed on the experimental configuration was on the optical filtering system used for suppressing the Raman spontaneous emission noise. Spontaneous Raman emission at 1.55 μm is generated when a pump at 1.45 μm propagates in the sensing fibre. Such emission noise has a broadband spectrum of 40 nm and it is amplified as it propagates in a counter-propagating direction to the Raman pump. The spectral profile of the CW Raman ASE noise is illustrated in figure 4.21. As mentioned in section 4.5.2, the CW Raman ASE noise is manifested by a DC offset on the measurement and causes the detector to saturate when the pump is increased to 250 mW. Using a pulsed pump helps to reduce the Raman ASE noise. Another solution is to use a narrower bandpass filter which coincides with the signal, thereby attenuating the other components of the ASE noise.

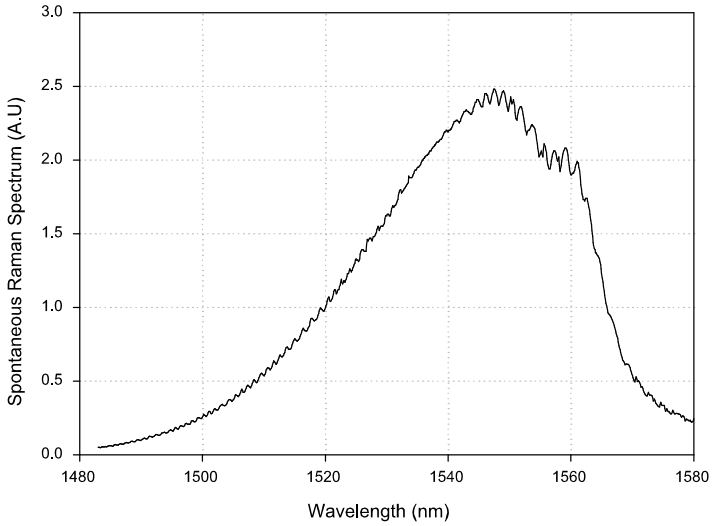

FIGURE 4.21: The spectrum of the spontaneous Raman ASE noise.

The other modification included replacing the DPMZ with two identical narrow linewidth FBGs, with a centre wavelength of 1532.9 nm at a room temperature of 22 ^{o}C, an optical bandwidth of 0.1 nm and a reflectivity of 99.4 %, for filtering the Rayleigh signal. Their spectrum is illustrated in figure 4.22. This optical filtering configuration yielded a 30 dB attenuation of the Rayleigh signal.

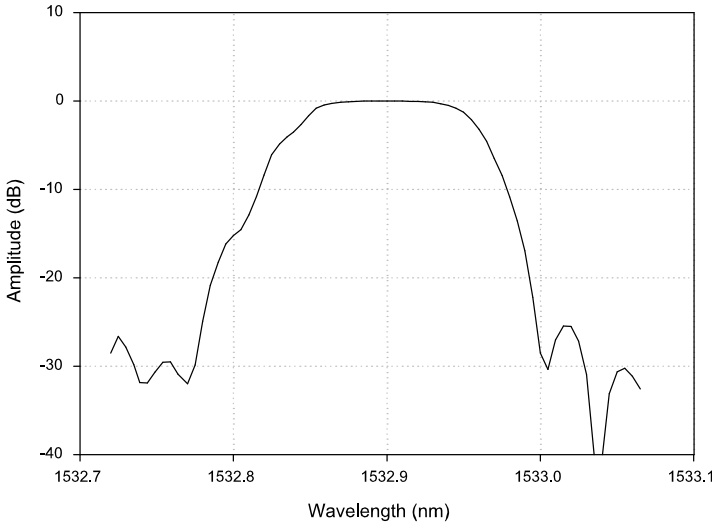

FIGURE 4.22: The spectrum of a narrowband FBG at 22 ^{o}C.

The schematic of using the FBGs to separate the Brillouin signal from the Rayleigh signal is illustrated in figure 4.23. The backscattered signals from the sensing fibre consists of the Rayleigh signal at 1533 nm, Brillouin Stokes signal at 1533.1 nm and Brillouin anti-Stokes signal at 1532.9 nm, shown in figure 4.23. The centre wavelength for the two identical FBGs (FBG 1 and FBG 3), located at the first and third port of the optical circulator, are thermally tuned using a Peltier element. The temperature dependence on the centre wavelength for both the FBGs was experimentally measured to be 10 pm/^{o}C. The two FBGs were tuned such that the centre wavelengths were matched to the wavelength of the incident Rayleigh signal at 1533 nm. In this configuration, the Rayleigh signal was reflected by FBG 1 and FBG 3, while the Brillouin Stokes and anti-Stokes signals were transmitted.

An additional FBG with a centre wavelength of 1533.14 nm at a room temperature of 22 ^{o}C, an optical bandwidth of 1 nm and a reflectivity of 99.0 % was used to reflect the backscattered signals from port 2 into port 3 of the optical circulator. The arms for each FBGs were kept at a different length to prevent the formation of a resonator. The broadband FBG can also be used to filter the Raman ASE noise when the Raman fibre laser was deployed in the system. The use of a broadband FBG will help to reduce the backscattered Raman ASE noise.

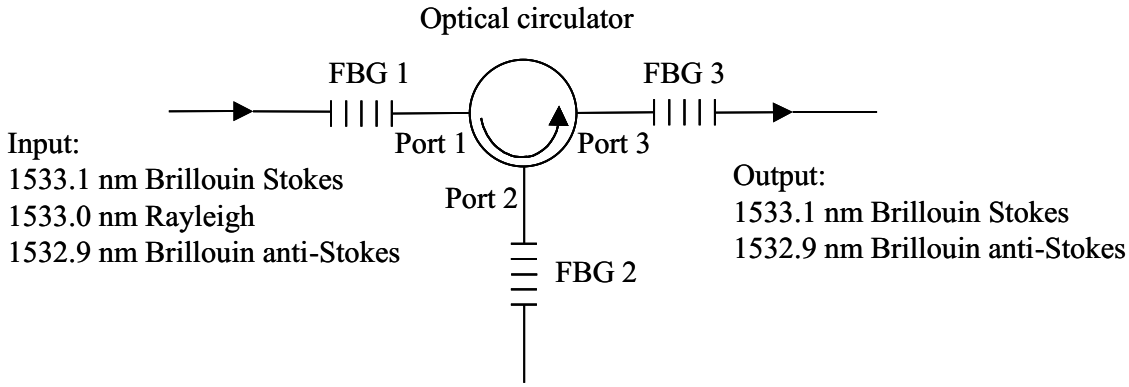

FIGURE 4.23: The FBGs used for filtering Rayleigh signal and Raman ASE noise.

An estimate of the ASE noise reduction with the broadband FBG is given by the following expression

$$R_{ASE} = \frac{\Delta B_{FBG}}{\Delta B_{ASE}} \tag{4.6}$$

where the ΔB_{FBG} is the optical bandwidth (FWHM) of the FBG and the ΔB_{ASE} is the linewidth of the Raman ASE Stokes noise. Assuming the linewidth of the ASE is 40 nm and the FBG is 1 nm, the ASE noise will be reduced by approximately 16 dB. The spectral characteristics of the broadband FBG is shown in figure 4.24

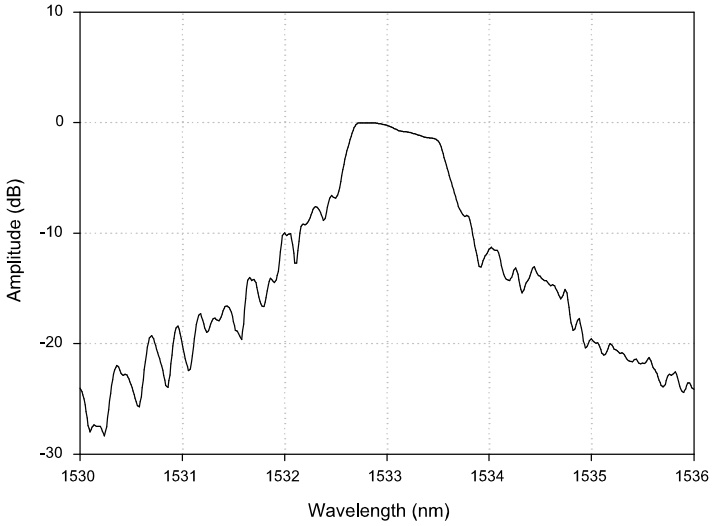

FIGURE 4.24: The spectrum of a broadband FBG at 22 ^{o}C.

The spectrum of the Brillouin backscattered signals observed using an OSA with a resolution bandwidth of 60 pm is shown in figure 4.25. It can be seen that with this current optical filtering configuration, the Rayleigh signal was no longer visible and that the two Brillouin signals were transmitted. The separation between the Brillouin peaks was approximately 0.18 nm.

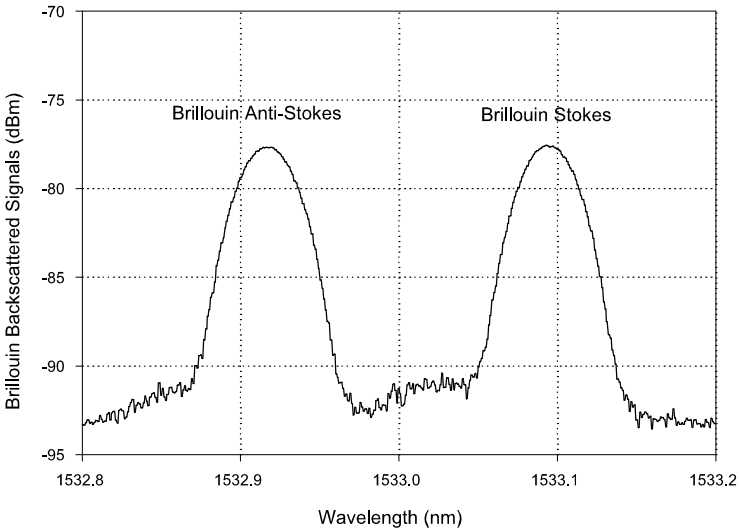

FIGURE 4.25: The spectrum of the spontaneous Brillouin backscattered signals.

4.7 Temperature Dependence of the Spontaneous Brillouin Backscattered Power

In the preceding section, the use of FBGs to filter the Raman ASE noise and Rayleigh signal has been described. This section describes preliminary testing of the optical filtering arrangement.

A 2 km fibre in the oven was heated in steps of 20 ^{o}C, from 20 ^{o}C to 80 ^{o}C. The remaining length of the fibre was maintained at a room temperature of 23^{o}C. The Brillouin signals corresponding to various temperatures were collected and were normalised using a broadband Rayleigh signal. The Brillouin backscattered signal was averaged 2^{12} times. The intensity change for the normalised traces at various temperatures is illustrated in figure 4.27. It can be seen that the percentage change in the intensity of the normalised trace is increased when the fibre is heated to a higher temperature.

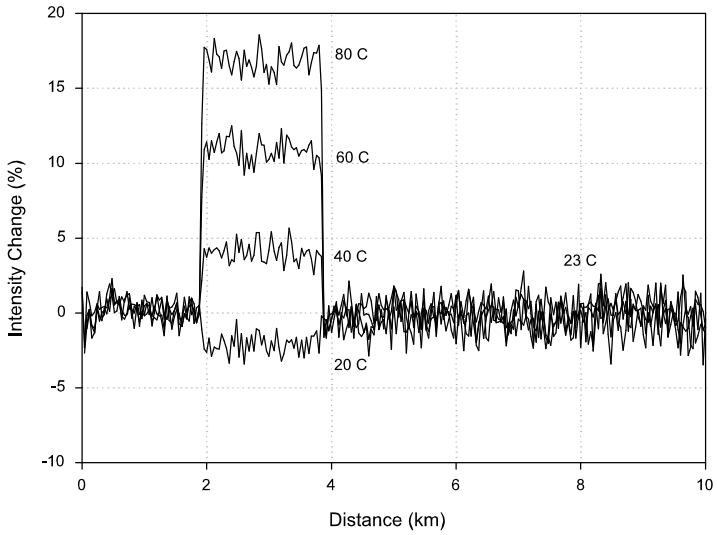

FIGURE 4.26: The percentage intensity change for the normalised Brillouin traces at different temperature.

The plot of the change in intensity of the normalised trace with temperature is illustrated in figure 4.27. The gradient of the line fitted to the data yielded an average value of approximately $0.30 \pm 0.006\,\%^{o}\mathrm{C}^{-1}$ for the temperature coefficient measurement and it is in close agreement with the previously reported value of $0.30\,\%^{o}\mathrm{C}^{-1}$ [13].

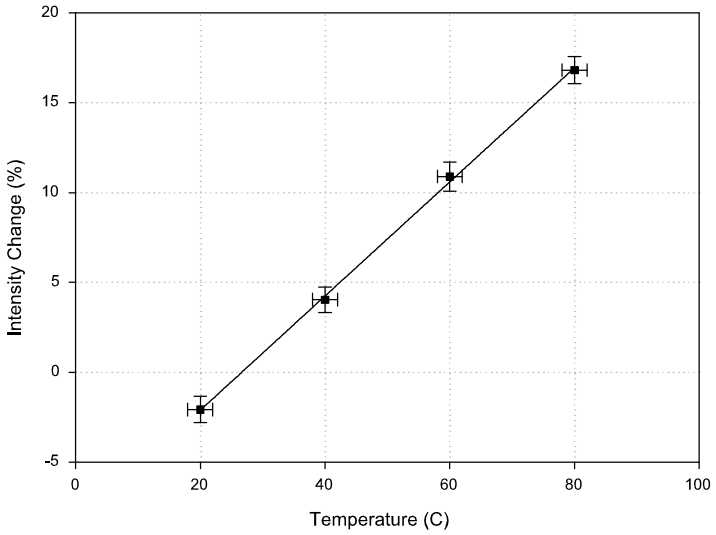

FIGURE 4.27: The plot of percentage change in intensity of the normalised trace with temperature. The gradient of the line fitted to the data provides an average value of the temperature coefficient for the power variation of the Brillouin signal.

This agreement indicates that the optical filter arrangement is achieving a satisfactory separation of the Rayleigh signal from the Brillouin signal.

4.8 Distributed Sensors Utilising Pulsed Raman Amplification

The delayed pulsed Raman amplification technique for enhancing the measurement range of distributed sensors was initially demonstrated for a Rayleigh based OTDR system operating at 1650 nm using a high peak power Q-switched fibre laser at 1530 nm [15, 16]. A probe pulse at 1650 nm was generated through stimulated Raman effect using a Q-switched fibre laser operating at 1530 nm. The two wavelengths were separated using a 1550/1650 nm WDM coupler and both the probe and the residual pump were then recombined in the sensing fibre. The probe pulse generated using stimulated Raman could not be used for applications in distributed Brillouin based sensors, because the spectrum of the probe is broadband ~ 40 nm at 1650 nm. Both the Rayleigh and Brillouin signals generated from such a probe would overlap and prevent separation of the two signals. This technique has now been applied to Brillouin based OTDR for the first time, as a narrow linewidth probe at 1533 nm and a high power Raman pump laser at 1450 nm are available.

The technique of pulsed Raman amplification utilises a Raman pump pulse to amplify the probe pulse in the sensing fibre. The Raman amplification of the probe pulse occurs when the two pulses overlap in the fibre. The overlapped distance between the two pulses is controlled by introducing time delay and allowing for the dispersion properties of the fibre. The probe pulse at 1533 nm is launched first, followed by a Raman pulse at 1450 nm. The Raman pulse travels faster than the probe pulse due to the anomalous dispersion characteristics of a standard singlemode fibre at this wavelength. The gain experienced by the probe pulse is primarily governed by the peak pump power and the interaction length is governed by the walk-off length.

4.8.1 Experimental Details

The experimental configuration is shown in figure 4.28. The setup consisted of two sources. An EDFA amplified DFB source at 1533 nm was used as a probe pulse to generate the Brillouin backscatter. The CW Raman fibre laser operated at 1450 nm was externally modulated with an AOM with a rise or fall time of 20 ns to produce the Raman pump pulse. The probe pulse, with a peak power of 100 mW and a pulsewidth (FWHM) of 100 ns, was launched into the sensing fibre via a three-port circulator. The probe pulsewidth was set to 100 ns in order to match the bandwidth of the detector of 3 MHz. The Raman pump pulse at 1450 nm, with a peak power of approximately 120 mW and a pulsewidth (FWHM) of 50 ns, was delayed such that it initially propagated behind the probe pulse at the front end of the sensing fibre. The pulsewidth for the pump was set to 50 ns to provide sufficient interaction length between the two pulses and also to ensure that the backscattered Raman ASE noise was smaller than the Brillouin backscattered signal. The walk-off length between the probe and pump can be expressed as

$$L_w = \frac{W_p + W_s}{D\,\Delta\lambda} \tag{4.7}$$

where W_p is the pulsewidth of the pump, W_s is the pulsewidth of the probe, D is the dispersion parameter and $\Delta\lambda$ is the difference between the probe and pump wavelength. The walkoff length for the two pulses was calculated to be 106 km assuming that the W_p was 50 ns, W_s was 100 ns, D was 17 ps/km nm and $\Delta\lambda$ is 83 nm. This value is much longer than the actual fibre length of 50 km used in the experiment.

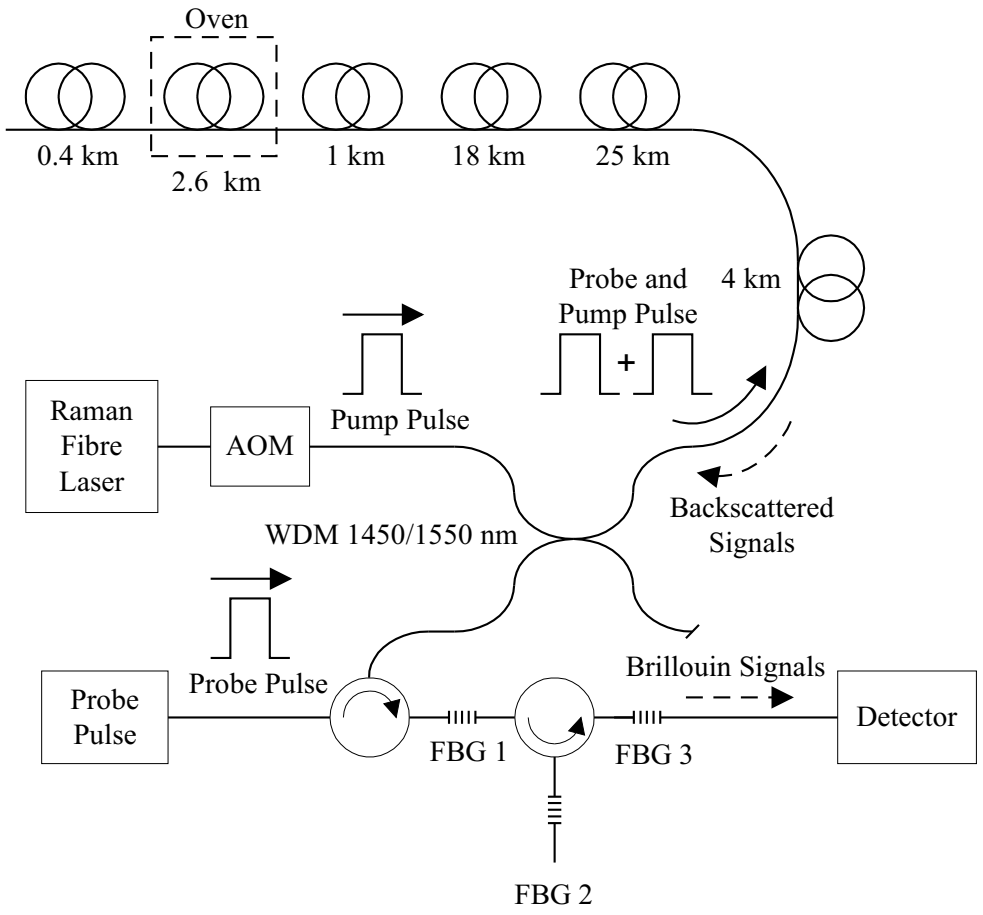

FIGURE 4.28: The experimental setup for Brillouin based OTDR using pulse Raman amplification. The solid line indicates the path of the optical probe and pump pulse, while the dashed line denotes the path of the backscattered signals.

The two pulses fully overlapped at approximately 30 km down the sensing fibre. The average walk-off rate between the probe and pump was measured to be 1.0 ns/km. The Brillouin backscattered signal was optically filtered from the Rayleigh signal by thermally tuning FBG 1 and 3. The Rayleigh signal generated by the probe was attenuated whilst the Brillouin signal was collected by the detector.

The Rayleigh and spontaneous Raman backscatter generated from the Raman amplifier was attenuated using FBG 2. A section of 2.6 km length of fibre at approximately 48 km was heated in an oven to a temperature of 80.0 ^{o}C. The remaining 5 sections of fibre were maintained at a room temperature of 22.0 ^{o}C. The Brillouin signal was collected using an InGaAs detector with a bandwidth of 3 MHz. The Brillouin backscattered trace was averaged 2^{19} times.

4.8.2 Experimental Results and Discussions

The Brillouin backscattered signals measured at a room temperature of 22.0 ^{o}C for the condition with (a) and without (b) Raman amplification are shown in figure 4.29. The improvement obtained for the Brillouin signal with Raman amplification is approximately 5.0 dB over 50 km. The Brillouin signal with and without Raman amplification decayed with an average gradient of 0.29 dB/km and 0.39 dB/km. This figure corresponded to the expected two-way fibre loss. The corresponding loss for the signal with a gradient profile of 0.29 dB/km and 0.39 dB/km over 50 km are 14.5 dB and 19.5 dB respectively. The difference between the two values is 5 dB and it is in agreement with the measurement.

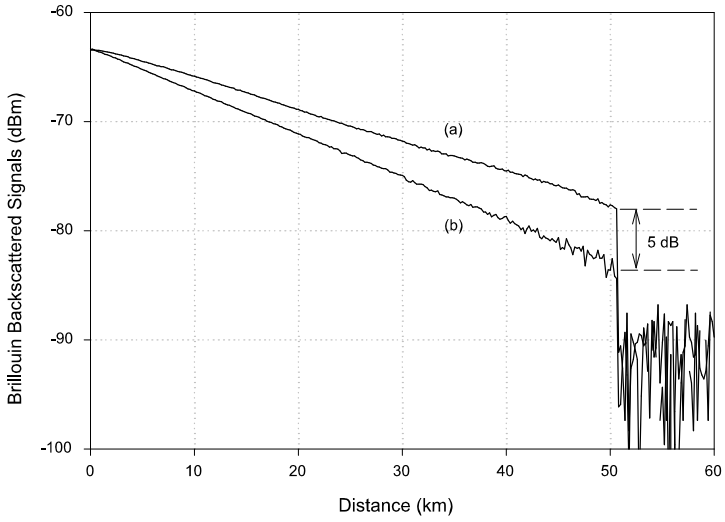

FIGURE 4.29: The Brillouin backscattered signals at a room temperature of 22 ^{o}C with (a) and without (b) Raman amplifications.

Figure 4.30 shows the comparison between the temperature resolution of the Brillouin signals with and without Raman amplification. It illustrates that up to a distance of about 30 km the temperature resolution was measured to be 4.0 ^{o}C for the experimental conditions with (indicated by squares) and without (indicated by triangles) Raman pulse amplification. The temperature resolution is defined as the standard deviation of the temperature measured over a section of fibre maintained at a uniform temperature. Beyond 30 km the traces diverge and the benefit of the Raman amplification is evident. At 50 km the temperature resolution was 40.0 ^{o}C for the condition without Raman amplification but improved to 13.0 ^{o}C with Raman amplification. This improvement in resolution (4.9 dB) closely matches the increase in signal level of 5.0 dB.

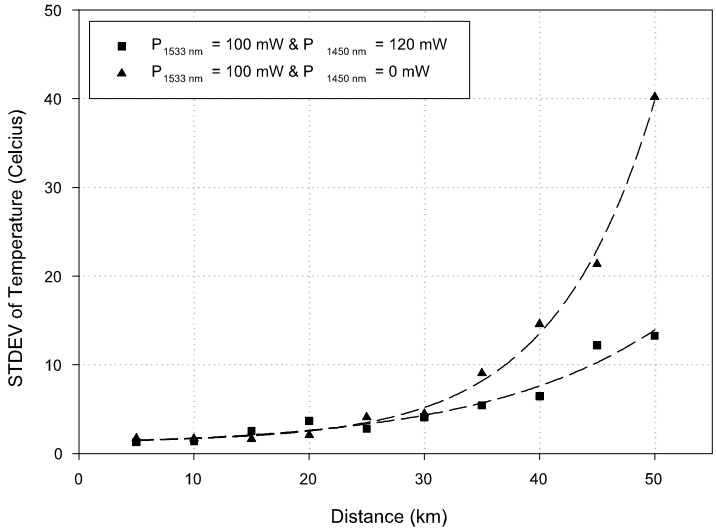

FIGURE 4.30: The temperature resolution measurement of Brillouin signals with and without Raman amplification at a room temperature of 22 ^{o}C.

The enlarged Brillouin backscatter at the far end of sensing fibre with (a) and without (b) Raman amplification is shown in figure 4.31.

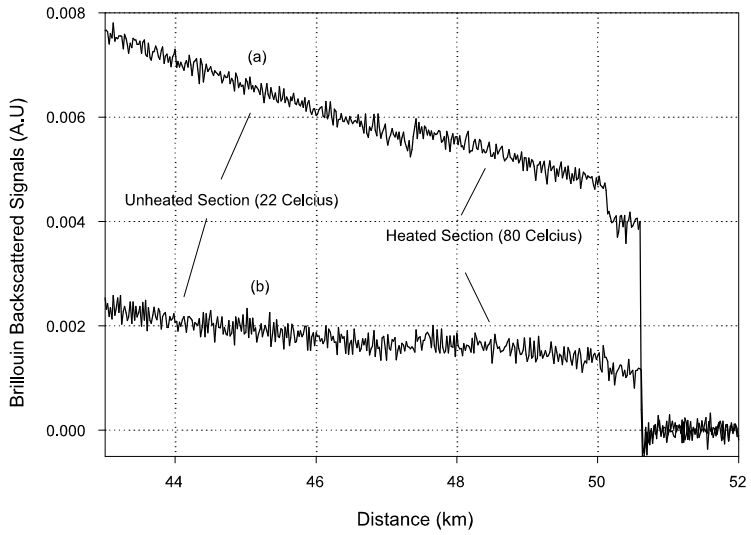

FIGURE 4.31: The enlarged Brillouin signals with (a) and without (b) Raman amplification.

The spatial resolution was measured to be 15 m and was defined by the 10 to 90 % response time with a sampling resolution of 2 m, shown in figure 4.32(a). The spatial resolution is determined by the combined effects of the pulse duration and the bandwidth of the detector and is independent of the range. The measurement was made close to the front end of the fibre to minimise the errors in estimating its value. The derived temperature profile at the far end is shown in figure 4.32(b).

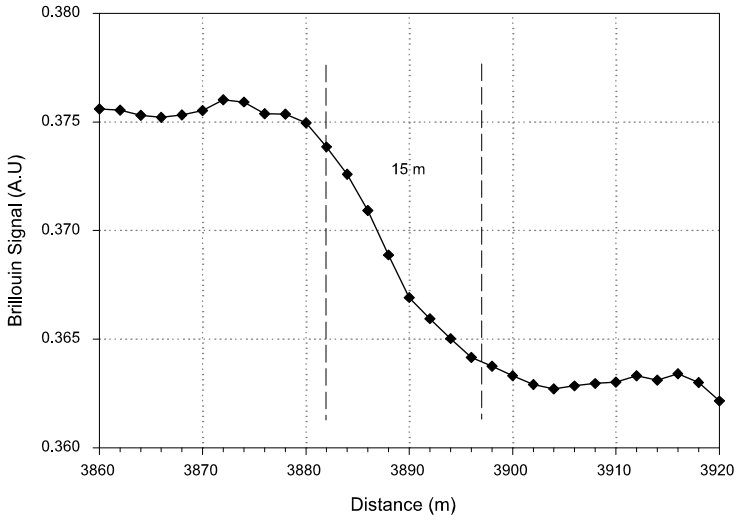

(a) The spatial resolution for the Brillouin signal.

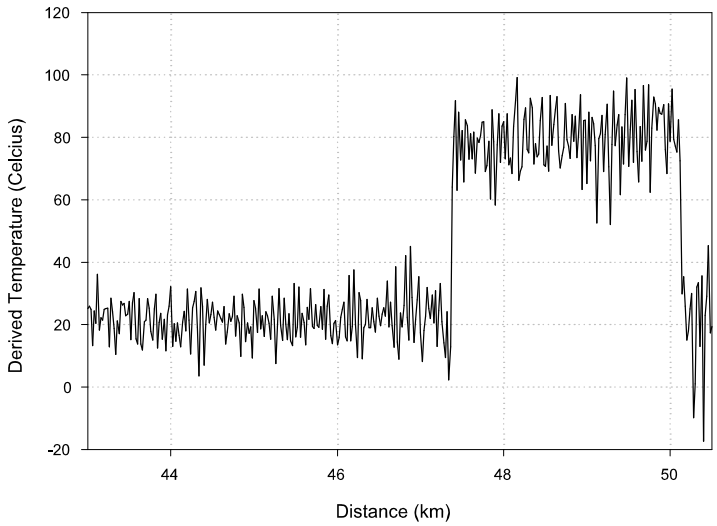

(b) The derived temperature profile.

FIGURE 4.32: The derived temperature profile together with the spatial resolution measurement.

4.8.3 Summary

The use of the pulsed Raman amplification technique for enhancing the intensity measurement of the Brillouin signal via amplification of the probe pulse has been demonstrated for the first time. The Raman gain of 5.0 dB matched the improvement obtained in the temperature resolution measurement of 13.0 ^{o}C and 40.0 ^{o}C for the condition with and without this technique. It is anticipated that further improvement in the temperature resolution measurement may be obtained with a higher power Raman pump pulsed source. Due to the passive loss in the AOM of more than 6.0 dB, this concept could not be explored further.

4.9 Conclusions

This chapter has investigated the use of Raman amplification in the CW and pulsed configurations for improving the performance of a single-ended Brillouin based system. An improvement was demonstrated for Rayleigh signal measurements in the CW pump configuration. However, the improvement in the performance of the Brillouin signal in this configuration was limited by the onset of nonlinear effects. The CW pump technique offered little advantage in long range sensing because the Raman gain primarily occurs in the first 30 km of the sensing fibre. At this distance the probe pulse power is relatively high and does not require much Raman gain. Moreover, the probe pulse power had to be reduced to avoid nonlinear effects. To overcome the problem, the technique of pulsed Raman amplification was investigated. Using such a technique, the Raman gain is delayed further down the sensing fibre such that the weaker probe pulse can be amplified. This technique demonstrated a temperature resolution of 13.0 ^{o}C at 50 km, compared to 40.0 ^{o}C at 50 km without Raman amplification.

It is anticipated that further improvements in the Brillouin signal measurement may be obtained using a higher pump pulse power and a faster modulator to provide more accurate control of the overlap position of the two pulses. Although significant advantage was obtained with this technique, the insertion loss of the modulator limited the amount of launched pump pulse power and hence the Raman gain. This effect limited the range to 50 km. This technique demonstrated the advantage of using Raman gain at some distance down the sensing fibre. To increase the measurement range beyond this distance, remote amplification is investigated in the following section.

Bibliography

[1] D.M. Spirit and L.C. Blank, "Raman Assisted Long Distance Optical Time Domain Reflectometry," *Electronics Letters*, vol. 25, no. 25, p. 1687, December 1989.

[2] R.H. Stolen, "Polarization Effects in Fiber Raman and Brillouin Lasers," *IEEE Journal of Quantum Electronics*, vol. QE-15, no. 10, p. 1157, October 1979.

[3] G.P. Agrawal, *Nonlinear Fiber Optics*, 2nd ed. Academic Press, 1995.

[4] M. Wuilpart, G. Ravet, P. Megret and M. Blondel, "Distributed Measurement of Raman Gain Spectrum in Concatenations of Optical Fibres with OTDR," *Electronics Letters*, vol. 39, no. 1, p. 88, January 2003.

[5] K. Toge, K. Hogari and T. Horiguchi, "Measurement of Raman Gain Distribution in Optical Fibers," *IEEE Photonics Technology Letters*, vol. 14, no. 7, p. 974, July 2002.

[6] H. Po, J.D. Cao, B.M. Laliberte, R.A. Minns, R.F. Robinson, B.H. Rockney, R.R. Tricca and Y.H. Zhang, "High Power Newodymium-Doped Single Transverse Mode Fibre Laser," *Electronics Letters*, vol. 29, no. 17, p. 1500, August 1993.

[7] S.G. Grubb, T. Strasser, W.Y. Cheung, W.A. Reed, V. Mizrachi, T. Erdogan, P.J. Lemaire, A.M. Vengsarkar and D.J. DiGiovanni, "High Power, 1.48 μm

Cascaded Raman Laser in Germanosilicate Fibers," *Proceedings on Optical Amplifiers and Their Applications (OAA)*, no. SaA4-1, p. 197, 1995.

[8] P. Mylinski, J. Chrostowski, J. A. Koningstein and J.R. Simpson, "High Power Q-Switched Erbium Doped Fiber Laser," *IEEE Journal of Quantum Electronics*, vol. 28, no. 1, p. 371, January 1992.

[9] F. Sequin and T. Oleskevich, "Diode Pumped Q-Switched Fiber Laser," *Optical Engineering*, vol. 32, no. 9, p. 2036, September 1993.

[10] G.P. Lees, A.H. Hartog , A. Leach, T.P. Newson, "980 nm Diode Pumped Erbium^{3+}/Ytterbium^{3+} Doped Q-Switched Fibre Laser," *Electronics Letters*, vol. 31, no. 21, p. 1836, October 1995.

[11] M. Nakazawa, M. Tokuda, K. Washio and Y. Asahara, "130-km Long Fault Location for Single Mode Optical Fibre Using 1.55 μm Q-Switched Er $^{3+}$:Glass Laser," *Optics Letters*, vol. 9, no. 7, p. 312, July 1984.

[12] G.P. Lees, P.C. Wait, M.J. Cole and T.P. Newson, "Advances in Optical Fiber Distributed Temperature Sensing Using the Landau-Placzek Ratio," *IEEE Photonics Technology Letters*, vol. 10, no. 1, p. 126, Jan 1998.

[13] P.C. Wait and T.P. Newson, "Landau Plazcek Ratio Applied to Distributed Fibre Sensing," *Optics Communications*, vol. 122, p. 141, Jun 1996.

[14] K. de Souza, "Fibre-Optic Distributed Sensing Based on Spontaneous Brillouin Scattering," Ph.D. dissertation, University of Southampton, June 1999.

[15] G.P. Lees, A.P. Leach, A.H. Hartog and T.P. Newson, "1.64 μm Pulsed Source for a Distributed Optical Fibre Raman Temperature Sensor," *Electronics Letters*, vol. 32, no. 19, p. 1809, 1996.

[16] H.H. Kee, G.P. Lees and T.P. Newson, "Extended Range Optical Time Domain Reflectometry System at 1.65 μm Based on Delayed Raman Amplification," *Optics Letters*, vol. 23, no. 5, p. 349, March 1998.

Chapter 5

Remote Amplification in Distributed Fibre Sensors

5.1 Introduction

The use of Raman amplification from the front end of the sensing fibre in Brillouin based OTDR was described in the preceding chapter. The improvement achieved in Brillouin based OTDR using the CW Raman pump was limited by the onset of nonlinear effects. To overcome this problem, the Raman gain was delayed to further down the sensing fibre using pulsed Raman amplification. However, the measurement range was limited to 50 km due to the low launched pump peak power arising from the loss of the acousto-optic modulator used to generate the pulsed pump.

One method of increasing the range is by using remote optical amplification. This involves amplifying a signal using an optical amplifier, ie. an EDFA or Raman amplifier, located at some point along the sensing fibre. The various ways of using remote amplification in distributed fibre sensors are described and evaluated in this chapter.

5.2 Remote Raman Amplification

The technique of remote Raman amplification involves deploying a Raman pump at some distance along the fibre to amplify the probe signal. This method is simple as it only requires a pump and the same optical fibre is used both as the gain and sensing medium. The investigation focussed on improving the signal level at the far end of a 100 km sensing fibre.

5.2.1 Experimental Details

The experimental configuration is illustrated in figure 5.1. A probe pulse, generated using an EDFA amplified DFB source, with a peak power of 100 mW and a pulsewidth of 200 ns, corresponding to a spatial resolution of 20 m, was launched into the sensing fibre. The spatial resolution of a Brillouin based OTDR is governed by the width of the pulse and the bandwidth of the detector. It was shown from section 4.8.2 that the receiver was able to measure spatial resolution of 15 m. Hence, the spatial resolution in this chapter was inferred from the width of the probe pulse used in the experiment. A Raman fibre laser was launched at the midpoint of the sensing fibre, in the forward direction co-propagating with the probe pulse. The Raman pump power used in the co-propagating configuration was limited to 660 mW to avoid the onset of nonlinear effects. To reduce the coherent Rayleigh noise [1], an erbium fibre ASE source with peak power of 30 mW and pulsewidth of 200 ns was used to generate a broadband Rayleigh signal. The effective optical bandwidth of the broadband Rayleigh signal is governed by the fibre Bragg grating (FBG 2). Both the Rayleigh and Brillouin backscattered signals were obtained from the same fibre and the Rayleigh signal was used to normalised the Brillouin signal.

Two identical FBGs were used to filter the Rayleigh signal from Brillouin signal and a 1 nm bandwidth FBG was used to attenuate the Raman amplified spontaneous emission (ASE) noise. This optical filtering configuration was previously described in section 4.8.1. Two sections of fibre with lengths of 2.0 km and 2.6 km located at 0 and 98 km respectively, were heated in an oven to 80.0 ^{o}C. The remaining fibres were kept at room temperature of 22.0 ^{o}C. The full length of optical fibre used in the system was approximately 100.8 km. The Brillouin signal was averaged 2^{20} times.

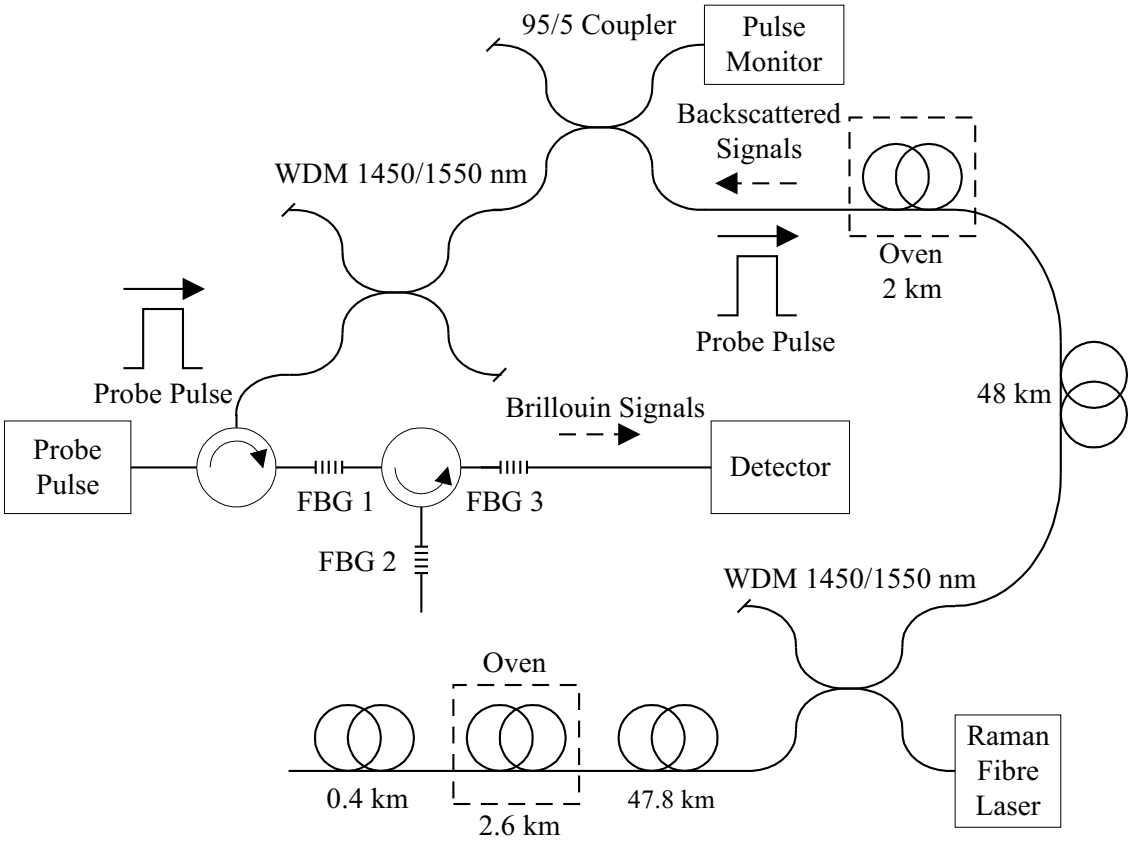

FIGURE 5.1: Experimental configuration in the forward pumped configurations. The solid line indicates the path of the optical probe pulse, while the dashed line denotes the path of the backscattered signals.

5.2.2 Experimental Results

The Brillouin and scaled Rayleigh backscattered signals over the entire sensing length are shown in figure 5.2 for the co-propagating Raman pump configuration. The amplified Rayleigh signal was scaled to facilitate comparisons with the amplified Brillouin signal. It can be seen that both the Brillouin (indicated by a solid line) and scaled Rayleigh (indicated by a dashed line) signals decayed linearly as a result of the two-way loss of 0.39 dB/km from 0 to 50 km. The probe pulse and the backscattered signals were not amplified up to this distance. Beyond 50 km, both the probe pulse and backscattered signals experienced Raman amplification, resulting in an increase in the signal levels, which peaked at around 70 km. Beyond 80 km, the Raman pump power had been significantly attenuated leading to reduced Raman amplification. From 80 to 100 km, both backscattered signals decayed with an average gradient of 0.28 dB/km as compared to the 0.39 dB/km at the front end. The Brillouin backscattered signal power at the far end of the sensing fibre was measured to be -76.6 dBm.

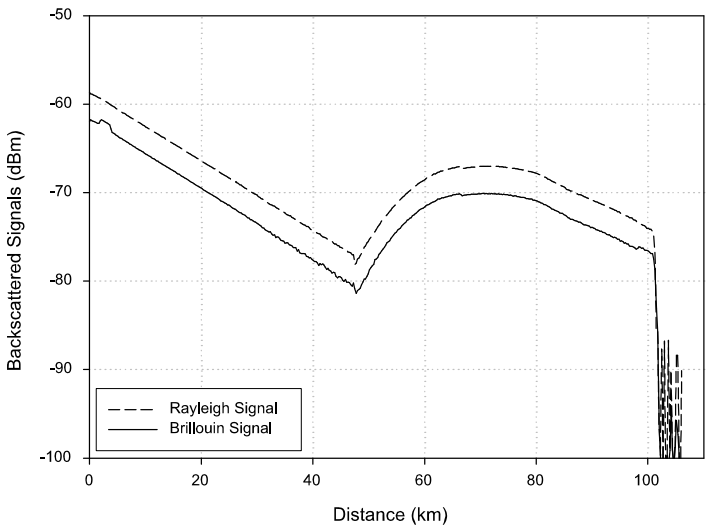

FIGURE 5.2: The scaled Rayleigh signal (indicated by a dashed line) and the Brillouin signal (indicated by a solid line) backscattered signals with a co-propagating Raman pump.

The derived temperature was obtained by normalising the Brillouin signal with the Rayleigh signal based on using the known coefficient of the Brillouin intensity change with temperature [2] and was verified to be $0.30\,\%^{o}\mathrm{C}^{-1}$ for this fibre, this equation is given by

$$B(T,z) = \left(\frac{P_B(T,z)}{P_R(z)} - 1\right)\frac{100}{K_{P,T}} + T_R \tag{5.1}$$

where $B(T,z)$ is the derived temperature as a function of distance, $P_B(T,z)$ is the Brillouin backscattered power, $P_R(z)$ is the scaled Rayleigh backscattered power, $K_{P,T}$ is the temperature coefficient of the Brillouin backscattered power and T_R is the room temperature. The derived temperature profile over the entire sensing length is illustrated in figure 5.3.

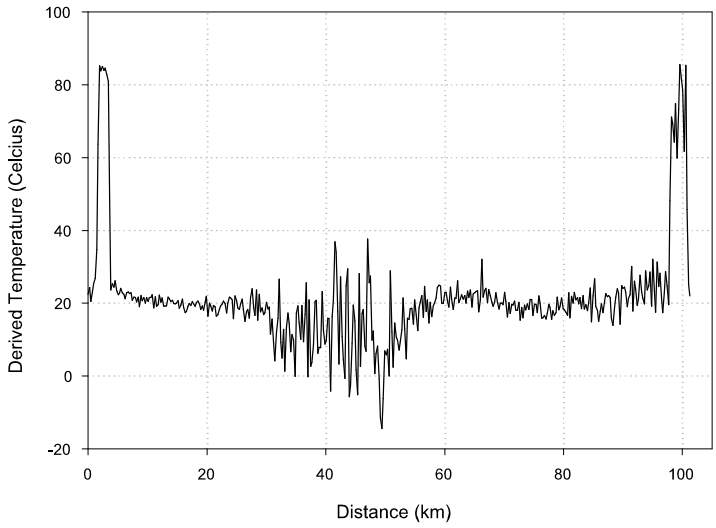

FIGURE 5.3: Temperature profile over the entire sensing length.

The temperature resolution measurement was obtained at intervals of 6 km over the whole length of the sensing fibre and it is illustrated in figure 5.4. The temperature resolution increased to almost 12.0 ^{o}C at 50 km. The advantage of using Raman amplification was observed beyond 50 km. The temperature resolution was improved to below 3.0 ^{o}C at 72 km and increased to approximately 4.0 ^{o}C at 96 km.

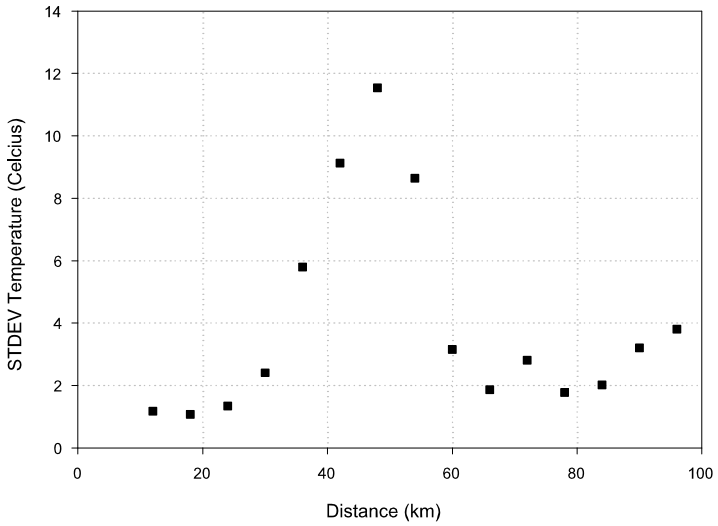

FIGURE 5.4: The temperature resolution measurement over the entire sensing length.

The time base scale of the oscilloscope was reduced to provide increased detail and also to increase the sampling points over the last 7 km of the sensing fibre. The enlarged Raman amplified Brillouin and Rayleigh signals are shown in figure 5.5. The amplified Rayleigh signal was scaled to facilitate comparison of the gradients for the two different signals. It can be seen that the two traces exhibit similar gradients of approximately 0.31 dB/km, which provided further confirmation that the technique of normalising Brillouin signal with Rayleigh signal is valid.

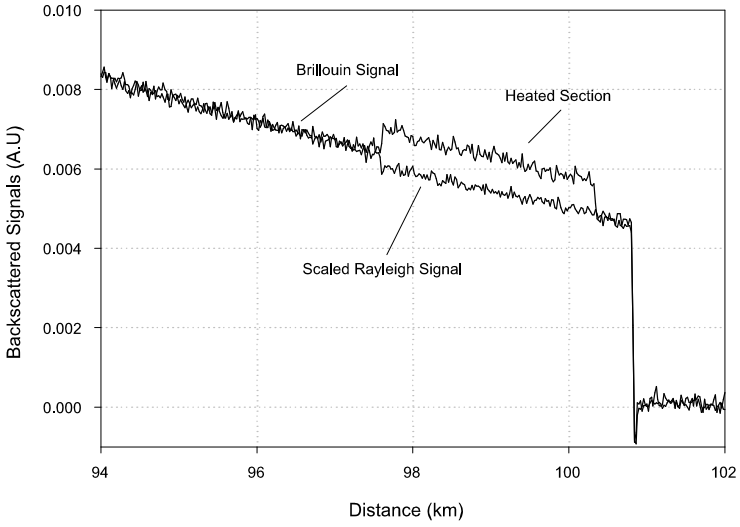

FIGURE 5.5: The enlarged backscattered traces of the Brillouin and Rayleigh signals at the far end of the sensing fibre.

Figure 5.6 illustrates the derived temperature profile based on the intensity measurement at the far end of the sensing fibre.

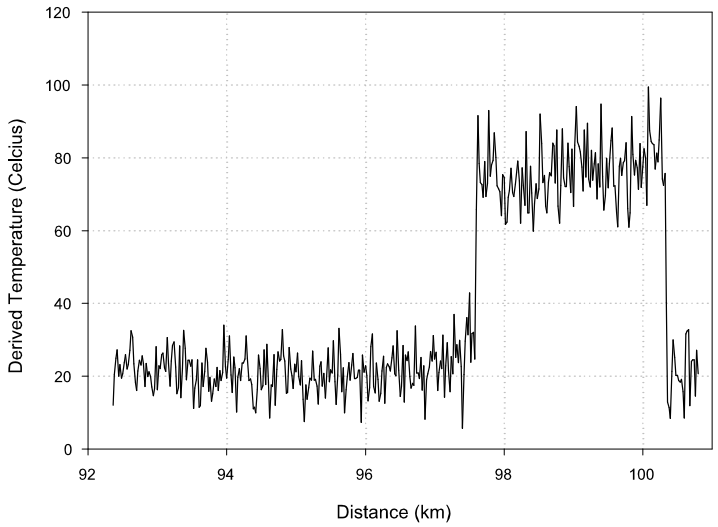

FIGURE 5.6: The derived temperature profile at the far end of sensing fibre.

The temperature resolution measurement obtained at intervals of 1 km over the last 7 km of the sensing fibre is shown in figure 5.7. The temperature resolution was measured to be less than 5.0 ^{o}C at 94 km and it increased to approximately 8.0 ^{o}C at 99.6 km.

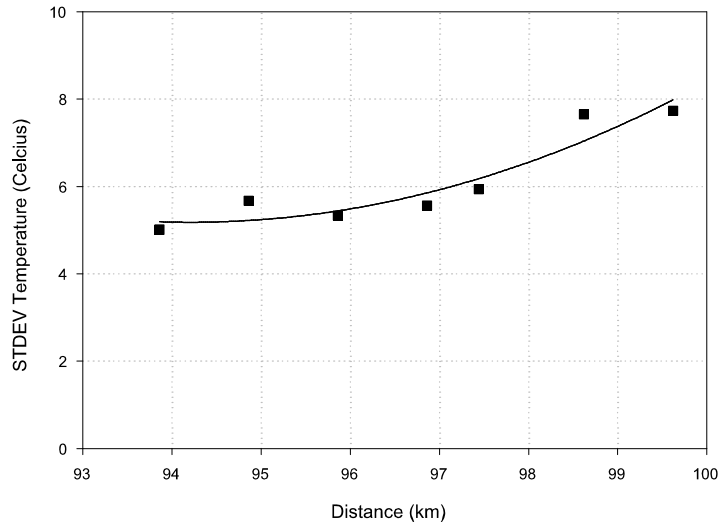

FIGURE 5.7: The temperature resolution measurement at 100 km.

5.3 Remote Amplification Using an EDFA

Alternatively, amplification of the probe and backscattered signal can be achieved using an EDFA located some distance along the sensing fibre. This EDFA may be pumped either by using a local pump, figure 5.8(a) or remotely pumped from a pump located at the front end of the sensing fibre, figure 5.8(b). Although better pump efficiency is achieved at 980 nm when pumped remotely it is preferable to use 1480 nm due to the lower propagation loss of 0.23 dB/km compared to 1.0 dB/km at 980 nm. When the EDFA is pumped remotely at 1480 nm the pump provides additional Raman gain to the probe pulse and backscattered signal.

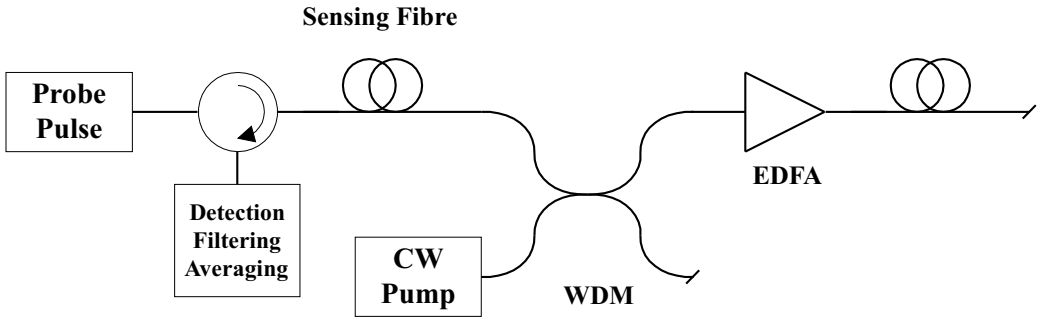

(a) Pumping the EDFA by using a pump located at some distance down the sensing fibre.

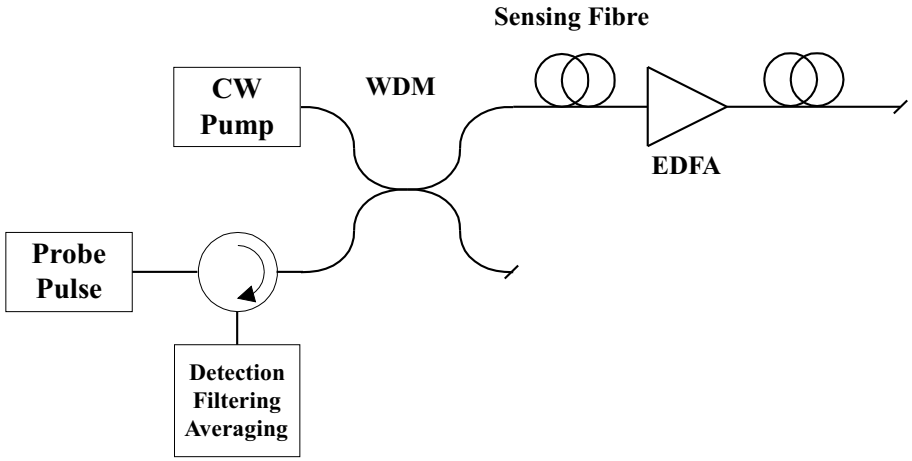

(b) Pumping the EDFA via the sensing fibre from the front end.

FIGURE 5.8: Remote amplification configurations using an EDFA.

5.4 Locally Pumped Remote EDFA

In this configuration, the EDFA at 50 km is pumped using a 980 nm laser diode. The EDFA is used to amplify both the probe pulse and backscattered signal for a sensing length beyond 50 km.

5.4.1 Experimental Details

The experimental schematic of a distributed fibre sensor containing a locally pumped EDFA is illustrated in figure 5.9. A probe pulse with a peak power of 100 mW and a pulsewidth of 200 ns was launched into the sensing fibre. The specifications of the EDFA were chosen based on the recommendation by Becker [3]. A 2 m length of EDFA with an erbium concentration of 100 ppm and a numerical aperture of 0.23 was used and pumped using a 980 nm laser diode with a CW power of 100 mW. It was operated in the saturation regime to ensure that the EDFA was fully inverted over its length thus providing the improved noise figure. The detected Brillouin signal was averaged 2^{20} times. The EDFA gain was such that the Brillouin signal power at the far end of the sensing fibre matched that achieved with the Raman amplification of the previous section.

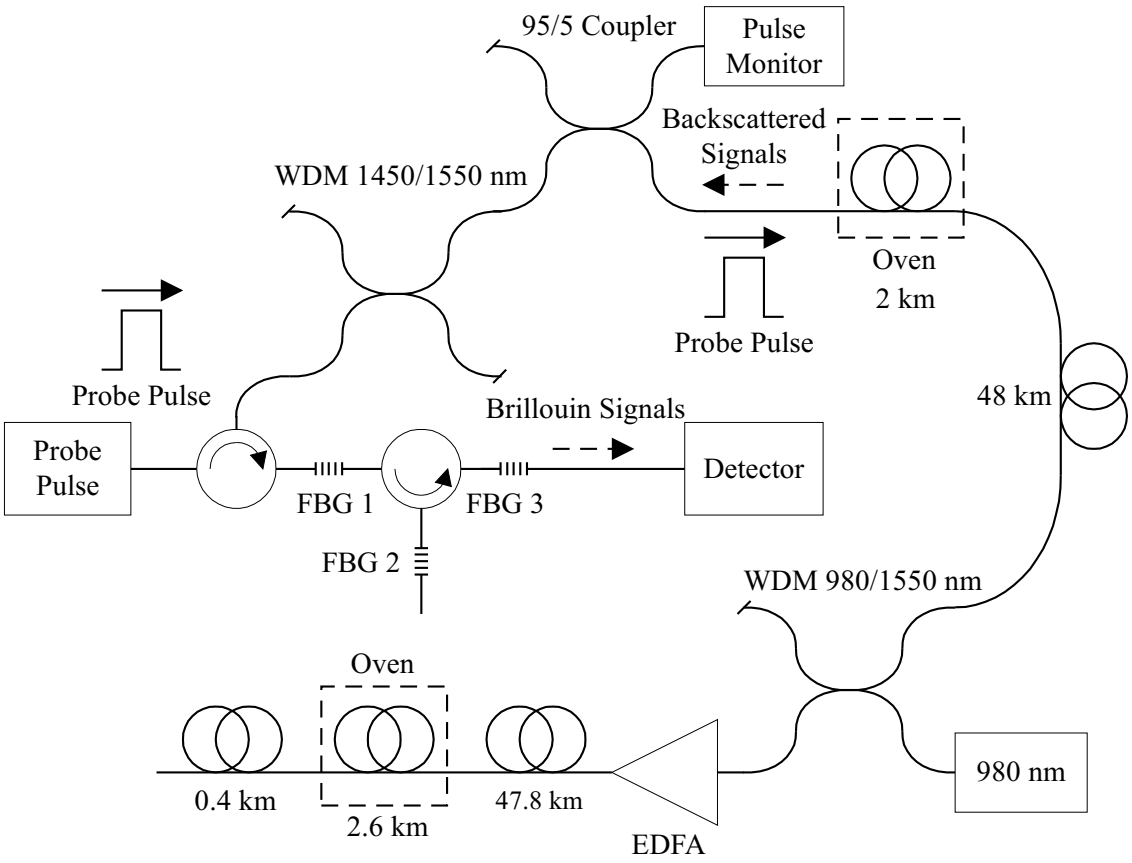

FIGURE 5.9: Experimental configuration for an in-line EDFA using a 980 nm pump located at about 50 km. The solid line indicates the path of the optical probe pulse, while the dashed line denotes the path of the backscattered signals.

5.4.2 Experimental Results

The Brillouin and Rayleigh backscattered signals amplified at 50 km using locally pumped EDFA are shown in figure 5.10. It can be seen that the Brillouin (indicated by a solid line) and Rayleigh (indicated by a dashed line) signals decayed linearly as a result of the two-way loss of 0.39 dB/km from 0 to about 50 km. The observed rise in the signal levels for both traces at approximately 50 km was due to amplification by the locally pumped EDFA. The two way EDFA gain at approximately 50 km was estimated to be 19.0 dB.

The estimated signal level at 100 km without the EDFA is -100.6 dBm, assuming the average loss coefficient over the full length of the sensing fibre is 0.39 dB/km. The measured backscattered power at the far end is -76.6 dBm. With remote amplification a gain of 24.0 dB is obtained compared to the expected gain of 19.0 dB. This was attributed to nonlinear effects. It can be seen that the slopes of the two backscattered traces are different beyond 50 km in figure 5.10. This effect was due to the contamination of the Brillouin signal by the Rayleigh signal, which caused the measured intensity of the Brillouin signal to be artificially increased and arises from spectral broadening of the probe power due to nonlinear effects. This results in a reduction in the temperature coefficient of the Brillouin backscattered power, which degrades the temperature resolution measurement. The presence of such a nonlinear effect was demonstrated by measuring the temperature coefficient of the Brillouin backscattered power along the sensing fibre.

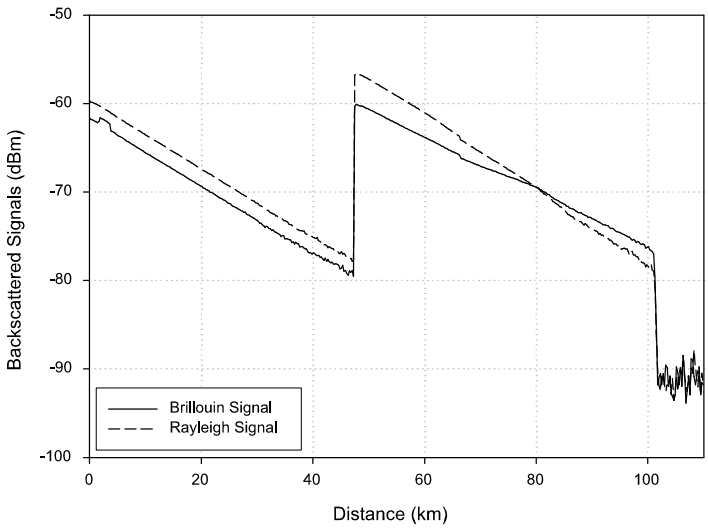

FIGURE 5.10: The Rayleigh and Brillouin signals with the in-line amplifier. The Rayleigh signal is indicated by a dashed line and the Brillouin signal is indicated by a solid line.

In the absence of strain, the temperature coefficient can be evaluated from the equation

$$K_{P,T} = \frac{P_B(T) - P_B(T_R)}{P_B(T_R)} \frac{100}{T - T_R} \tag{5.2}$$

where $K_{P,T}$ is the temperature coefficient of the Brillouin backscattered power, $P_B(T)$ is the Brillouin backscattered power at temperature, T, and $P_B(T_R)$ is the Brillouin backscattered power at a room temperature, T_R. The temperature coefficient of the Brillouin backscattered power was measured from 50 km to 100 km in figure 5.11. It was obtained by measuring the percentage change in the Brillouin signal of a fibre heated in an oven at various position along the sensing fibre. From figure 5.11, the temperature coefficient degraded from 0.30 $\%^o\mathrm{C}^{-1}$ at 70 km to approximately 0.21 $\%^o\mathrm{C}^{-1}$ at 100 km. This observation indicated that the contamination was more severe closer to the far end of the sensing fibre. To account for these changes, a value of 0.30 $\%^o\mathrm{C}^{-1}$ was used up to approximately 70 km and a value of 0.21 $\%^o\mathrm{C}^{-1}$ was used for calibration beyond this length. The uncertainty introduced with the calibration for the distance between 70 km and 80 km was within the experimental error of $\pm 1.0\,^o\mathrm{C}$.

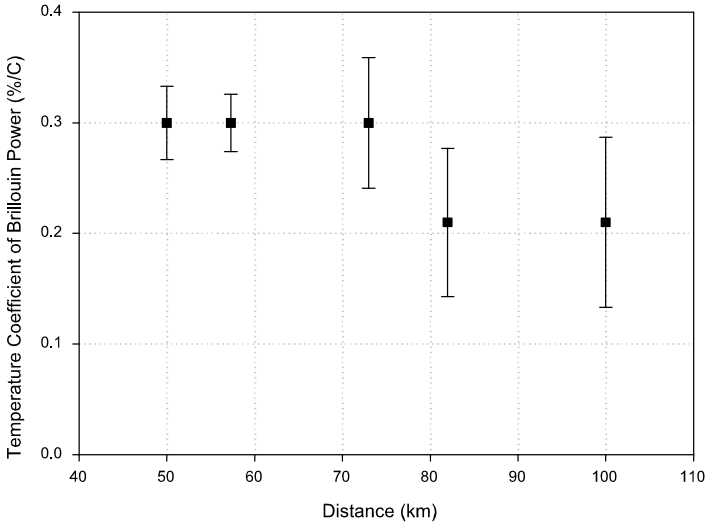

FIGURE 5.11: The temperature coefficient of the Brillouin backscattered power measurement as a function of sensing length.

The usual technique of normalising Brillouin signal with Rayleigh signal is no longer valid and so the Brillouin signal obtained at 80.0 ^{o}C was normalised using a Brillouin signal obtained at a room temperature of 22.0 ^{o}C. The temperature resolution measurement was performed at intervals of 6 km, over a range of 96 km, illustrated in figure 5.12. The temperature resolution was increased from 1.0 ^{o}C at the front end to approximately 12.0 ^{o}C at 50 km. A temperature resolution of 1.0 ^{o}C at 50 km was achieved with amplification by EDFA and it increased to approximately 6.0 ^{o}C at 96 km.

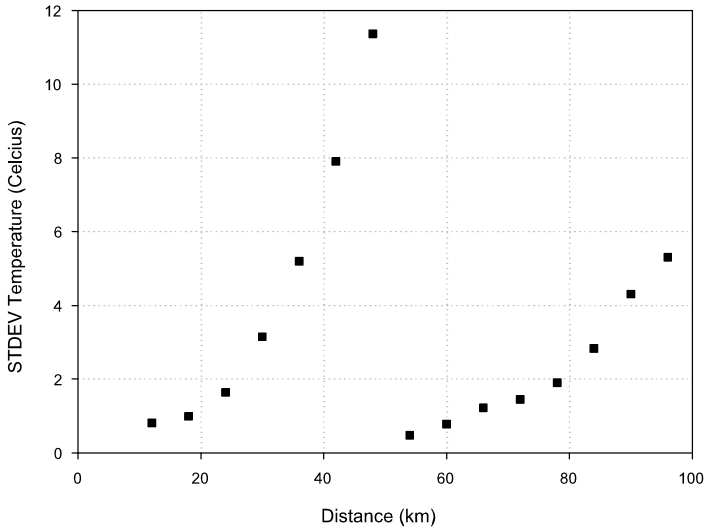

FIGURE 5.12: The temperature resolution measurement up to 96 km.

The enlarged Brillouin backscattered signal at the far end of the sensing fibre is illustrated in figure 5.13. The intensity change which corresponded to a temperature change of 60.0 ^{o}C at 98 km was measured to be 12.5 %. This value was much lower compared to the intensity change of 17.4 % measured at the front end of the sensing fibre.

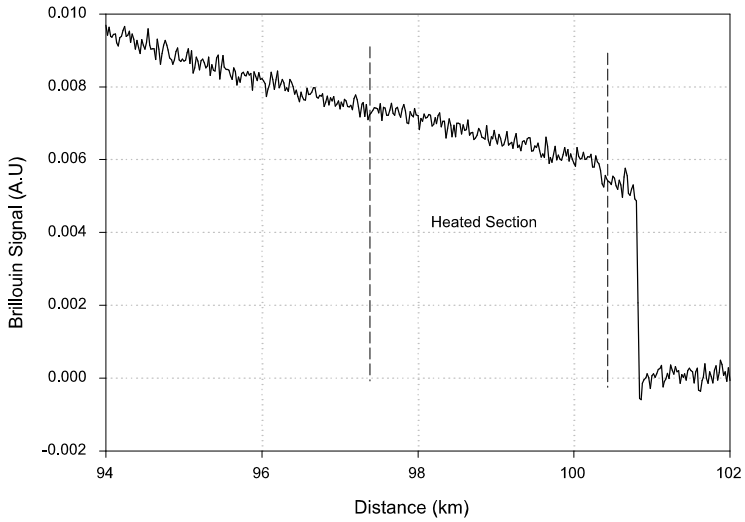

FIGURE 5.13: The enlarged Brillouin signal at the far end of the sensing fibre.

Figure 5.14 shows the temperature resolution measurement, performed in steps of 1 km, in the last 7 km of the sensing fibre. The standard deviation of temperature was increased from about 6.0 ^{o}C at 94 km to 12.0 ^{o}C at 100 km.

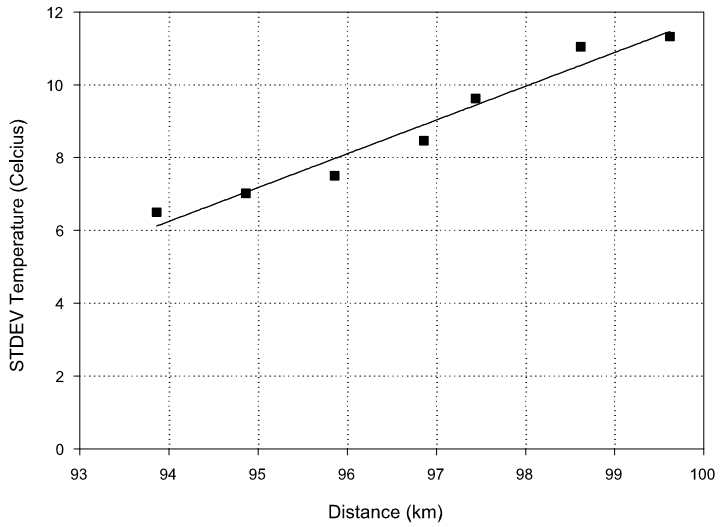

FIGURE 5.14: The temperature resolution measurement at the far end of the sensing fibre.

5.5 Remotely Pumped EDFA

In this configuration a 1480 nm Raman fibre laser source was used to remotely pump an EDFA. The 1480 nm pump also provides Raman gain to both the probe pulse and to the backscattered signal.

5.5.1 Experimental Details

The experimental setup for a remotely pumped EDFA is illustrated in figure 5.15. In this configuration, both the pump and probe can be operated at the front end of the sensing fibre. A CW Raman pump at 1480 nm, with an optical bandwidth of 0.5 nm and a pump power of 730 mW (below the calculated SBS threshold of 2.6 W), co-propagated in the sensing fibre with a 200 ns probe pulse with a peak power of approximately 40 mW at 1533 nm. In the first section of fibre at approximately 50 km, both the probe pulse and backscattered signals were amplified by the CW pump via Raman amplification. The EDFA provided further amplification at approximately 50 km. The 1480 nm pump power had fallen to 40 mW and was used to pump a 2 m section of EDFA with an erbium concentration of 100 ppm. The Brillouin signal was averaged 2^{20} times. To facilitate comparison of the temperature resolution measurements, the backscattered signal level at the far end of the sensing fibre was maintained at a similar amplitude as in other configurations.

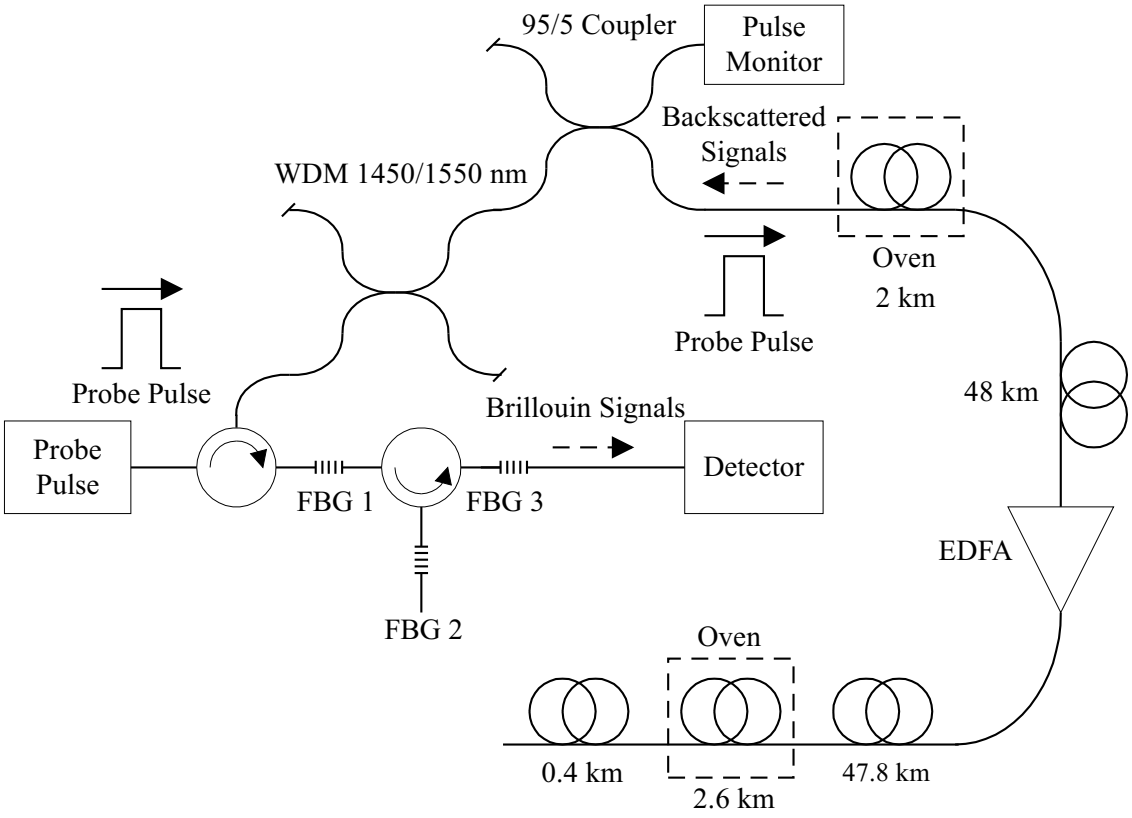

FIGURE 5.15: The experimental setup for the distributed temperature sensors employing remotely pumped EDFA. The solid line indicates the path of the optical probe pulse, while the dashed line denotes the path of the backscattered signals.

5.5.2 Experimental Results

The intensity profile of the Brillouin and Rayleigh backscattered signals using the remotely pumped EDFA is illustrated in figure 5.16. The peaks observed at approximately 16 km for the Brillouin (indicated by a solid line) and Rayleigh (indicated by a dashed-line) signal in the first 50 km were the result of Raman gain provided by CW pump at 1480 nm. A 7.8 dB increase in the amplitude of the signal was observed close to 50 km as a result of amplification by the EDFA. The Raman gain provided by the 1480 nm pump was estimated to be 16.2 dB at 50 km, based on the difference between the Raman amplified Brillouin signal to the unamplified Brillouin signal.

The Brillouin signal power at the far end was measured to be -76.6 dBm. This value was obtained by adjusting the pump power. As shown in figure 5.16, the two backscattered signals had different slopes after optical amplification at 50 km. This effect is again attributed to contamination of the Brillouin signal by the Rayleigh signal causing a reduction in the temperature coefficient of the Brillouin backscattered power, shown in figure 5.17.

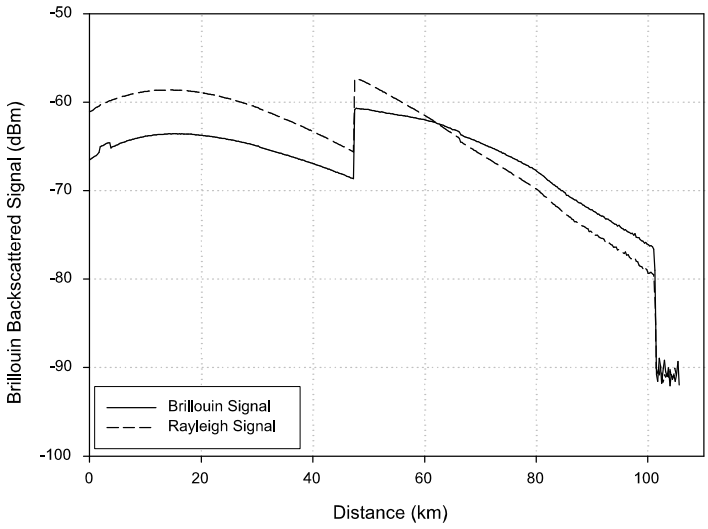

FIGURE 5.16: The Brillouin and Rayleigh backscattered signals with a remotely pumped EDFA. The Rayleigh signal is indicated by a dashed line and the Brillouin signal is indicated by a solid line.

It can be seen that the temperature coefficient of the Brillouin backscattered power was reduced from 0.26 $\%^oC^{-1}$ at to 0.10 $\%^oC^{-1}$ over the last section of the sensing fibre. These values were much lower compared to the value of 0.30 $\%^oC^{-1}$ obtained at the front end. It can be seen that the contamination of the Brillouin signal in this configuration was much more severe as compared to the locally pumped EDFA configuration.

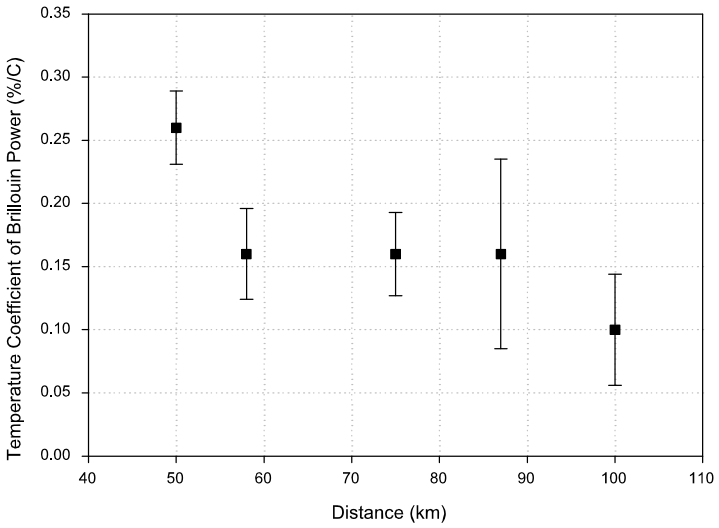

FIGURE 5.17: The temperature coefficient of Brillouin backscattered power as a function of sensing length.

Figure 5.18 shows the measured temperature resolution with distance. The reduction in the temperature coefficient mentioned earlier was taken into account, when deriving the temperature resolution. The temperature resolution was measured to be less than 3.0 ^{o}C over the first 80 km, and it increased to approximately 13.0 ^{o}C at 96 km.

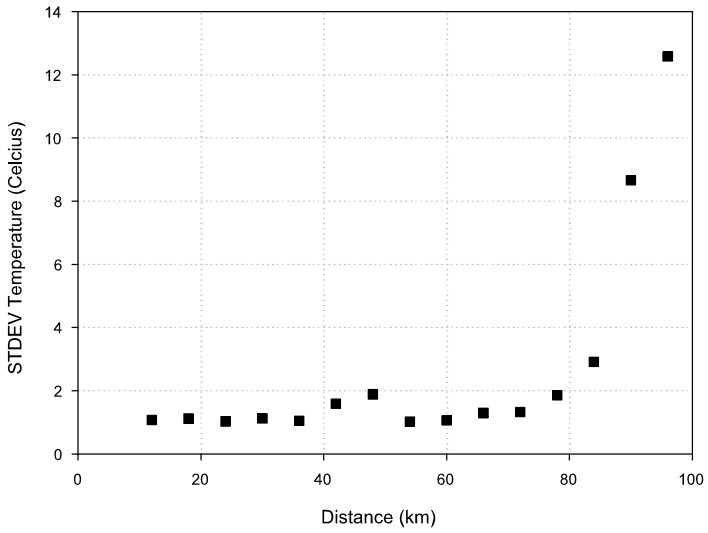

FIGURE 5.18: The measured temperature resolution with distance.

The enlarged Brillouin backscattered signal at 100 km is illustrated in figure 5.19. The measured intensity change was approximately 5.8 % at the far end and this value was lower than the intensity change of 17.4 % obtained at the front end of the sensing fibre.

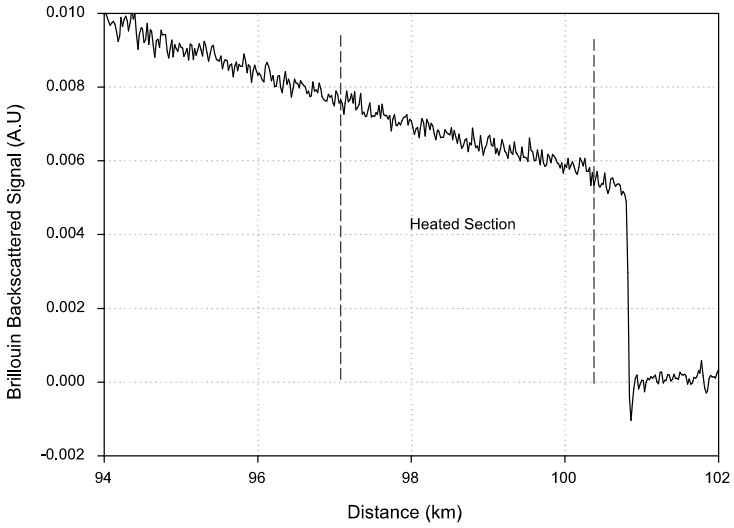

FIGURE 5.19: The enlarged Brillouin backscattered signal obtained at the far end of the sensing fibre.

The temperature resolution measurement, performed in steps of about 1 km in the last 7 km at 100 km, shown in figure 5.20. It can be seen that the temperature resolution was increased from 10.0 ^{o}C at 94 km to 20.0 ^{o}C at 99.6 km.

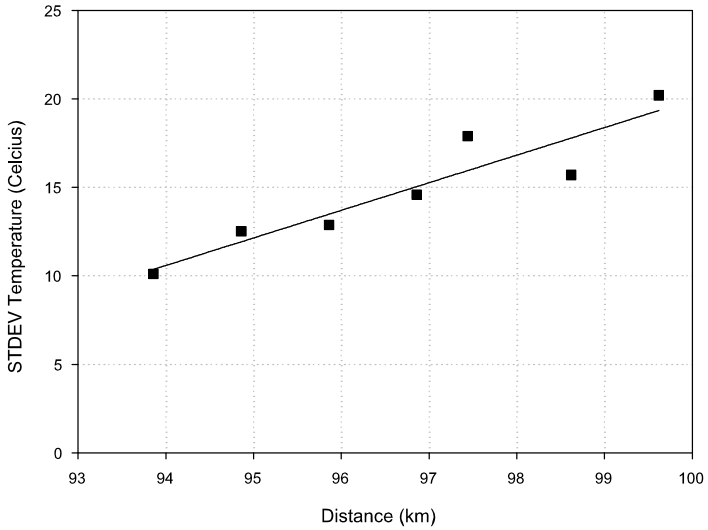

FIGURE 5.20: The temperature resolution measurement at 100 km.

5.6 Discussions

The performance of each distributed temperature sensor using various remote amplification techniques was assessed by comparing the temperature resolution at the far end of the sensing fibre.

The configurations containing locally pumped EDFA (indicated by triangles), a CW Raman fibre laser (indicated by squares) and without amplification (indicated by diamonds) demonstrated identical temperature resolution in the first 50 km as the launched probe power was similar for all the three cases, illustrated in figure 5.21. A temperature resolution of less than 1.0 ^{o}C at the front end rising to 12.0 ^{o}C at 50 km was obtained for all the three configurations. The distributed fibre sensor with the use of remotely pumped EDFA (indicated by circles) demonstrated an improved temperature resolution in the first 50 km in comparison to the latter three configurations. This improvement was the result of Raman gain, which leads to a temperature resolution of 1.0 ^{o}C increasing to less than 3.0 ^{o}C at a similar distance. However, the temperature resolution measurement deteriorated from 3.0 ^{o}C at 80 km to 13.0 ^{o}C at 96 km, as the nonlinear effects became more severe.

Beyond 80 km, the best result was obtained using remote Raman amplification. This was achieved whilst maintaining a temperature coefficient of 0.30 %^{o}C^{-1} for the Brillouin backscattered power over the full range of the sensing fibre. This led to the achieved temperature resolution measurement of 4.0 ^{o}C at 96 km. Without optical amplification and with a launched probe power of 100 mW, the temperature resolution deteriorated from 1.0 ^{o}C at the front end to 820.0 ^{o}C at 96 km. The value at the far end was estimated by extrapolating the temperature resolution from 50 km to 96 km. The temperature resolution obtained with remote Raman amplification was 1.5, 3.0 and 200.0 times better compared to the system using locally pumped EDFA, remotely pumped EDFA and without amplification at the far end respectively.

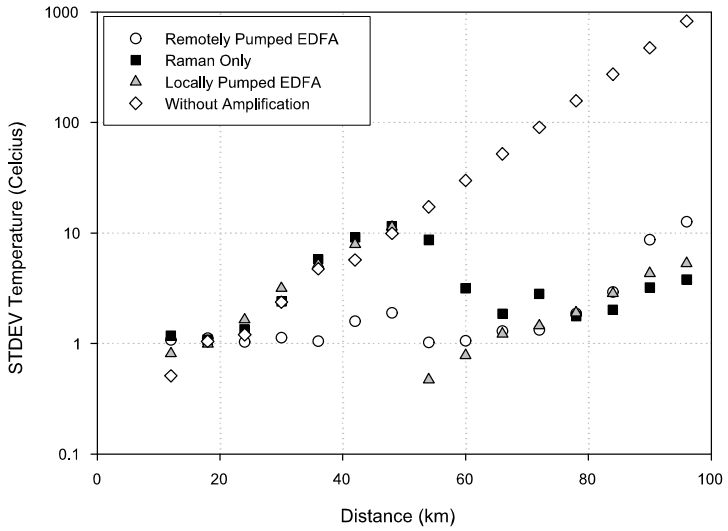

FIGURE 5.21: A comparison of the temperature resolution measurements over 100 km for different configurations. Temperature resolution measurements with Raman amplification (indicated by squares), locally pumped EDFA (indicated by triangles), remotely pumped EDFA (indicated by circles) and without amplification for a launched probe power of 100 mW (indicated by diamonds).

5.6.1 Summary

The performance of long range distributed fibre sensors utilising remote amplification has been investigated. Overall, remote Raman amplification at the midpoint of the sensing fibre demonstrated the best temperature resolution at the far end. This was followed by the locally pumped EDFA and remotely pumped EDFA configurations. The performance of the latter configurations at the far end was affected by the nonlinear effects.

5.7 Conclusions

This chapter has investigated and demonstrated the use of optical amplifiers namely EDFA and Raman in different remote amplification topologies, to enhance the sensing range of a distributed sensor. It consisted of remote Raman, locally pumped EDFA and remotely pumped EDFA configurations.

Using remote Raman amplification at 50 km, a temperature resolution of 4.0 ^{o}C was achieved at 96 km whilst ensuring a temperature coefficient of 0.30 %C^{-1} over the full length of the sensing fibre. A temperature resolution of 6.0 ^{o}C was achieved at 96 km for a similar experimental conditions using the locally pumped EDFA configuration. However, the temperature coefficient of the Brillouin backscattered power was reduced. This was attributed to the presence of Rayleigh contamination of the Brillouin signal arising from the spectrally broadened probe pulse. A temperature resolution of 13.0 ^{o}C was achieved at the far end of the sensing fibre using a remotely pumped EDFA. This configuration highlighted the advantage of using Raman gain in the first 50 km, in which the temperature resolution was the best among all the various configurations. However, the use of Raman amplification also lead to the occurrence of nonlinear effects further down the sensing fibre. The Raman gain increased the effective length and hence the amount of spectral broadening, for nonlinear effects such as SPM. Without optical amplification and using the maximum launched probe power of 100 mW, a temperature resolution of less than 1.0 ^{o}C at the front end rising to 12.0 ^{o}C was achieved at 50 km. By extrapolating this value to 96 km, the temperature resolution had deteriorated to 820.0 ^{o}C and further signal averaging is required to enable temperature measurement at this distance. This result demonstrated that without optical amplification, it is difficult to perform distributed measurement up to 100 km.

Although the signal level at the far end was maintained at a similar amplitude in all the three configurations, the remote Raman amplification demonstrated the best temperature resolution at the far end. Such amplification distributes the gain over the remaining length of the fibre and hence allows the signal to be amplified further down the sensing fibre and avoids significant spectral broadening due to SPM.

Bibliography

[1] K. Shimizu, T. Horiguchi and Y. Koyamada, "Characteristics and Reduction of Coherent Fading Noise in Rayleigh Backscattering Measurement for Optical Fibers and Components," *IEEE Journal of Lightwave Technology*, vol. 10, no. 7, p. 982, July 1992.

[2] P.C. Wait and T.P. Newson, "Landau Plazcek Ratio Applied to Distributed Fibre Sensing," *Optics Communications*, vol. 122, p. 141, Jun 1996.

[3] P.C. Becker, N.A. Olsson and J.R. Simpson, *Erbium-Doped Fiber Amplifiers: Fundamentals and Technology.* Academic Press, 1999.

Chapter 6

Discussions, Recommendations and Conclusions

A summary of the achievements and the future directions of the research is presented in this chapter.

6.1 Discussions

Distributed fibre sensors based on spontaneous Brillouin scattering provide an excellent technique for performing distributed temperature measurements. However, the sensing range is limited by the attenuation of the signal in the optical fibre. To enhance the measurement range of such a fibre sensor, the use of optical amplification was investigated.

The characteristics of various types of optical amplifiers and their applications for improving the performance of the long range distributed fibre sensor were discussed. The research was focussed on using Raman amplification and it was modelled to determine the optimum parameters. Numerical simulation shows that the optimum operating pump and probe wavelengths were located at 1450 nm and 1550 nm respectively.

In the first experiment, a sensing length of 35 km was demonstrated using the CW Raman amplification provided at the front end of the sensing fibre. However, the performance of the system was deteriorated due to the onset of the nonlinear effects. The temperature coefficient of the Brillouin backscattered power was reduced when the Raman pump power was increased. This effect was due to contamination of the Brillouin signal by the Rayleigh signal, which arose from the spectrally broadened probe pulse. Moreover, the backward travelling Raman ASE occurring at the signal wavelength led to the saturation of the receiver and this consequently limited the launched pump power. To fully utilise the Raman gain, the nonlinear effects have to be reduced.

To achieve this, the Raman gain was delayed until further down the sensing fibre using pulsed Raman amplification. A pump pulse at 1450 nm was produced by gating the CW Raman fibre laser using an acousto-optic modulator (AOM). The pump pulse at 1450 nm was used to amplify the probe pulse at 1533 nm when the two pulses overlapped in the sensing fibre. Using this technique, the Raman gain was delayed whilst keeping the nonlinear effects to a minimum. The use of a pump pulse, instead of a CW pump, reduced the amplitude of the backward propagating Raman ASE. A temperature resolution of 1.0 ^{o}C at the front end rising to 13.0 ^{o}C at 50 km was achieved.

Without Raman amplification, the temperature resolution was measured to be 40.0 ^{o}C at 50 km. The Raman gain is primarily governed by the amplitude of the pump pulse. However, the amplitude of the pump pulse and hence the Raman gain was limited by the loss of the modulator. This restricted the measurement range to 50 km.

The aforementioned technique highlighted the benefit of delaying the Raman gain further down the fibre. To increase the sensing range beyond 50 km, remote amplification was investigated. Such a method involves amplifying the probe signal at the midpoint of the sensing fibre. This technique allows a much higher launched pump power, which lead to a higher gain. Three configurations were finalised and investigated. They were remote Raman amplification, locally pumped EDFA and remotely pumped EDFA configurations. The performance for each configuration was assessed and compared based on the temperature resolution measurement at the far end. Among the three configurations, the remote Raman amplification technique demonstrated the best temperature resolution at the far end of the sensing fibre. A temperature resolution of 4.0 ^{o}C was obtained at 96 km. It was 1.5, 3.0 and 200.0 times lower at 96 km compared to using locally pumped EDFA, remotely pumped EDFA and without amplification, performed under similar experimental conditions. Although the temperature measurement at the far end with the remotely pumped EDFA was inferior to the locally pumped EDFA and remote Raman amplification configuration, its temperature resolution was much better in the first 80 km. A temperature resolution of less than 3.0 ^{o}C was achieved over this distance.

6.2 Recommendations for Future Work

The results obtained from the study suggested that to extend the measurement range of a distributed fibre sensor whilst keeping the nonlinear effects to a minimum, the Raman gain should be delayed until further down the sensing fibre. The work on the pulsed Raman amplification technique may be further improved by investigating high power pulsed lasers operating at 1450 nm. This includes investigating the thulium-doped fluoride fibre amplifier as the gain medium for a Q-switched fibre laser operating at 1450 nm. A peak power of 70 W and a pulsewidth of 450 ns at 1470 nm have been demonstrated using such a fibre laser [1]. The spectral broadening of the probe pulse with Raman amplification should be investigated in further detail. The results obtained from such an investigation may provide an improved understanding for choosing the optimum launched pump and probe power for a particular sensing length.

The sensing range of the distributed fibre sensor can be optimised by operating the probe wavelength at a lower loss wavelength of 1550 nm. The use of an erbium doped fibre preamplifier and optical mixing with local oscillator light have enhanced the sensitivity of the coherent detection. This detection system when combined with the pulsed Raman amplification technique may improve the measurement range further and it is now under investigation. The optical fibres used in distributed fibre sensors consist of standard singlemode fibre. In such an optical fibre, the attenuation from 1360 nm to 1450 nm is increased due to absorption of hydroxyl ions. Recent advances in fibre fabrication techniques have made it possible to develop an optical fibre with reduced absorption of light by hydroxyl ions [2]. The use of such an optical fibre would reduce the attenuation of a pump at 1450 nm, increasing its transmission length and allowing higher Raman gain.

Special design fibres such as large area non-zero dispersion shifted fibre (NZDSF) with higher power carrying capacity should be investigated. The use of such a fibre allows a higher launched power and this indicates a longer sensing range.

6.3 Conclusions

The objective of the research was to investigate the use of optical amplification to enhance the sensing range of distributed fibre sensors. The main achievements are:

1. A 50 km single-ended distributed temperature sensor based on spontaneous Brillouin scattering with a spatial resolution of 15 m was demonstrated using pulsed Raman amplification. A temperature resolution of 13 ^{o}C was achieved at 50 km.

2. A single-ended distributed temperature sensor with a sensing range of 80 km and a spatial resolution of 20 m was demonstrated using a remotely pumped EDFA at 50 km. A temperature resolution of less than 3 ^{o}C was achieved over this measurement range.

3. A 100 km distributed temperature sensor with a spatial resolution of 20 m was demonstrated using remote Raman amplification at 50 km. A temperature resolution of 8 ^{o}C was achieved at 100 km.

These results represent a significant advance compared to the results obtained without optical amplification.

Bibliography

[1] T. Komukai, T. Yamamoto, T. Sugawa and Y. Miyajima, "Efficient Upconversion Pumping at 1.064 μm of Tm^{3+}-Doped Fluoride Fibre Laser Operating Around 1.47 μm," *Electronics Letters*, vol. 28, no. 9, p. 830, April 1992.

[2] G.A. Thomas, B.I. Shraiman, P.F. Glodis and M.J. Stephen, "Towards the Clarity Limit in Optical Fibre," *Nature*, vol. 404, p. 262, March 2000.

Appendix A

List of Publications

Journal Publications

1. Y.T. Cho, M. Alahbabi, M.J. Gunning and T.P. Newson, "Enhanced Performance of Long Range Brillouin Intensity Based Temperature Sensors Using Remote Raman Amplification", Measurement Science and Technology, Vol. 15, No. 8, p. 1548, August 2004.

2. Y.T. Cho, M. Alahbabi, M.J. Gunning and T.P. Newson, "50 km Single-Ended Spontaneous Brillouin Based Distributed Temperature Sensor Exploiting Pulsed Raman Amplification", Optics Letters, Vol. 28, No. 18, p. 1651, September 2003.

3. M. Alahbabi, Y.T. Cho, P.C. Wait, A. Hartog and T.P. Newson, "Influence of Modulation Instability on Distributed Optical Fiber Sensors based on Spontaneous Brillouin Scattering", Journal of Optical Society of America B (JOSA B), Vol. 21 No. 6 p. 1156, 2004.

4. M. Alahbabi, Y.T. Cho and T.P. Newson, "Comparison of the Methods for Discriminating Temperature and Strain in Spontaneous Brillouin-Based Distributed Sensors", Optics Letters, Vol. 29, No. 1, p. 26, January 2004.

5. M. Alahbabi, Y.T. Cho, and T.P. Newson, "100 km Distributed Temperature Sensor Based On Coherent Detection of Spontaneous Brillouin Backscatter", Measurement Science and Technology, Vol. 15, No. 8, p. 1544, August 2004.

6. M. Alahbabi, N.P. Lawrence, Y.T. Cho and T.P. Newson, "High Spatial Resolution Microwave Detection System for Long Range Brillouin-based Distributed Sensors", Measurement Science and Technology, Vol. 15, No. 8, p. 1538, August 2004.

Conference Presentations

7. Y.T. Cho, M. Alahbabi, and T.P. Newson, "Brillouin Based OTDR With Measurement Range of 85 km Using Combined EDFA and Raman Amplification", Conference of Lasers and Electro-Optics Technical Digest (CLEO), CWM5, May 2004.

8. Y.T. Cho, M. Alahbabi,M.J. Gunning and T.P. Newson, "Enhanced Performance of Long Range Brillouin Intensity Based Temperature Sensors Using Remote Raman Amplification", 16^{th} International Conference on Optical Fiber Sensors Technical Digest, p. 392, October 2003.

9. Y.T. Cho and T.P. Newson, "Brillouin-based Distributed Fibre Temperature Sensor at 1.53 μm Using Raman Amplification", 15^{th} Optical Fiber Sensors Conference Technical Digest, p. 305, May 2002.

10. M. Alahbabi, Y.T. Cho and T.P. Newson, "Simultaneous Distributed Measurements of Temperature and Strain using Combined Spontaneous Raman and Brillouin Scattering", Second European Workshop on Optical Fibre Sensors (EWOFS), SPIE Vol. 5502 p.488, June 2004.

11. M. Alahbabi, Y.T. Cho and T.P. Newson, "100 km Distributed Temperature Sensor Based On Coherent Detection of Spontaneous Brillouin Backscatter", 16^{th} International Conference on Optical Fiber Sensors Technical Digest, p. 388, October 2003.

12. M. Alahbabi, N.P. Lawrence, Y.T. Cho and T.P. Newson, "High Spatial Resolution Microwave Detection System for Long Range Brillouin-based Distributed Sensors", 16^{th} International Conference on Optical Fiber Sensors Technical Digest, p. 384, October 2003.